# STUDY OF EFFECTS OF SOLAR ACTIVITY ON IONOSPHERIC PLASMA

**THESIS**

***Submitted in fulfillment of the requirement for the award of the degree of***

**DOCTOR OF PHILOSOPHY**

***to***

***J. C. BOSE UNIVERSITY OF SCIENCE & TECHNOLOGY, YMCA***

***by***

**GEETA RANA**
**Registration No: YMCAUST/Ph/04/2011**

***Under the Supervision of***

**DR. MANI KANT YADAV**
**Supervisor**
**Assistant Professor**


**DEPARTMENT OF PHYSICS**
**FACULTY OF SCIENCES**
**J. C. BOSE UNIVERSITY OF SCIENCE & TECHNOLOGY, YMCA**
**SECTOR-6, MATHURA ROAD, FARIDABAD-121006,**
**HARYANA (INDIA)**

**2021**

# DEDICATION

*This Ph.D. Thesis is dedicated to….*

*My Father-in-Law,* ***Sh. Raj Karan Rana!***

# DECLARATION

I hereby declare that this entitled **"STUDY OF EFFECTS OF SOLAR ACTIVITY ON IONOSPHERIC PLASMA"** by **GEETA RANA**, being submitted in fulfillment of the requirements for the Degree of Doctor of Philosophy in **PHYSICS** under Faculty of Sciences of J.C. BOSE University of Science & Technology, YMCA, Faridabad, during the academic year 2020, is a bona fide record of my original work carried out under guidance and supervision of **Dr. MANI KANT YADAV**, **Assistant Professor, Department of Physics,** J.C. BOSE University of Science & Technology, YMCA, Faridabad, and has not been presented elsewhere.

I further declare that the thesis does not contain any part of any work which has been submitted for the award of any degree either in this university or in any other university.

**(Geeta Rana)**
Registration No: YMCAUST/Ph/04/2011

# CERTIFICATE

This is to certify that this thesis entitled, **"STUDY OF EFFECTS OF SOLAR ACTIVITY ON IONOSPHERIC PLASMA"** by **GEETA RANA,** submitted in fulfillment of the requirement for the Degree of Doctor of Philosophy in **PHYSICS** under Faculty of Sciences of J.C. BOSE University of Science & Technology, YMCA, Faridabad, during the academic year 2020, is a bona fide record of work carried out under my guidance and supervision.

I further declare that to the best of my knowledge, the thesis does not contain any part of any work which has been submitted for the award of any degree either in this university or in any other university.

**(Signature of Supervisor)**

**Dr. Mani Kant Yadav**
Assistant Professor
Department of Physics
Faculty of Sciences
J.C. BOSE University of Science and Technology, YMCA, Faridabad

Dated:

# ACKNOWLEDGEMENT

*I express my gratitude to almighty God for giving me the strength and courage to complete this work*

I would like to express my sincere and deep gratitude to my Ph.D. supervisor, Dr. Mani Kant Yadav, Assistant Professor, Department of Physics, J. C. BOSE University of Science and Technology, YMCA, Faridabad for allowing me to work in this area. It would never be possible for me to take this thesis to this level without his continuous guidance, constructive criticism, and valuable advice. His knowledge of various perspectives of research provided me with the opportunity to make significant work in this direction.

I am seriously thankful to our Vice-chancellor Dr. Dinesh Kumar, Dean and Chairman Dr. Rajkumar, Ph. D. Coordinator Dr. Manisha Garg, Dr. Anuradha, and all the staff members, for being kind enough and helpful during my entire research work. Here I cannot forget to thank Mr. Bishan Pal for his continuous help and concern from the beginning till the completion of this long journey.

I am deeply indebted to Professor Dr. D K Sharma and Dr. Ananna Bardhan from Manav Rachna University for their wholehearted motivation, incessant support, and appreciation which culminated in the successful completion of this research work. Their sharp and inclusive intellect, innovative ideas, and deep insight of the subject and research kept me sailing through the tough times of my Ph.D. marathon. I am truly short of words to express my gratitude from the bottom of my heart to both of them.

I want to express my special thanks to my in-laws, my parents, my sister, and brother, and all my friends for their blessings, caring words, invaluable suggestions, and support. My sincere heartiest special thanks to my husband Mr. Sudhir Rana (Barrister & Solicitor) for his constant encouragement and support. Without his patience, faith, and inspiration, it would have been impossible to complete this research journey.

At last, I would like to bow with words of special thanks to my mother-in-law Mrs. Shashi Rana for her utmost patience, love and faithful support without which it was never possible to finish my Ph.D.

Big thanks to all!!

**(Geeta Rana)**
Registration No: YMCAUST/Ph/04/2011

# ABSTRACT

The interplanetary space, Earth's magnetosphere, and the ionosphere form a single system driven by the Sun or Solar activities. Variations in solar activities cause variations in the ionospheric plasma and its parameters (electron & ion temperature, density, and ionic composition, etc).

Since the beginning of the space era in the 1950s, space weather has become a hot topic, and the ionosphere which is considered the most dynamic and complex region of the Earth's atmosphere plays an utmost important role in it. Any deviation in conditions on the Sun, interplanetary space, magnetosphere, and ionosphere influences the performance and reliability of space-born technological systems such as satellite communication and navigation systems, ground-based technological systems as power outage and can even endanger astronauts, human lives, or health.

In the present thesis, the effects of solar activities on ionospheric plasma have been studied mainly with the help of ROCSAT-1 and SROSS-C2 satellites. The dataset is analyzed for the diurnal, seasonal, and annual behavior of ion density and temperature of especially the F2 layer of the ionosphere over the equatorial and low latitude region.

The behavior of total ion density (Ni) and ion temperature (Ti) as measured by SROSSS-C2 satellite at an average altitude of about 500 km have been analyzed and compared with estimations of the IRI-2012 model during low solar activity year (LSA-1995) and high solar activity year (HSA-2000). Ni is found to increase by a factor of $10^2$ with the increase of solar activity. The Ni values obtained from SROSS-C2 and IRI-2012 show asymmetrical behavior during both low and high solar activity years. The relative variation of Ti between SROSS-C2 and IRI-2012 values is observed in good agreement with each other during low and high solar activity years, except for an asymmetry during nighttime in the year 1995. The relationship between Ni and Ti itself shows a weak/poor co-relation. The correlation factor is weaker in the low solar activity year as compared to the high solar activity year.

The behavior of Ni and Ti has also been analyzed with the help of ROCSAT-1 satellite and then a comparison has been made with the estimations of the IRI-2016 model, during different phases of solar activity years (1999-2003).

During all the considered years (1999-2003), IRI-2016 model overestimates Ni data, specifically in the nighttime and pre-sunrise hours. On the contrary, the model underestimates Ni during the daytime. Also, the IRI model predicts evening enhancements in Ni which are not observed in ROCSAT-1 measurements.

The annual diurnal analysis of Ti (measured by ROCSAT) shows that Ti exhibits a morning peak (morning overshoot, ~07:00 LT), a daytime trough, and a secondary peak (evening enhancement) followed by nighttime minima and a minimum before the sunrise. According to ROCSAT-1 measurements, secondary peaks of Ti are of higher magnitude (~1500K) for years 2000-2002 as compared to the years 1999 and 2003 (~1400K ). On the contrary, the IRI-model cannot model the Ti secondary peaks measured by ROCSAT-1.

The Ionosphere gets perturbed due to solar phenomena as high-speed solar winds, solar flares, and coronal mass ejections, etc. The magnetic field associated with solar phenomena, when enters inside the Earth's magnetic field it disturbs the geomagnetic field and produces a storm known as a geomagnetic storm. Hence, to a weak (30 July 1999) and a moderate (13 November 1999) geomagnetic storm (GS) at low latitude Indian region (5-35º geog N and 65-95º geog E), the behaviour of ionospheric parameters- ion densities ($O^+$ and $H^+$) and ion temperature (Ti) has been analyzed using ROCSAT-1 satellite measurements and estimated values of IRI-2016 model. The ionospheric plasma parameters show anomalous behaviour during disturbed days compared to quiet days. For the weak GS, both the average $O^+$ and $H^+$ density have been increased by a factor of around 1.8 during disturbed and quiet days respectively as calculated by ROCSAT-1. For the moderate GS, the average $O^+$ and $H^+$ density has been increased by a factor of around 2.7 and 6.3 respectively during disturbed and quiet days respectively, as calculated by ROCSAT-1. And the least or negligible variation has been observed in Ti for both measured and modelled values during weak and moderate GS.

# TABLE OF CONTENTS

# LIST OF TABLES

# LIST OF FIGURES

# LIST OF ABBREVIATIONS

| | |
|---|---|
| **AE-C** | Atmosphere Explorer |
| **ASLV** | Augmented Satellite Launch Vehicle |
| **CIR** | Co-rotating Interaction Region |
| **CME** | Coronal Mass Ejection |
| **COSPAR** | Committee on Space Research |
| **DEMETER** | Detection of Electromagnetic Emission Transmitted from Earthquake Regions |
| **DMSP** | Defense Meteorological Satellite Program |
| **Dst** | Disturbance Storm Time Index |
| **EEJ** | Equatorial Electrojet |
| **EIA** | Equatorial Ionisation Anomaly |
| **EISCAT** | European Incoherent Scatter Scientific Association |
| **ESF** | Equatorial Spread F |
| **ETWA** | Equatorial Temperature and Wind Anomaly |
| **EUV** | Extreme Ultra Violet |
| **GCR** | Galactic Cosmic Rays |
| **GNSS** | Global Navigation Satellite System |
| **GS** | Geomagnetic Storm |
| **HAS** | High Solar Activity |
| **IMF** | Interplanetary Magnetic Field |
| **IP** | Initial Phase |
| **IPEI** | Ionospheric Plasma and Electrodynamics Instrument |
| **IRI** | International Reference Ionosphere |
| **ISR** | Incoherent Scatter Radar |
| **ISRO** | Indian Space Research Organization |
| **LSA** | Low Solar Activity |
| **MP** | Main Phase |
| **MU** | Middle and Upper Atmosphere Radar |
| **Ni** | Total Ion Density |
| **OGO** | Orbital Geophysical Observatory |

| | |
|---|---|
| **PRE** | Pre-Reversal Enhancement |
| **ROCSAT** | Republic of China Satellite |
| **RP** | Recovery Phase |
| **RPA** | Retarding Potential Analyzer |
| **SID** | Sudden Ionospheric Disturbances |
| **SROSS** | Stretched Rohini Satellite Series |
| **SSC** | Storm Sudden Commencement |
| **SUPIM** | Sheffield University Plasmasphere Ionosphere Model |
| **Ti** | Ion Temperature |
| **URSI** | International Union of Radio Science |
| **UT** | Universal Time |
| **VTEC** | Vertical Total Electron Content |

# CHAPTER 1

# GENERAL INTRODUCTION

## 1.1 THE ATMOSPHERE OF THE EARTH

Our Earth is the only planet in the solar system that can sustain life because of the existence of an atmosphere. The huge blanket of gas encircling the entire Earth is called its Atmosphere. This atmosphere contains breathable gas and keeps the Earth warm by day and cold at night. Also, it protects us from solar radiations and blasts of heat emanating from the sun.

The Earth's atmosphere is governed by the Sun as solar radiations are absorbed in various latitudes which lead to heating and dissociation of various atmospheric constituents. Hence, the atmosphere is categorized based on variations in altitude, latitude, temperature, composition, and homogeneity. On the basis of altitude, the atmosphere is divided as lower atmosphere-below 15 km, middle atmosphere-15 to90 km, and upper atmosphere- above 90 km. Based upon the latitudinal extent, the region between ±30º is known as 'low latitude', between ±30° and ±60º as mid-latitude, and as 'high latitude' for the region lying above ±60º. The atmosphere consists of various gas particles out of which molecular nitrogen ($N_2$) and molecular oxygen ($O_2$) exists abundantly with smaller amounts of water vapour and some trace gases [1].

The absorption of solar radiation is the major source of heating in different regions of the Earth's atmosphere and hence, forms the thermal structure of the atmosphere. Depending upon the temperature variation, the Earth's atmosphere is divided into five main layers, as shown in figure 1.1. Starting from the bottom, these layers are the troposphere, the stratosphere, the mesosphere, the thermosphere, and the exosphere. Although there is no distinct boundary between the atmosphere and space, an imaginary line at around 100 km from the surface, known as the Karman line is considered the boundary where the atmosphere encounters the outer space.

The troposphere is the layer closest to the Earth's surface- the region where we live in. Most of the weather phenomena such as cloud formation, rain, snow, etc. occur in the troposphere, which extends up to about 7 km at the poles and around 17 km at the equator. In this region, at a rate of 6.5º C per km, the temperature decreases

continuously with the height above the earth. The upper boundary of the troposphere is the tropopause which is an inversion layer, where the air temperature ceases to decrease with height and remains constant through its thickness [2].

The next layer above the troposphere, extending up to around 50 Km from the earth's surface is called the stratosphere. Ozone is found abundantly here which protects us from harmful UV radiations of the sun. The temperature gradient is reverse in the stratosphere. The temperature increases with an increase in height due to the absorption of ultraviolet (UV) radiation. This increase in temperature with height results in strong thermodynamic stability with little or restricted turbulence and vertical mixing (mixing of the atmosphere). Due to the increased temperature, the air here is very dry and thinner with an almost cloud-free volume. This is why jet aircraft and weather balloons fly in this region.

The upper boundary of the stratosphere is known as stratopause.

The third layer of the atmosphere directly above the stratosphere is the mesosphere. It starts from about 50 km above the ground and goes up to 85 km high. Here, the temperature again decreases with increasing height and reaches a minimum of about 172 K at the boundary of the mesosphere known as mesopause. This is the highest layer of the atmosphere up till which the gases are thoroughly mixed by turbulence in the atmosphere. The mesosphere has been accessed only through sounding rockets, which provide mesospheric measurements for a few minutes per mission. This is why the mesosphere is poorly studied relative to other layers and hence is also named as '*ignorosphere'*.

Above the mesopause, the layer of the atmosphere is the thermosphere which extends from about 90 km to between 500 and 1000 km. The temperature in the thermosphere again increases with height because of the absorption of energetic UV and X-Ray radiations and it ranges from about 500 K to 2000 K. The thermosphere is the region where space shuttles and the International space station orbit the Earth.

The part of the thermosphere where charged particles are found in abundance is known as the ionosphere. Solar UV radiations cause photoionization of molecules and results in the formation of ions in the ionosphere. The ionosphere is an electrically

conducting region that enables the reflection of radio waves and thus allows long-distance radio communication possible.

The last known layer of the atmosphere is the exosphere which begins at about 600 km from the Earth's surface and then gradually fades into outer space. This region is extremely thin and is composed of widely dispersed gaseous particles, mainly hydrogen and helium.

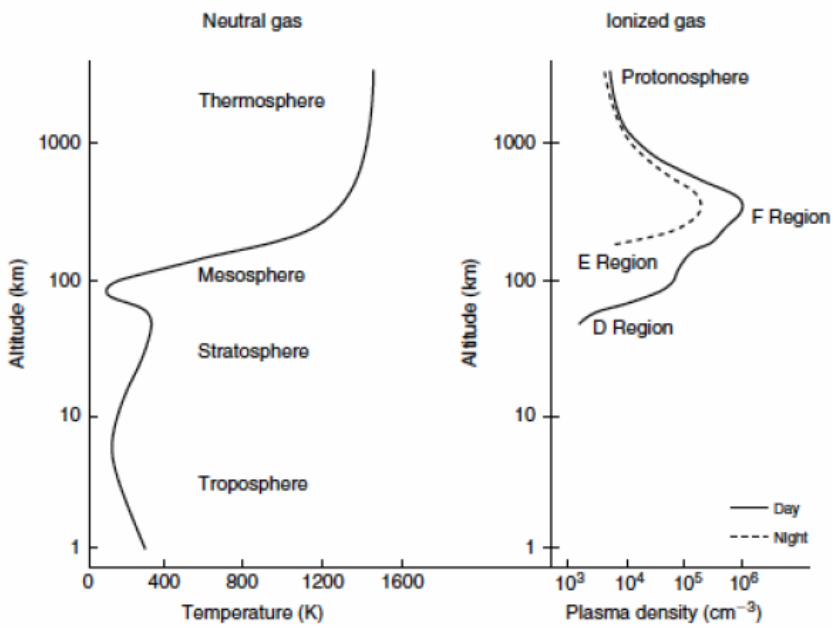


Figure 1.1: The neutral atmosphere temperature (left) and ionospheric plasma density (right), M.C. Kelley, 2009.

## 1.2 FORMATION OF THE IONOSPHERE AND ITS LAYERS

In 1839, C. F. Gauss, a German mathematician, and physicist hypothesized about an electrically conducting layer of the atmosphere, accountable for varying geomagnetic field. Then in December 1901, Guglielmo Marconi surprised the world by making transatlantic communication possible for the very first time, from Cornwall, England to Newfoundland, Canada. In 1902, British scientists Heaviside and Kenelly in the United States suggested the existence of the ionosphere. They concluded that the waves had to follow the curvature of the earth along electrically conductive layers in the upper atmosphere. So they proposed a region "ionosphere" that acted as a mirror for radio waves with avelength $\lambda >\approx 20$ m and hence, decided to measure the electrical properties of the upper atmosphere. About 25 years later (1925), the actual

existence of the ionosphere could experimentally be proved by Appleton and Barnett and Brut and Tufe. They inferred that at different heights three ionized layers viz. E, F1and F2 exists, with their ionization maxima. Later, a D-layer was discovered from the sudden ionospheric disturbance (S.I.D) phenomenon in 1931 by Mogel. Prof. Chapman was the first who gave the classical theory on the production of ionization and the formation of different ionized layers in the upper atmosphere.

The ionosphere is that part of the atmosphere which contains a sufficient amount of atoms and molecules and various ionized species to affect the radio wave propagation. It lies approximately 50-1000 km above the Earth's surface. The ionospheric layer or plasma is formed primarily due to the photoionization of neutral atmospheric constituents by solar extreme ultraviolet (EUV) and X-ray radiation [1, 3]. Cosmic rays and solar wind particles considered as secondary ionizing factors also play a role in causing ionization, but their effect is of lesser importance when compared to that due to radiation.

The activities of the ionosphere are controlled through dynamic, chemical, and energy processes which involve conservation laws of mass, momentum, and energy. The production of ions and their loss comes under chemical processes, whereas ionization's movement is a dynamic process. The chemical reactions prevail in the bottom side ionosphere and the dynamic processes dominate in the upper ionospheric region. The F2 layer is the region that lies at a level of transition between the chemical and dynamic process [4].

*Production of Ionization processes in the ionosphere*

*(a) Photoionization*: When the incoming solar radiation or a photon interacts with a neutral atom or molecule, enough energy is absorbed by the atom so that in result an electron knocks out leaving a positively charged ion. This process of removal of an electron from an atom and producing a positively charged ion is known as photoionization [4].

The ionization rate (q) depends upon the intensity of the radiation (i) and concentration of the neutral gas (n). At high altitudes, though (i) is large, 'q' will be small because (n) is small. When radiation enters deeper inside the atmosphere, its intensity degrades due to absorption, but the gas concentration

increases. Below a certain height ' $h_m$ ' the radiation is very weak in such a way that its rate of loss is greater than the rate of increase of gas concentration. Thus there is a definite height $h_m$, where the rate of production of ions reaches utmost.

*(b) Corpuscular Ionization*: Corpuscular radiation (cosmic rays with energy above 109 eV) from the sun also contributes to the production of ionization especially at low altitudes. Corpuscular radiation is responsible for the production of D region and part of E region of the ionosphere by ionizing triatomic molecules.

*Loss of Ionization processes in the ionosphere:* As there is the production of ionization in the ionosphere, its destruction is also obvious. The various loss mechanisms in the ionosphere are broadly classified into chemical reactions and transport phenomena such as diffusion, neutral winds, and electric fields. The various photochemical reactions are described below where X and Y denote either an atom or a molecule, asterisks indicate that the atoms are in an excited state and M denotes a neutral particle that exchanges energy and momentum, but does not take part in the chemical reaction.

*a. Ion-ion recombination* $X^+ + Y^- \rightarrow X + Y$

*b. Electron-ion recombination*

*1. Three-body* $X^+ + e^- + M \rightarrow X + M$

*2. Radiative* $X^+ + e^- \rightarrow X' \rightarrow X + h\nu$

*3. Dissociative* $XY^+ + e^- \rightarrow X' + Y'$

*c. Ion-atom interchange* $X^+ + YZ \rightarrow XY^+ + Z$

*d. Collisional detachment* $X^- + M \rightarrow X + e^- + M$

*e. Associative and dissociative attachment* $X^- + Y \rightleftarrows XY + e^-$

*f. Photodetachment and radiative attachment* $X^- + h\nu \rightleftarrows X + e^-$

The most significant chemical loss reactions are radiative and dissociative recombination reactions. The radiative recombination reaction is important for the loss of $O^+$, the chief ion in the upper region of the ionosphere. Whereas,

the dissociative recombination is imperative for the loss of $N_2^+$, $NO^+$, and $O_2^+$ ions, which are the crucial ions in the lower regions of the ionosphere.

The chief ion $O^+$ is created through photoionization of the O atom and is lost generally through rearrangement with $N_2$ and $O_2$ and the resulting molecular ions are simply lost through dissociative recombination reaction. Therefore, the strength of the ionosphere depends on the O/ $N_2$ and O/ $O_2$ ratios.

***Stratification of the ionosphere:*** The construction of the ionosphere is not plain everywhere. Due to the presence of different molecules and atoms in the atmosphere and their different rates of absorption, a series of distinct regions or layers of electron density exists. These are denoted as D, E, F1, and F2 and usually are collectively referred to as the bottom side of the ionosphere. The part of the ionosphere between the F2 layer and the upper boundary of the ionosphere is termed as the topside of the ionosphere.

The different regions of the ionosphere can be understood as follows:

### 1.2.1 D Layer

The D layer extends from about 60 to 90 km in height and is present only during day time and affects the radio waves noticeably. The major ion species of the D region are $NO^+$ and $O_2^+$. In addition to that different clusters of positive and negative ions are also observed in the D region. The presence of different categories of positive and negative ions makes the D region the most complex part of the ionosphere from the chemical point of view. In general, the recombination rate of molecular ions is large. On the other hand, the cluster ions possess a much higher recombination rate than the simple molecular ions such as $NO^+$ [5]. Hence, as a result of fast dissociative recombination rate, the plasma density in the D region vanishes after sunset. Only a feeble ionization produced by galactic cosmic rays remains in the D region throughout the night. A peak electron density of the order of $3 \times 10^3$ el/ $cm^3$ occurs at about 80 km by noon. In 70-85 km range, the electrons are chiefly generated by the ionization of traces of NO gas present in the atmosphere by H-Lyman $\alpha$ (a strong spectral line of 1216 $A^o$); Solar X-rays interacting with molecular Oxygen and molecular Nitrogen also contribute to the ionization. Below 70 km corpuscular ionization by Cosmic rays dominates. This layer disappears by the night because the source of ionization is

removed and the electrons get attached to atoms and molecules to form negative ions. However, by the day, due to interaction with solar radiation, the electrons detach themselves from the ions causing the D layer electrons to re-appear [6].

### 1.2.2 E Layer

The E layer above the D layer stretches from about 90 km to 150 km above the ground and is also known as the Kennelly-Heaviside layer after its prediction by A.D Kennelly and Oliver Heaviside independently and simultaneously in 1902. It bears a maximum daytime electron density of $10^5$ el / $cm^3$ at about 115 km, close to noon, and almost disappears at night. The 90-110 km region is mainly ionized by X-rays in the 30-100 Aº range (figure 1.2). Above around 100 km, the ionizing agency is soft X-rays and UV radiation. The small amount of ionization present in this region during nighttime could be due to micro meteoric bombardment. The main ions in this region are $NO^+$, $O_2^+$, $N_2^+$, and $O^+$. Many meteors burn up themselves in the E region after entering the Earth's atmosphere and this results in the deposition of the metallic ions such as $Fe^+$, $Ca^+$, $Si^+$, and $Mg^+$ in this region. The primary loss process of the molecular ions present in the E region is the dissociative recombination, which has a large reaction rate. As a result, the E region plasma recombines fast after sunset and the plasma density reduces drastically from the average daytime value of ~$10^5$ per $cm^3$ to ~$10^3$ per $cm^3$ at night. One of the reasons the E region plasma does not vanish completely after sunset is the metallic ions. The primary loss process of the metallic ions is radiative recombination which has a very slow reaction rate, providing a considerably larger lifetime to these ions. In the region between 100 and 120 km, sometimes the electron densities may exceed even that of F region. This highly conducting irregular E region is termed as the sporadic E because of its sporadic nature of the occurrence. This sporadic E layer is now believed to be associated with the interaction of wind structure with the geomagnetic field lines. Some connection between sporadic E, thunderstorm, and electrojet currents has also been suggested [6].

### 1.2.3 F Layer

The F layer, also known as the Appleton layer is the topmost layer of the ionosphere and is found above 150 km. It coexists with the thermosphere and part of the exosphere. During the day time in the presence of sunlight, F layer is divided into two

layers i.e. F1 and F2 and during night, these F layers merge into a single layer. The dominant ion loss mechanism above the F region peak is the radiative recombination process while below the peak; the charge exchange reaction becomes more dominant. The reaction rates of both of these processes are much smaller in comparison to the molecular ion loss process (i.e. dissociative recombination). Also in the upper F region, the recombination rate becomes lower than the ionization rate as the intensity of radiation increases with the altitude. Hence, there will be a larger ion density at an altitude above F1 region. The F region plasma (mainly $O^+$ and $H^+$) does not decay drastically after the sunset and retains a relatively high density of ~$10^4$ to $10^5$ per $cm^3$ at the night as well. The observed daytime peak plasma density in the F region is about $10^6$ per $cm^3$ at around 350 km altitude and moves slightly upward at night time.

*F1 layer:* The F1 layer is the lower region of the F layer and extends roughly between 150 km and 200 km above the surface of the earth. Here, the maximum electron density observed during day time, at about 180 km is approximately $2\times10^5$ el / $cm^3$. The principal ionizing source is solar UV radiation in the 200-900 Aº range (figure 1.2), which acts basically on atomic oxygen. This region merges with the F2 layer at night.

*F2 layer:* It extends roughly between 200 km and 1000 km and has a daytime maximum of $5\times 10^5$ el/ $cm^3$ at about 250 km. During the nighttime, there is just a single layer having a maximum electron density of $10^5$ el / $cm^3$ in the vicinity of 350 km. The ions present in the region are $O^+$, $He^+$, and $H^+$ of which $O^+$ is the dominant one. Earth's magnetic field plays a dominant role in the complex dynamics of the F region plasma [6].

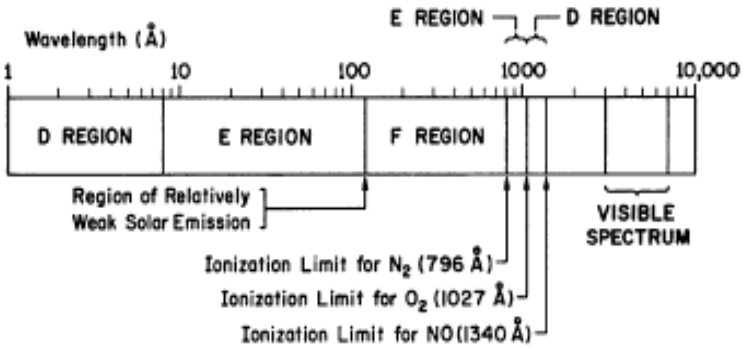


Figure 1.2: The regions of solar spectrum responsible for different regions of the ionosphere. Image credit: Reid, G. C., Ionospheric Effects of Solar Activity

## 1.3 IONOSPHERIC PLASMA PARAMETERS VARIATIONS

The behaviour of the ionosphere is not stable and is subjected to many variations such as the diurnal, annual, latitudinal, and seasonal changes. Due to the different magnetic field geometry with latitudes, the ionosphere shows great spatial variability and due to the variable solar input energy, it shows vast temporal variability too. These variations are systematic and regular and can be predicted in advance with rational precision.

**Temporal Variations:** At sunrise, the production of photoelectrons in the ionosphere starts via the ionization of the neutral particles. When these energetic photoelectrons interact with the ambient electrons, sharing of energy takes place which consequently, increases the electron temperature (Te). This increment in Te is at a faster pace in the early hours of morning time because a few electrons are present at that time. But as the electron concentration increases, sharing of energy to each electron decreases. Eventually, with the progress of the day, a steady-state is acquired with a maximum decrement. A secondary maximum is also observed before sunset. Finally, nighttime stability is attained [7]. The D, E, and F1 layers also vary depending upon the solar activity and the solar zenith angle over the location. The E layer does not completely fade away at night. The F1 layer becomes a separate layer during day time and vanishes after sunset to form a single F-layer located at a higher altitude. The variations in F2-layer are more complex. The foF2 rises rapidly after sunrise due to photoionization, amplifies during the day then decreases at sunset but never vanishes.

The ionosphere exhibits seasonal variations with the solar zenith angle as the relative position of the sun moves from one hemisphere to the other causing different seasons. According to the Chapman ionization theory, Ne should be larger in summers than in equinoxes and smallest during winters. However, previous studies have revealed quite different (anomalous) features in contrast to the prediction of the Chapman ionization theory. It is presented that the F2 layer does not follow this pattern. It is noticed that the daytime values of NmF2 at mid-latitude in the northern hemisphere are much greater in winter than that in summer, but this anomaly disappears at night. This difference is known as the ‘mid-latitude seasonal anomaly’ [8, 9].

Similarly, in the ionosphere, strong annual and semiannual variations occur in daytime Ne, which have a distinct latitudinal and altitudinal dependency. The 'annual anomaly or non-seasonal anomaly' expresses that the NmF2 (in the whole world or in the entire Northern to Southern hemispheres) is greater in December than in June during both day and nighttime. Whereas the semiannual anomaly ('equinoctial asymmetry') describes that the electron density is higher at on equinox than that at the solstice.

**Spatial Variations:** The spatial variations are altitudinal or latitudinal and longitudinal dependent. As in the early morning, the sun is relatively low in the sky, so that radiation must penetrate a large column of air before reaching a given level of the atmosphere. Consequently, the rate of ionization is lower, and the location of ionized layers shifts to higher altitudes. As the day progresses, the D, E, and $F_1$ layers shift in altitude. The layers are at lowest altitude with highest electron densities at noon. In contrast, at night the ionization in the D, E, and $F_1$ regions tends to disappear as electrons and ions recombine to form neutral gases.

The solar zenith is again responsible to cause latitudinal variations in the ionosphere. Different latitudes warm and cool with the seasons as the intensity of sunlight vary from place to place due to the tilt of Earth's axis. As a result, the critical frequencies corresponding to different layers show a substantial variation at low, mid, and high latitudes [10].

## 1.4 EQUATORIAL AND LOW LATITUDE IONOSPHERE

The region under the geographic latitudes $0^o$ to $\leq 20^o$ is known as equatorial and low latitude ionosphere, $20^o$ to $50^o$ region represents mid-latitude ionosphere and beyond $50^o$ region represents polar or high latitude ionosphere. The equatorial and low latitude ionosphere represents considerably different behaviour in comparison to mid and high latitude ionosphere. The main reason behind this is that here Earth's magnetic field lines are almost horizontal, and the Earth's atmosphere is most exposed to Sun's ionizing radiation. And hence, according to Lorentz force, the charged particles move readily along the field lines than perpendicular to it.

### 1.4.1 Features and Dynamics of Equatorial and Low Latitude Region

Due to the unique horizontal orientation of north-south magnetic field lines and east-west electric field perpendicular to it, the equatorial and low latitude ionosphere exhibits some characteristic geophysical phenomena viz. Equatorial Electrojet (EEJ), Equatorial Ionisation Anomaly (EIA), Pre-Reversal Enhancement (PRE), etc. [11,12].

#### a) Equatorial Ionization Anomaly (EIA)

EIA is one of the peculiar geophysical features present over the equatorial and low latitude ionosphere. Near the geomagnetic equator, the zonal electric field generated by the global E-region wind dynamo, together with horizontal magnetic field causes a vertical plasma drift at F-region altitudes. This vertical plasma drift rises upward during the daytime. But under the influence of strong meridional pressure gradient (poleward winds) and gravitational force, this risen accumulated plasma starts diffusing along the geomagnetic field lines to regions away from the dip equator. This process is known as plasma fountain which produces a double-humped structure with two plasma density crests at around 15º-20º on either side of the dip equator (in both hemispheres) and a plasma density trough centered right on the dip equator. This particular rearrangement of plasma density is referred to as EIA (figure 1.3). Post sunset, the plasma drift is downward and the plasma density starts drifting from EIA crest region to the dip equator. This equatorward movement of the plasma density which is opposite to the daytime behaviour is known as reverse fountain [1, 6].

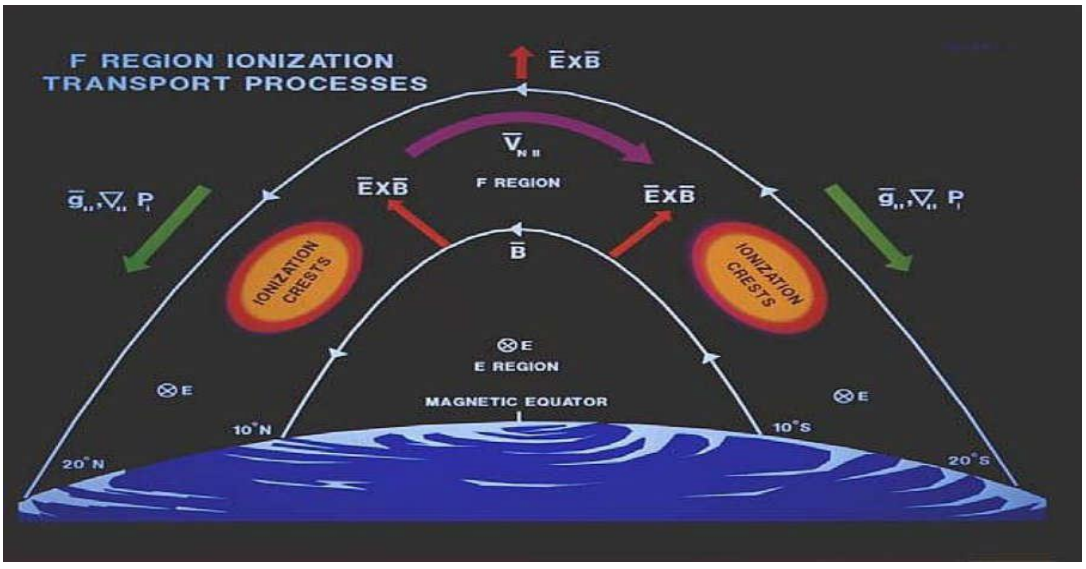


Figure 1.3: Schematic representation of equatorial anomaly or the Appleton anomaly, image credit: AFRL, USA.

**b) Pre Reversal Enhancement (PRE)**

During nighttime, the electric fields are westward and cause a downward E x B plasma drift. However, near sunset, the eastward electric field usually shows a significant and fairly sharp enhancement, just before the eastward daytime field reverses to the westward direction. This enhancement in the eastward electric field during near-sunset hours, just before switching its direction is called the Pre-Reversal Enhancement (PRE) [13, 14]. Any alteration in the east-west electric field is reflected in the plasma drift driven by E×B mechanism. So, the enhancement in electric field results in a height increase of the F-layer in the equatorial ionosphere, before electric field reverses [15]. The PRE is observed depending upon various factors viz. the phase of the solar cycle, the season, and the level of magnetic activity [16].

**c) Equatorial Spread F (ESF)**

ESF is referred to an ionospheric irregularity occurring mainly near the equatorial and low latitude regions. It is a nighttime phenomenon, which displays large-scale electron density depletions (plasma bubbles) and can be observed in ionograms as a spread of the regular ionogram traces [17]. ESF is stated by various names depending on its nature of appearance in different instruments. In Radar measurements, ESF becomes visible as towering structures of irregularities and is generally called as plumes. In the context of in-situ satellite measurements, it is known as bite-outs when ESF appears as steep reductions of the background plasma density. In the GPS satellite studies, ESF is mentioned as scintillation. This equatorial F-layer irregularity is also referred to as a plasma bubble when a strong depletion of background emission intensity is observed in airglow measurements [6, 18].

**d) Equatorial Electro Jet (EEJ)**

EEJ is an intense eastward electric current flowing in a narrow latitudinal band of ±3° (i.e. ±300 km) over the dip equator at an altitude around 105 km (figure 1.4). This ionospheric current chiefly generated in the E-region is a consequence of the dynamo action of the neutral wind system. The electrojet current flows eastward during daytime and westward during nighttime, but the strength of the nighttime current is very weak compared to daytime because of the reduction in the electron density during the night due to recombination [19].

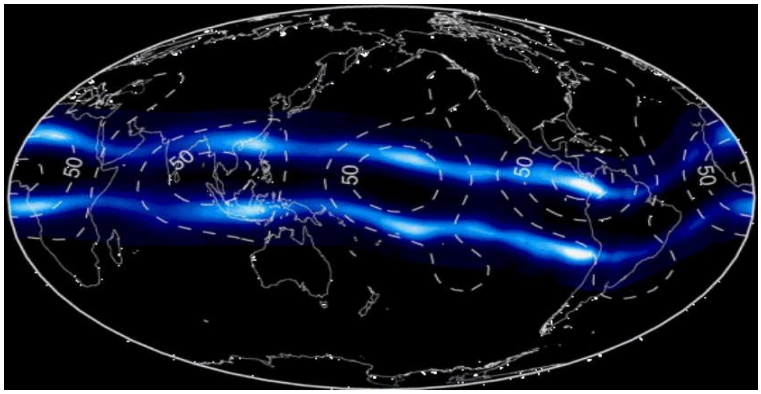


Figure 1.4: Location of the Equatorial Electrojets in the ionosphere (image credit: http:// www.ice-ageahead-iaa.ca)

**e) Equatorial temperature and wind anomaly (ETWA)**

The Equatorial temperature and wind anomaly (ETWA) being a similar kind of phenomenon to the EIA is a prominent feature in the mid, low-latitude nighttime ionosphere/thermosphere. An ETWA in the upper thermosphere, characterized by the formation of two crests of enhanced neutral temperature on either side of a prominent trough at the magnetic equator has been reported [20]. The zonal wind reaches a maximum near the equator with two minima on either side of it. The zonal wind's maximum, temperature's trough, and the trough of the EIA are collocated. The two crests in temperature and the two minima in the zonal wind are collocated at the crests of EIA. However, the ETWA occurs at latitudes slightly poleward from the EIA. The configuration develops vertical wind that triggers the spread-F.

Recent studies have revealed that neither heat transport due to zonal winds nor chemical heating can explain the formation of the ETWA crests. However, it is observed that plasma-neutral collisional heating and the field-aligned ion drag are the major contributors in producing the ETWA crest and trough respectively [21, 22].

## 1.5 SOLAR ACTIVITIES

The sun, a hot gaseous ball contains its own atmosphere within which some natural phenomena take place periodically and non-periodically. Those phenomena are called solar activities. These activities are in the form of solar wind, solar flux, solar flares, and sunspots, etc. Many solar phenomena show a periodic variation over an average interval of around 11years, known as solar cycle.

### 1.5.1 Solar Cycle

The sun has its powerful magnetic field because of the presence of electrically-charged hot gases. The magnetic field of the sun and the resulting solar activities get rise and fall within an average 11-year time span. This regular variation of solar activities or its magnetic field is known as the solar cycle. In every 11 years, the sun's magnetic field turns over i.e. the north-south poles of the sun change places, and then in the next 11 years, the poles flip back again. So, in the context of the magnetic field, the solar cycle is half completed in 11 years.

Each cycle is defined as starting with a solar minimum and lasting until the following solar minimum. A classic solar cycle takes four years to rise from solar minimum to solar maximum, and then approximately seven years to fall back to solar minimum. The solar cycle is measured in terms of sunspot numbers. Although the number of sunspots may vary from cycle to cycle in general, the highest numbers of sunspots denote the high activity period of the sun (solar maximum) and lowest sunspot numbers denote least activity period (solar minimum). Increased solar activity results in enhanced extreme ultraviolet radiations and X-ray emissions which produce effects in Earth's upper atmosphere. As a consequence, atmospheric heating increases both the temperature and density of the atmosphere at higher altitudes.

### 1.5.2 Sunspots

Sunspots are dark regions on the sun's visible surface (the photosphere) and are located within 35º solar latitudes on either side of the sun's equator. Sunspots appear dark because they are only 10 to 20 percent as bright as the surrounding photosphere. The temperature of the gases in sunspots is about 4000º -5000º K whereas the temperature of the normal photosphere is about 6000º K. Sunspots are cooler regions because of the existence of strong magnetic fields of magnitude about 3000 G which is believed to be thousand times stronger than the average magnetic field of the normal photosphere. A sunspot can last from a few hours to several weeks or months depending upon its size. Although recurrent individual sunspots can be observed very often, generally they occur in groups and are huge (around the size of the earth) and complex. The number of sunspots and their location fluctuates with the solar cycle and solar rotation. The regions where sunspots occur are called the active regions and

are mostly bipolar with two main spots and surrounding spots. The main westward spot is called a leading spot and the main eastward spot is called a follower spot. These active regions having enormous energy are believed to be responsible for other solar events like solar flare and coronal mass ejection etc. [23].

### 1.5.3 Solar Flare

A solar flare is a sudden, rapid and intense flash of increased brightness from active regions over the surface of the sun (figure 1.5). It occurs due to the formation of a large amount of magnetic energy in the solar atmosphere. Solar flares release many millions of energy in just a few minutes and emit radiations at all wavelengths of the electromagnetic spectrum, ranging from radio waves to gamma rays. The frequency of occurrence of solar flares coincides with the solar cycle ones. So, when there is solar minimum, active regions are small and rare and few solar flares are spotted. The number of flares increases as the sun approaches its solar maximum. The solar flares are classified as A, B, C, M, or X (in watts per square metre, $W/m^2$) based upon the peak flux of 1 to 8 Angstroms X-rays near Earth, as measured by the GOES satellite (table 1.1). Each X-ray class category is divided into a logarithmic scale from 1 to 9. For example B1 to B9, C1 to C9, etc. so an X2 flare is two times as powerful as an X1 flare and is four times more powerful than an M5 flare. The X-class category is slightly different and does not at X9 but continues on. Solar flares of X10 or stronger are sometimes also called ‘Super X-class solar flares.

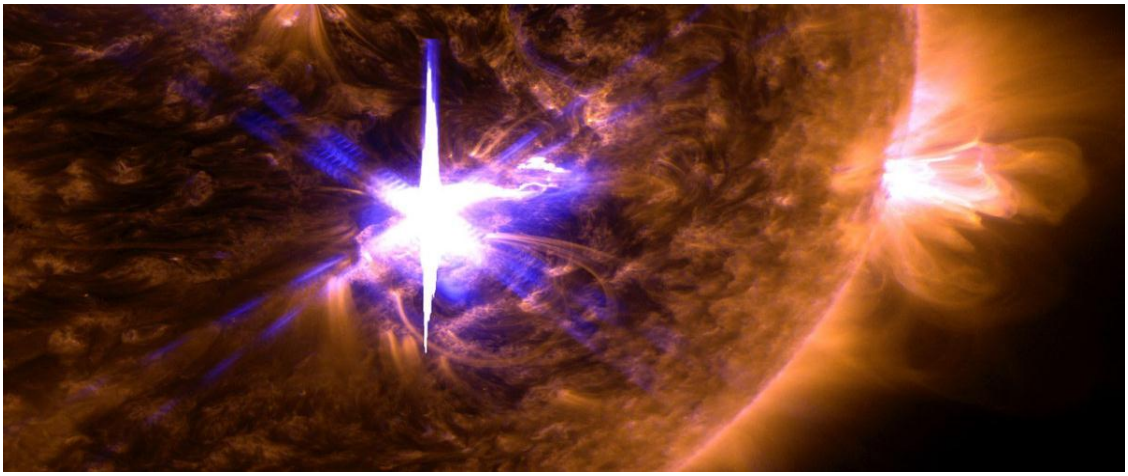

Figure 1.5: Solar flare, Image courtesy: NASA/GSFC/SDO

Table 1.1: Categories of Solar Flares

| **Class** | **Peak Flux Range ($W/m^2$ between 1-8 Angstroms)** |
|---|---|
| A | $A < 10^{-7}$ |
| B | $10^{-7} - 10^{-6}$ |
| C | $10^{-6} - 10^{-5}$ |
| M | $10^{-5} - 10^{-4}$ |
| X | $> 10^{-4}$ |

### 1.5.4 Solar Wind

The solar wind is the continuous flow of charged particles (ions, electrons, and neutrons) that scatter out from the sun in all directions. The source of the solar wind is the sun's outer atmosphere, corona from where wind spreads out in all directions at a speed range of about 300-400 km/s and may achieve a maximum speed up to about 900 km/s. It varies in density, temperature, and speed with time and solar longitude. Solar winds containing high-energy particles carry a large amount of kinetic and electrical energy. This energy enters into Earth's magnetosphere and triggers magnetic storms which can disrupt communications and navigational equipment, damage satellites, and even cause blackouts [23, 24].

### 1.5.5 Solar Flux

Solar radio flux at 10.7 cm (2800MHZ), an excellent indicator of solar activity is one of the longest-running records of solar activity which can be measured accurately from the ground in all weather conditions. The sun emits radio energy with a slowly varying concentration. It is generally mentioned as F10.7 index and expressed in solar flux units (sfu), where 1 sfu = $10^{-22}Wm^{-2}Hz^{-1}$. The F10.7 radio emissions originating from the chromospheres and corona follow the solar cycle and correlates well with the sunspot number and extreme ultraviolet radiations [23, 25].

### 1.5.6 Coronal Mass Ejection (CME)

A coronal mass ejection is a significant release of plasma and accompanying magnetic field that is blown away from the Sun's corona (Figure 1.6). In other words, the sun very often burps, with the power of 20 million nuclear bombs. These hiccups are known as *coronal mass ejections* or CME. A CME travels outward from the Sun at speed ranging from slower than 250 km/s to as fast as near 3000 km/s. A CME is observed rare, like one coronal mass ejection every week when the Sun is in solar minimum phase. Whereas, when the Sun's activity increases during solar maximum, multiple coronal mass ejections can be observed every day. Generally, a coronal mass ejection erupts out along with other solar events like solar flares and filament eruptions. However, not every event is associated with a coronal mass ejection and a CME can also occur in the absence of either of these events.

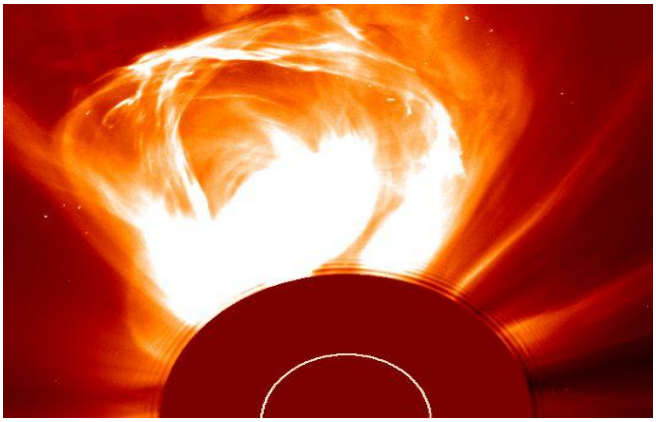

Figure 1.6: Coronal mass ejection of February 27, 2000. A disk is being used to block out the light of the sun. The white circle indicates the sun's surface. Image: NASA's Solar and Heliospheric Observatory (SOHO).

The Earth-directed CMEs are very important because these are the prime source of producing strong geomagnetic storms which can affect the earth's magnetosphere and ionosphere. Therefore it is very essential to keep an eye on a CME.

## 1.6 SOLAR ACTIVITY INFLUENCE ON IONOSPHERE

Solar activity refers to firstly, the intensity of electromagnetic radiations, particularly of X-rays and extreme ultraviolet rays (EUV), and secondly to the events like CMEs, solar wind, and solar flares, etc. Variations in solar activity are the chief source of influencing and controlling the ionosphere. The effect of EUV and X rays on the ionosphere is already studied in detail under ionospheric temporal and spatial

variations. The effect of other solar events is discussed here. The solar wind and the interplanetary magnetic field interacting with the earth's magnetic field, strongly drive the earth's magnetosphere. The solar wind particles trapped in the magnetosphere gyrate along the magnetic field lines; result in a drift across the magnetic field lines depending upon the polarity of the charge (electrons drifting to east and protons to the west) and thus causes a belt-like configuration or a ring current around the globe known as Van Allen Belt.

The dynamics of the ionosphere also get affected by the solar flares. The solar flares depending upon their type (C, M, and X) cause sudden ionospheric disturbances (SIDs) such as electron density enhancement in the D region, short wave fadeouts, frequency anomalies, and a sudden increase in total electron content [26].

When the Earth's magnetic field is severely disturbed, a "magnetic storm" is said to occur in the near-Earth environment in response to solar activity. The Earth's magnetic field gets disturbed by the solar phenomena like solar flares, high-speed solar wind streams, and coronal mass ejections which results in geomagnetic field disturbances and causing geomagnetic storms. A large amount of energy is transmitted from the solar wind to the Earth's magnetosphere. This energy transfer between solar wind and the magnetosphere is most effective when the solar wind speed is high (~ > 400 km/s) and the interplanetary magnetic field (IMF Bz) is heading towards southward at the dayside magnetosphere for an extended time (~2-3 hr) and is of noticeably large magnitude (IMF Bz ~ < -5 nT). This southward IMF Bz opens up a path for efficient energy transfer through the process of magnetic reconnection. The largest storms result when the energy transfer is associated with the coronal mass ejections (CMEs). And another solar wind disturbance that causes storms is co-rotating interaction regions (CIRs). When a high-speed solar wind stream interacts with the slower-moving solar wind in front of it, a CIR generates. CIRs can deposit more energy in the magnetosphere over a longer interval [27, 28].

The storms can be categorized depending upon their Dst values. A storm is said to be weak if Dst ≤ -30 nT, moderate for Dst ≤ -50 nT, strong for Dst ≤ - 100 nT, severe for Dst ≤ -200 nT, and great magnetic storm if Dst ≤ -350 nT [29].

The storms can be explained with three different phases based upon the Dst values, as described below.

*Storm Sudden Commencement (SSC)*–when a solar wind encounters the magnetopause, geomagnetic field lines surrounding the Earth are compressed due to which pressure in the magnetosphere raises. As a result of this impact, the enhanced magnetospheric current induces an additional field to the existing terrestrial magnetic field. This induced magnetic field brings a boost in the horizontal (H) component of the earth's magnetic field in the low to mid-latitude region. This phenomenon of swift positive increase in the H component is known as storm sudden commencement. The rise time due to SSC is generally in the range of a few minutes. However, each storm is not accompanied by an SSC.

*Initial Phase (IP)*– Initial phase is the period over which the magnitude of the H component of the earth's magnetic field remains above its pre-storm value and can last from minutes to hours. This phase results due to the continuous pressure applied by the solar wind on the magnetopause and compressing it inward. This phase also is not common to all storms.

*Main Phase (MP)*– The main phase or the growth phase is the most remarkable phase of any storm. Initiation of the main phase is generally termed as storm onset (SO). It is marked by a decrease of the H component of the earth's magnetic field below its pre-storm value and shows major fluctuations for a longer time, and with larger amplitude than the initial phase. This decrease in the H component is caused by the westward flow of magnetospheric ring current during the storm. A measure of this magnetospheric ring current is termed as disturbance storm time (Dst) index and is generally used to characterize the strength of a storm. A minimum Dst index of -50 to -100 nT is generally observed during a storm though during a very severe storm this value could be of the order of 100s nT and even more [30]. The main phase of the storm generally lasts for 12-24 hr.

*Recovery Phase (RP)*– This is the last phase of a storm. The start of this phase generally coincides with the northward turning of IMF Bz. The ring current starts decaying in strength during this stage and as a result of which H component of the earth's magnetic field gradually returns to its pre-storm value. In a recovery phase, the

storm spends its greatest time (one day to several days) in gradually returning to an undisturbed level.

However, it is found that SSC and initial phases are not necessary features of a geomagnetic storm. The only essential feature characterizing a magnetic storm is the significant development of the ring current and its subsequent decay [31].

Geomagnetic storms that commence with a sudden increase at the start of the initial phase are typical of storms produced by a solar flare. These storms arise as a result of the shock front from the solar flare hitting the Earth's geomagnetic field and suddenly compressing it. Storms with gradual commencement are produced by high-speed solar wind streams. They start gradually as the high-speed solar wind stream overtakes the Earth, and tend to reoccur every 27 days or so, following the Sun's rotation[32,33,34].

## 1.7 MOTIVATION

The ionosphere is one of the important layers of our Earth's atmosphere. The ionosphere contains a sufficient number of free electrons and ions due to which it behaves as a reflecting layer and makes it possible to communicate and navigate the signals through Earth. Several communication operational systems and scientific organizations rely upon the behaviour of the ionosphere. The larger the irregular behaviour of ionosphere larger is the degradation in radio signals. Hence, this technology-based era forces us to study the variability in the ionosphere.

The predominant factor to drive the ionosphere is the Sun or solar radiation flux. The formation and dynamics of the ionosphere are related to solar activities. Extensive work has been done to relate the ionosphere with solar activities. But still one can find work to be performed to study the relationship between solar parameters and ionospheric parameters.

This solar activity-based ionospheric study becomes more significant over the low latitudes. The low latitudinal regions are different from mid and high latitudes because of some unique phenomena occurring there. Hence the study of the ionosphere over the low latitudes becomes very essential.

The Indian subcontinent also falls under the low latitudes. Studies related to variability in ionospheric parameters over the Indian subcontinent region still lack, hence it attracts one to do an intensive study on this region which will be beneficial to have complete knowledge about the atmosphere/climatology of this region.

Based upon the earlier researches it is found that sufficient theories and observations are available for total electron content TEC and electron density but lacks for ion densities and ion temperature. So, the present study has been done to analyze the variations in total ion density (Ni) and ion temperature (Ti), in the topside ionosphere of low latitudes with different phases of solar activity (1999-2003).

There exist, different empirical models, to estimate the behaviour of the ionosphere. One of them is the International Reference Ionosphere (IRI) model. The IRI model is continuously used in various research areas of the magnetosphere and ionosphere and is being progressively improved [32]. The model's estimated values depend upon the data collected from other sources due to which they sometimes lack in finding appropriate estimations. Hence, it gives us an idea to do more comparative studies to facilitate the IRI developers, researchers, and scientists with better findings or results.

## 1.8 RESEARCH OBJECTIVES

The main objectives of the research are:

i. To study the variations in ionospheric plasma density and temperature with respect to time, season, and location:

   The annual diurnal variation in total ion density ($N_i$) and ion temperature ($T_i$) has been studied by using ROCSAT-1 and SROSS-C2 satellite data.

ii. To study the equinoctial variations of plasma density and temperature:

   Asymmetric behaviour of ion density and ion temperature is observed during moderate to high solar activity years.

iii. To analyze and compare the results of satellite data with IRI models:

   The behaviour of $N_i$ and $T_i$ observed by ROCSAT-1 and SROSS-C2 satellite data measurements have been compared with the estimated data of IRI-2012

and 2016 model and some significant discrepancies have been observed in the modelled data.

iv. To study the variations in ionospheric parameters ($N_i$ and $T_i$) with changing solar activity or solar flux (F10.7):

The linear or non-linear dependency of $N_i$ and $T_i$ with F10.7 has been observed during low and high solar activity years.

v. To study geomagnetic storms (occurred due to solar flares, coronal mass ejections, interplanetary magnetic fields, etc.) over low latitudinal regions:

The effect of two geomagnetic storms on ionospheric ion density ($O^+$ and $H^+$) and ion temperature ($T_i$) has been studied over the low latitude Indian region.

## 1.9 ORGANISATION OF THESIS

The present study deals mainly with the variations in the ionospheric plasma due to solar activities. The behaviour of the ionosphere or ionospheric parameters is analyzed during different solar activity years by several datasets and the results have been compared with the IRI models too.

The entire research work has been organized into seven chapters. The content of each chapter is outlined below.

**Chapter 1** starts with brief information about Earth's atmosphere, ionosphere, its formation, and stratification (D, E, and F layers). The ionosphere undergoes through regular and irregular variations. The regular variations which are very systematic can be further categorized on a temporal and spatial basis. Temporal variations include changes in the ionosphere on a time scale for example- diurnal, seasonal, annual, solar cycle variations (11 year and 27-day sunspot cycle). Spatially ionosphere varies with altitude, latitudes, and longitudes. The irregular variations are sporadic E and sudden ionospheric disturbances (SID). All these variations are briefed here.

The equatorial and low latitudes are the most interesting and important regions as compared to mid and high latitudes. The unique features (plasma fountain, EIA, EEJ, ESF, ETWA) exhibited by equatorial and low latitudes and the dynamics of this region are also discussed here. As the Sun is the predominant factor in the formation

of the ionosphere hence a light has been put on the solar activities (Solar cycle, Sunspots, Solar flare, Solar wind, Solar flux, and Coronal mass ejections). Due to the effect of these solar phenomena, the Earth's magnetic field is disturbed and a geomagnetic storm is produced. This has been discussed here with detailed information about the geomagnetic indices -Kp, Ap, Dst, and IMF. In addition to the solar activity effects on the ionosphere, the effects of other factors as earthquakes and tsunamis have also been briefed here. The chapter ends with the motivation behind the research work, objectives of the proposed work, and the organization of the thesis.

**Chapter 2** describes the literature review. It covers the reviewed study for low latitude ionosphere (specifically over the Indian region), factors affecting the ionospheric plasma density and temperature, IRI models, and the Geomagnetic storms. This chapter reveals the extent of work done by other researchers in the same field.

**Chapter 3** is based upon the methodology adopted for the present study. It explains the data selection methods, measurements, and analysis. The data was collected from SROSS-C2 and ROCSAT-1 satellites. So the information about the data retrieval method, the payloads mounted on these satellites, the mission of the satellites, and derivation of ion density and ion temperature, are discussed in detail here. The other supporting data as IRI model data Seismic activity data, Dst data, IMF Bz data, etc. have also been dealt with within.

**Chapter 4** explains the variations in ionospheric ion density and temperature at low latitudes during the low solar activity (LSA-1995) and high solar activity (HSA-2000) years. The total ion density (Ni) and ion temperature (Ti) data are obtained from SROSS-C2 satellite and IRI-2012 model. The results obtained from satellite measurements are compared with results obtained from modelled values. The relative variations of Ni and Ti for both measured and estimated values are discussed and the linear or non-linear relationship of Ni with Ti is also discussed here for the years 1995 and 2000.

**Chapter 5** explains the variations in ion density and temperature at low latitudes during the rising, high, and declining phase of solar activity years (1999-2003). The data for ion density and ion temperature is collected from ROCSAT-1 satellite

measurements and estimations from IRI-2016 model. A comparative study is done for the results obtained by both measured and modelled values. Relative variation $Ni_{(ROCSAT)}$ / $Ni_{(IRI)}$ and $Ti_{(ROCSAT)}$ / $Ti_{(IRI)}$ is calculated. Correlation coefficients are observed for hourly averaged Ni in the day time (10-16 LT), measured by ROCSAT-1 and IRI-2016. Similar correlation coefficients are observed for $T_i$. The relationship between ion density and temperature with solar flux index (F10.7) is also analyzed during the years 1999-2003.

**Chapter 6** explains the response of low latitude ionosphere to weak and moderate magnitude geomagnetic storms. Two geomagnetic storms are selected for the present study, occurred on 30 July 1999 and on 13 November 1999. Anomalous variations in $O^+$, $H^+$ density, and ion temperature during storm events are observed and compared during normal and quiet days. Further a comparative analysis is also carried out with the IRI-2016 model.

**Chapter 7** outlines the conclusion of the present study. It deals with all the results and discussions drawn through the study. The scope of future work is also discussed here.

# CHAPTER 2

# LITERATURE REVIEW

## STUDIES ON IONOSPHERIC PLASMA

The ionosphere being a very dynamic and complex region of the atmosphere is very sensitive to the phenomena occurring below and above it. Its parameters vary spontaneously in response to solar flares, CMEs, geomagnetic storms, earthquakes, thunderstorms and lightning/sprites, etc. [35-38]. An extensive study has been done on variations in Earth's ionospheric parameters through ground-based and in-situ observations [39-41] and theoretical calculations [42-45]. Empirical models have also been presented to show variations in plasma density and temperature variations [46-48].

## 2.1 IONOSPHERIC PARAMETERS VARIATIONS

Previous studies based upon various techniques, methods, or missions have proved that ionospheric plasma density and temperatures vary with latitude, longitude, local time, season, altitude, and solar activity which are found relatively significant over equatorial and low latitude regions [49-51].

It is well known that the electron temperature varies with local time (diurnal) and is characterized by morning peak and evening peaks [52-54]. This morning peak is prominent over the low latitudes due to the vertical E x B drift which increases the morning Te and decreases the daytime Te [50, 55]. The topside radar data at Jicamarca was compared with other conventional data during solar minimum and was found an increase in electron to ion temperature ratio at pre-sunrise hours with a diurnal minimum of plasma temperature at afternoon [56]. Whereas Alexander et al. 2004 employed SROSS-C2 satellite data to make a comparison of electron and ion temperatures at the low-latitude upper ionosphere. In their results, they concluded that the nighttime mean values of Te and Ti increased with solar activity indicated by the solar radio flux. While the daytime mean values of Te decrease with solar activity and the daytime mean value of Ti do not exhibit the solar cycle evolution.

From Hinotori satellite measurements, Oyama et al. [1997] reported high $T_e$ during evening-night time hours over the equatorial region. In the plasma temperature, an anomaly was noticed during the evening-midnight hours while studying low-latitude ionosphere under equinoctial conditions at low, medium, and high solar activity by using the Sheffield University Plasmasphere Ionosphere Model (SUPIM) and Hinotori satellite observations [57]. In the context of seasonal variations, it is observed that during summer solstice $T_e$ shows a higher morning peak than winters morning peak whereas in nighttime $T_e$ is found independent of season and solar activity. The ion temperature, Ti is noticed to follow solar flux during summer and winter solstice but is independent for equinox [58].

At low latitudes, the relation between electron-ion-neutral temperatures and their ratio comparisons has also been studied by [59].

The ionospheric temporal variations have also been studied by analyzing measurements from incoherent scatter radar and ionosonde over Millstone Hill [60]. They found increment in the peak parameters (NmF2 and hmF2) of the F2 layer with daily F10.7 index and saturate (or increase with a much lower rate) for large F10.7.

The ion densities also represent a distinct behaviour over equatorial and low latitude regions. $O^+$ ions produced during the daytime diffuses to the topside ionosphere, thereby increases the expected $O^+$ - $H^+$ transition height. The zonal and meridional components of neutral winds play a significant role in increasing or decreasing the $O^+$ - $H^+$ transition height [61]. Using satellite measurement from AE-C, OGO-6 and IK-24 effect of solar activity on topside ion density on a global scale for a period from 1960's to1990's has been explained [62]. Effect of high and low solar activity on ion composition over Indian region using SROSS-C2 measurements have been also studied [63]

It has been revealed [64] in previous studies that at an altitude of about 500 km $O^+$ and $H^+$ ion densities own opposite diurnal behavior i.e. during daytime $O^+$ ion density is higher in magnitude whereas $H^+$ ion density is higher during nighttime. Similarly, $O^+$ ion density is observed minimum during pre-sunrise whereas, $H^+$ ion density is noticed minimum during the day time.

In general Ne and Te over equatorial and low latitudes region are found to be inversely correlated during daytime and for the low solar activity phases and almost independent for the nighttime [65]. In the studies on the global and seasonal variations in the topside ionosphere, by using DEMETER satellite measurements between 2006 and 2009, [66] revealed a strong negative correlation between Ne and Te in the low and mid-latitude regions in the daytime. This negative correlation arises because local electron heating by photoelectrons was balanced by collisions between electrons and ions. However, in certain conditions, a positive correlation has also been reported. For example, the observations made by the incoherent scatter radar at Millstone Hill from 1976 to 2001 provided a positive correlation between Ne and Te during all the local times in July in the $F_2$ region [67]. Similarly, a positive correlation between Ne and Te in summer during the low solar activity phase has been observed by [68] by using satellite measurements and the field line interhemispheric plasma model. Whereas [69] found a negative correlation between Ni and Ti during the solar minimum phase. The main cause for positive correlations is the increase of heating more rapidly than the electron density which allows heating to dominate the energy balance [70]. However, the physical mechanism for this positive correlation has not yet been completely understood.

Numerous studies have been executed to compare the measured values of the ionospheric parameters with the results of empirical (Bent Ionospheric model, Klobuchar model, NeQuick model, IRI model, etc.) and theoretical models (SAMI2 model, SUPIM model, etc.) [71-78]. Since the IRI modelled values are predicted or estimated values depending upon other data sources, consequently, some discrepancies arise. For example, [79] compared the ionospheric parameters Te, Ti, and Ni measured by utilizing SROSS-C2 satellite observations with the estimated values of IRI-2007 and IRI-2012 models during the low and high solar activity years. They found that the modelled Te (by IRI-2007) agrees throughout the day during high solar activity whereas for the low solar activity it is overestimated in nighttime and underestimated during morning and noontime over the low latitude region. The IRI estimated Ti during high solar activity is in agreement during the daytime whereas during low solar activity it is higher in nighttime and lower in morning hours. On the other hand, the estimated Ni is in accordance with the measured Ni over both the equatorial and low latitudes.

[80] also evaluated the performance of IRI-2016 model over the east African sector of the equatorial ionosphere during different geomagnetic conditions and time scales. And observed that IRI-2016 model does not respond to geomagnetic storms in the East African equatorial region.

[78] proposed depletion of electron density at geomagnetic equatorial latitudes in the altitude range of 1500-2500 km with the help of SAMI2 model which is a low latitude ionospheric model developed at Naval Research Laboratory. [76] also utilized the SAMI2 model to retrieve $H^+$ and $O^+$ ion temperature and verified dependence of ion temperature upon ion composition. Their study showed that in the topside at middle latitudes when a single ion is dominant, $O^+$ or $H^+$ is heated by electron collisions and cooled by conduction as expected. However, in the intervening altitude region where both $O^+$ and $H^+$ are present, $O^+$ is heated by collisions with $H^+$ and cooled by conduction, while $H^+$ is heated by collisions with electrons and cooled by collisions with $O^+$.

## 2.2 GEOMAGNETIC STORM STUDIES

The Earth's outer space of atmosphere known as the magnetosphere is a highly dynamic structure that responds dramatically to solar activities. When an enormous amount of solar energy exchange takes place at the magnetosphere, the geomagnetic field gets disturbed which persists for a long interval of time and consequently, a geomagnetic storm is said to occur. Geomagnetic storm brings intense variations in the magnetosphere, radiation belts, and in the ionosphere. They generate perturbations in neutral composition, enhanced electric fields, currents, and can produce heating in the ionosphere-thermosphere system [81-86].

The two major sources of storm time disturbance in low latitude ionosphere are namely (1) prompt penetration of electric field (PPEF) originated from magnetosphere [87, 88]. (2) The ionospheric disturbance dynamo electric field (DDEF) generated from storm time neutral winds [89-91]. The PPEF is an immediate response to geomagnetic storms because as soon as the geomagnetic storm is initiated on account of the southward ward turning interplanetary magnetic field, the expansion of convection currents in the high latitude ionosphere takes place rapidly. This expansion is so fast that it cannot resist more there and hence penetrates promptly into the low

latitude ionosphere which results in the dawn-dusk electric field into the low latitude ionosphere [92].

The DDEF resulting from the enhanced energy deposition into the high latitude ionosphere comparatively varies slowly with respect to PPEF. During geomagnetic storms, the meridional winds are reinforced to generate equatorward winds towards the low latitude which alters the motion of electrons and ions along the magnetic field lines and hence varies low latitude F region electron density peak height [91, 93, 94].

During the geomagnetic storms energy transfers to high latitude regions, in excess, in the form of particle precipitation and joule heating which results in the expansion of air and increment in the molecular to the atomic ratio in F2 region. The storm triggers the wind circulation towards the low latitude regions where it undergoes adiabatic compression and hence rises the temperature of low latitude regions [95].

Several researchers have studied the geomagnetic storm effects on ionospheric parameters and have validated the variations in electron density, total electron content (TEC), peak electron density (NmF2), peak height (hmF2), etc. over low latitude F2 regions. For instance, [96, 97] investigated the effect of geomagnetic storms on TEC and observed significant variations in TEC over Indian low latitude and EIA region. Chakraborty et al. [2015] analyzed the effect of two geomagnetic storms (24$^{th}$ April and 15$^{th}$ July 2012) over the Indian low latitude and EIA region by using (GPS-TEC) data. They noticed depressions and enhancements in vertical total electron content (VTEC) during the geomagnetic storms in comparison to normal days. They inferred that during both the storms the perturbed VTEC was caused due to PPEF, DDEF, and thermospheric composition changes. Bagiya et al. (2009) explained the TEC variation by utilizing GPS dual-frequency measurements at Rajkot, during the geomagnetic storm on 24$^{th}$ August 2005. They observed enhanced TEC on the storm day while a little diminished TEC on the next day of the storm. The response of the low latitude ionosphere over the Indian EIA crest region has also been analyzed by using GPS data, during the moderate geomagnetic storm of 7-8$^{th}$ May 2005 [98]. They found an increment in TEC during the storm and a decrement during the recovery phase of the storm. A longitudinal study of the ionospheric response to the geomagnetic storm of 15$^{th}$ May 2005 was performed by [99] utilizing the TEC data, collected from three different GPS stations situated near the northern crest of EIA region. They explained

the simultaneous existence of maximum southward interplanetary magnetic field Bz and eastward Interplanetary electric field which as a consequence resulted in a peak in TEC. They attributed the large enhancement in TEC and [O/N2] ratio to the travelling atmospheric disturbances (TADs). All the cases (weak, Moderate, and intense) of geomagnetic storms over low latitude ionosphere in association with the interplanetary magnetic field were analyzed by [100]. They reported a long duration enhancement of ionospheric electric field (measured by Jicamarca and Millstone incoherent scatter radar) during the main phase of a geomagnetic storm, as a consequence of the penetration of interplanetary electric field.

## 2.3 EFFECTS OF OTHER PHENOMENA ON IONOSPHERE

### 2.3.1 Tsunami and Seismic Activity Effects

Earthquakes and Tsumami are natural disasters that cause devastation in the affected regions. During an Earthquake when the ground shakes, it causes tiny atmospheric waves that can propagate right up to the ionosphere. These atmospheric waves reach the ionosphere in 10 min or so and cause notable variations of electron density in F - layer occupying the area over the epicentre with a diameter of more than 1000 km [101-104]. These changes can be recorded and measured when signals from global navigation satellite systems (GNSS) or GPS, travel through the ionosphere.

The same satellites can also detect disturbances in the ionosphere caused by tsunamis. When a tsunami forms and moves across the ocean, the crests, and troughs of its waves compress and extend the air above them, creating motions in the atmosphere known as gravity waves. These undulations of gravity waves are amplified as they travel upward into an atmosphere that becomes thinner with altitude. These gravity waves propagating up to the ionosphere and generating disturbed electron densities in the E and F regions also can be detected using the GNSS satellites circling Earth [105, 106].

During the occurrence of these kinds of activities, not only the electron density but also the temperature, height scale, ion compositions are observed to show variations [107, 108].

### 2.3.2 Thunderstorm and Lightning Effects

A thunderstorm is basically an electrical storm described by lightning and thunder. Thunderstorms also known as electric generators, taking place generally in the lower atmosphere, produce ionospheric disturbances through the effect of the electric field associated with lightning. Actually, in a convective cloud, on account of electric breakdown, division of charge takes place with a negative charge at the bottom of the cloud and a positive charge at the cloud's top and thus creates a high electric field. The thunder cloud induces a positive charge along the ground which concentrates and rises up to a tall object. The negative charge channelling down (known as stepped leader) from the cloud connects with the positive charge over the ground which also reaches out through its own channel, "streamer". On the connection of these channels the electron transfer results in lightning. The first stroke, which carries the largest current (approximately 30000 A) is followed by subsequent strokes within a few milliseconds. The lightning flash results in the increased temperature of air through which it passes, to more than 30000 K in fractions of a second. This extremely hot air expands so rapidly that it explodes with a great sound wave which we hear as thunder. Thunder is generally heard within 25 km from lightning discharge [23].

**Transient Luminous Events:** These are short-lived optical phenomena that occur above the lightning or thunderclouds. Some of them proliferate upward towards the ionosphere, above a thunderstorm. These different optical events are collectively known as transient luminous events (TLE).

**Sprites:** Sprites are the phenomena which are observed as momentary luminous flashes directly above thunderstorm and extending to about ~90 km in lower ionosphere [109]. Sprites correspond to large electrostatic fields triggered by intracloud or cloud-to-ground lightning stroke [110]. Their spatial structures might be kind of small single spot or multiple vertically elongated spots which can spread horizontally in more than 40 km region. Sprites are mostly red with tendrils of declining intensity.

The sprites coupled with a thunderstorm may affect the conductivity, electric field, and temperature of the stratosphere, mesosphere, and ionosphere [111]. Various researchers [112-115] have expansively studied the consequence of sprites on the ionosphere.

**Elves:** Elves (Emission of Light and Very Low-Frequency perturbations due to Electromagnetic Pulse Sources) are great, scattered and ring-shaped flashes occurring in the ionosphere at about 100 km altitude above the ground and can expand up to around 500 km in diameter. These are initiated by atmospheric heating, because of the electromagnetic pulse generated by lightning stroke. Elves last for few microseconds (0.001seconds) and are almost invisible to naked eyes.

**Blue Jets:** Blue jets are cone-shaped transient luminous flashes that propagate upward in narrow cones from the interior of a thundercloud to with a vertical speed of ~ 100 km/s and then disappearing at an altitude of about ~40 km. These are partially ionized with a short life of ~100-200 ms. Sometimes blue jets turn on sprites but these are not observed to be directly associated with the cloud to ground lightning [116-117].

# CHAPTER 3

# DATA INFORMATION AND INSTRUMENTATION

## 3.1 MISSION OF SROSS-C2

SROSS-C2 satellite was an Indian satellite which was launched from Sriharikota on 4 May 1994 by the Indian Space Research Organization (ISRO) to perform experiments on Gamma-ray astronomy and ionospheric science. SROSS-C2 was the fourth satellite of Stretched Rohini Satellite Series program of ISRO which was planned, developed, and tested at the ISRO Satellite Centre (ISAC), Bangalore (figure 3.1). SROSS-C2 satellite weighing 113 kg was injected into an orbit of 938 km apogee and 437 km perigee with the help of a rocket Augmented Satellite Launch Vehicle-D4 (ASLV-D4) with an orbit inclination of 46º. After operating for two months the satellite's orbit was lowered to 630 km by 430 km. SROSS-C2 satellite was the most successful mission in its series and it provided excellent data coverage over the Indian lat-long, for almost half of the 23rd solar cycle from minima to solar maxima at an altitude of ~500 km, over the low latitudes, and then finally ended on 12 July 2001. A detailed explanation about SROSS-C2 and its functioning has been provided in [118-119].

## 3.2 SROSS-C2 SATELLITE CONFIGURATION

The satellite was octagonally prismoidal-shaped implanted with eight solar panels on the eight sides of the prismoid to generate 50 W of electric power, backed up by 18 Ah Ni-Cd rechargeable batteries whereas, payload sensors and telemetry antennae were fixed over the top deck (figure 3.1). The retarding potential analyzers (RPA) sensors were mounted on the top deck over the cylindrical-shaped sensor mounts. The PP sensor was arranged on a gold plated cylindrical boom (electrically insulated from the probe) at the centre spot of the top deck near the ion RPA sensor and 2 cm above the ground plane. The rest of the electronics for RPA payload contained in an electronic box was mounted below the top deck, inside the central structure of the satellite.

The satellite body was spin-stabilized moving in cartwheel mode, keeping the spin axis perpendicular to the orbital plane. The spin axis was parallel to one of the lateral

axes while its longitudinal axis rotated in the orbital plane. Thus, the top deck of the satellite, carrying payload sensors and the ground plane, faced the plus roll axis and the satellite velocity vector once in every spin rotation figure 3.2. The satellite spun at a rate of 5 revolutions per minute (rpm) and the angle between satellite spin axis and orbital plane normal was maintained within ±10°. Satellite orbit was inclined by 46.3° and covered a latitude range of 46° S to 46° N with an orbital period of 90 minutes. The longitude range of satellite tracking was 50° to 100° E.

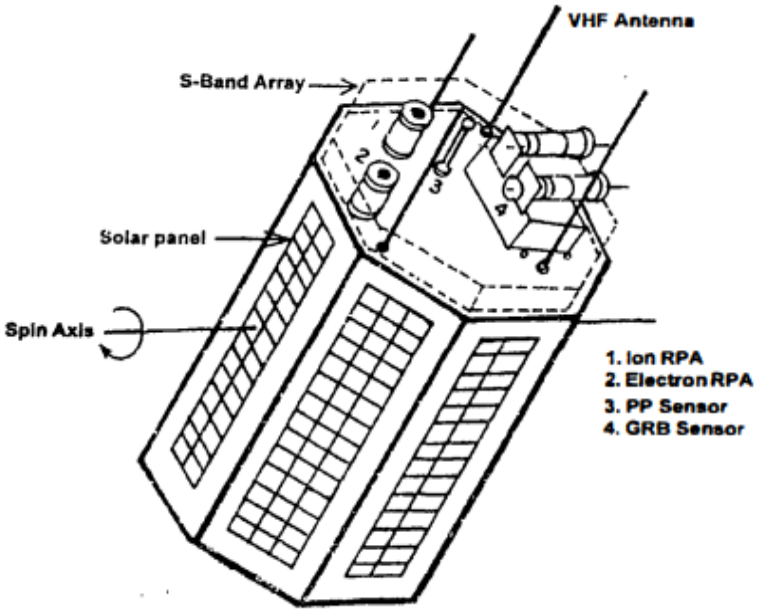


Figure 3.1: Top deck layout of SROSS-C2 satellite, Garg et al. 2003

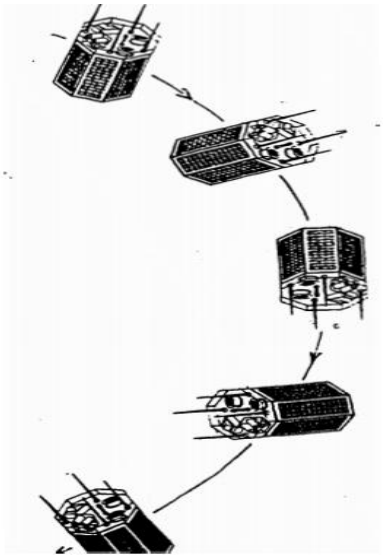

Figure 3.2: SROSS-C2 satellite orientation in orbit, Garg et al. 2003

As the satellite moves in the orbit motion keeping the spin axis perpendicular to the orbital plane, in this kind of spin arrangement of the satellite, the angle in between the sensor face normal and the satellite velocity vector ($\theta$) keeps on changing constantly between 0° and 360° (figure 3.2). The RPA measurements are taken when the sensor normal faces the satellite velocity vector. But in a spin-stabilized satellite, this situation remains for fraction of a second. The RPA sensors collect data within ±30˚ (for ions) and within ±90˚ (for electrons) of the satellite velocity vector at once in each spin period.

### 3.2.1 RPA Payload and Sensors

The laboratory techniques, Langmuir probes, or retarding potential analyzers (RPA) used for space purposes were developed and explained [120] by Irving Langmuir and co-workers over seventy years back. The RPA probes onboard numerous satellites and rockets is a very well-established technique which has been effectively used in the past for depiction of ionosphere such as to derive ion and electron temperatures, ion and electron densities, and thermal and supra-thermal electron fluxes.

The SROSS-C2 satellite carried two specific payloads- the gamma Ray Burst Experiment (GRB) detector payload and the Retarding Potential Analyser (RPA) payload. The GRB payload was an astronomy payload planned and developed by ISRO Satellite Centre (ISAC), whereas the RPA payload separate for electron and ion was an aeronomy payload which was planned and fabricated at the National Physical Laboratory (NPL), New Delhi.

The payload collected simultaneous samples of electron and ion plasma in the altitude range of 420–620 km. Payload data was collected at Banglore ground station, (12.5° N, 77.3° E), Lucknow (26.8° N, 80.8° E), and Mauritius (20° S, 56° E). And the satellite potential was measured with the help of the Potential probe.

The RPA payload consisted of the sensors with allied electronics. The sensor employed planar geometry and had a multigridded cylindrical structure (Faraday cup), a number of grids, and a collector electrode. The sensor was similar to a pentode vacuum tube devoid of a cathode, where the ionospheric plasma entering through the open aperture acted as a source of plasma.

The two RPA sensors had four mechanically identical grids as (i) Entrance grid, (ii) Retarding grid, (iii) Suppressor grid, and (iv) Collector shield grid. These grids were made from 100 × 100 and 50 × 50 counts (wires for square inch) gold plated tungsten wire mesh (wire diameter of 0.001 inches) having 90 to 95 % optical transparency. The 50 mesh has optical transparency as high as 92% and 100 counts mesh 82%. The entrance and the retarding grids were double grids each one made of a 50 × 50 mesh and a 100 × 100 mesh. The suppressor and collector shield grids were single grids each one made of a 50 × 50 mesh in both sensors. Thus, one ion sensor contains 2 grids made from 100 × 100 mesh and four grids made from 50 × 50 meshes. The two sensors were mechanically alike but had diverse grid voltages appropriate for the collection of electrons and ions respectively hence, the electrons and ions having energy more than the threshold energy (voltage applied on retarding grid) were able to cross different grids and get eventually collected at the collector electrode to produce collector current. RPA sensors can be operated in different modes: in fixed bias mode, density and irregularities are measured while in swept bias mode, temperature and other parameters are measured. The electron and ion sensors are synchronized in such a manner that one sensor operates in fixed bias mode and the other remained in sweep mode to avoid any interference among them.

### 3.2.2 Derivation of Ionospheric Parameters

The ion RPA, Electron RPA, and a Potential probe made simultaneous measurements of the plasma parameters. The potential probe, like a spherical Langmuir probe, estimated the deviations in the satellite potential during the spinning and motion of the satellite. It could operate in both current and voltage modes. In current mode, it gave characteristic current-voltage curves (*I-V)* of ambient plasma, independent of RPA, while in voltage mode it measured the difference between probe floating potential and potential acquiring satellite [118, 121-123].

Non-linear curve fitting is opted for characteristic *I-V* curves of ion RPA because of the composite nature resulting from the presence of more than one type of ionic species in plasma (figure 3.3). Individual plasma quantities are estimated by fitting the observed non-linear curve theoretical curve with the different values of variables for minimizing the coefficient of fitness.

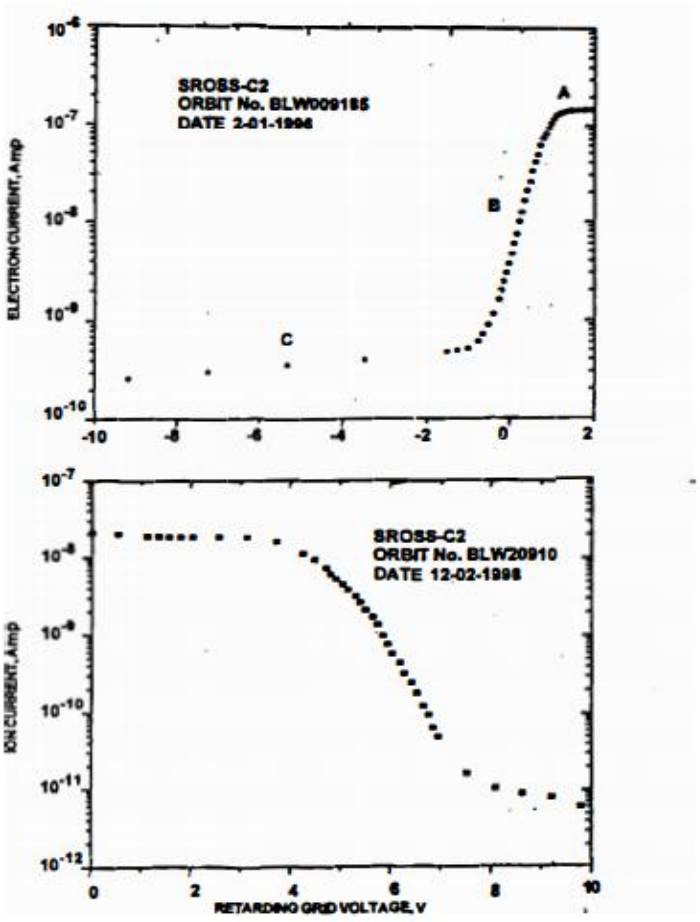


Figure 3.3: Typical electron and ion *I-V* curves, Garg et al. 2003

The following ionospheric parameters can be derived from the characteristic *I-V* curve.

*Measurements by the ion RPA:* the total ion density, irregularities in the Ni, the temperature of the ions, and densities of the different ions ($H^+$, $He^+$, $O^+$, $O2^+$, $NO^+$) present in the ionosphere.

*Measurements by the electron RPA*: the total electron density, irregularities in the Ne, temperature of the electrons, and the supra-thermal electron flux (STEF) up to 30 eV.

The electron-ion parameters were derived from the characteristic curves of the collector current versus retarding grid voltage obtained with some limits and accuracies, as shown below in table 3.1

Table 3.1: Plasma parameters measurements with their limits and accuracies

| Parameter | Limits of measurement | Accuracies |
|---|---|---|
| Ni | $5 \times 10^2$ to $5 \times 10^6$ $m^{-3}$ | ±5% |
| Ti | 500 to 5000 K | ±50K |
| Te | 500 to 5000 K | ±50K |
| STEF | $1x10^7$ to $1 \times 10^9$ $cm^{-2}$ $s^{-1}$ | ±10% |

## 3.3 MISSION OF ROCSAT-1 SATELLITE

The National Space Program Office (NSPO) is a governmental organization of Taiwan, Republic of China (ROC) which executes the national space programs along with providing an infrastructure for space science and technology missions. Republic of China Satellite (ROCSAT) series was also conducted by NSPO whose main objective was to carry out scientific observations and experiments on the ionosphere and oceans [124]. In December 2004, the ROCSAT program was renamed FORMOSAT-1. The ROCSAT-1 satellite and its instrumentation were developed jointly by TRW (Space & Electronics Group) and NSPO, and it was launched on 26 January 1999 from Cape Canaveral Air Force Station, US, on Lockheed Martin's Athena-1 vehicle. The 400-kg ROCSAT-1 being a low earth orbit satellite was placed into a circular orbit of 600 km altitude and 35 degrees inclination. Being at low inclination orbit it circulated the Earth every 97 min, provided a high-quality spatial coverage in local time and longitude and consequently Taiwan's receiving stations collected satellite transmitted data approximately six times a day [125]. All the satellite functioning and data processing were performed at Hsin-Chu city in Taiwan. The ROCSAT-1 satellite served successfully for 5 ½ years during the active period of solar cycle 23. The mission ended on 17 June 2004 and the satellite was decommissioned on 16 July 2004.

## 3.4 ROCSAT-1 SATELLITE CONFIGURATION

The ROCSAT-1 was three-axis stabilized hexahedron-shaped satellite with dimensions of width 1.1 m and height of 2.1 m. It was 7.2 m extensively wide, organized with solar arrays of size 1.16 m x 2.46 m that provided the power of 450 W. Whereas, during the eclipse period a, 21 AH Ni-Cd battery cell provided power to the satellite [126]. It was module designed to accommodate multiple payloads. Like most

of the other spacecraft, ROCSAT-1 was also composed of six major subsystems viz. Structure and Mechanical Subsystem (SMS), Command and Data Handling/Tracking, Telemetry and Control Subsystem (C&DH / TT&C), Electrical Power Subsystem (EPS), Attitude and Determination and Control Subsystem (ADCS), Thermal Control Subsystem (TCS), and Reaction Control Subsystem (RCS). The C&DH Subsystem consisted of onboard computers, remote interface units, solid-state recorder, GPS equipment, and transponder interface electronics.

### 3.4.1 IPEI Payload and RPA

The ROCSAT-1 satellite was instrumented with three payloads—(1) Ocean color imager (OCI), (2) Ionospheric Plasma and Electrodynamics Instrument (IPEI), and (3) Experimental Communications Payload (ECP) (figure 3.4 and 3.5). The OCI collected the data on visible and near-infrared radiances over low latitude oceans. The ECP studied the system performance and different implementation schemes for LEO mobile satellite communication using Ka-band frequency. The IPEI measured the F-region's ionic parameters at low to medium latitude ionosphere.

***IPEI Payload:*** The IPEI consisted of two chief packages- the Sensor Electronics Package (SEP) and the Main Electronics Package (MEP), along with an interconnecting cable. The dimensions of SEP and MEP were 47 cm x 42 cm x 19 cm and 28 cm x 13 cm x 14 cm, respectively. Both the packages were made from aluminium alloy. The total mass of the IPEI, including the cable, was 9.26 kg. Both the SEP and MEP were mounted on the payload adapter of ROCSAT-1. The IPEI was thermally protected by multi-layer insulation (MLI) and had heaters on the mounting adapter to control the operational thermal environment in orbit. The SEP carried four ion sensors: an Ion Trap (IT), two Horizontal and Vertical Drift Meters (DM), and a Retarding Potential Analyzer (RPA) along with intimately associated electronics and power supplies. These sensors measured ion concentration, ion temperature, and ion drift velocity, and major ion composition, within the latitude band of ± 35º of the low-mid latitude ionosphere at the satellite position along the ROCSAT-1 orbit. The MEP contained four major parts: a digital processing unit (DPU), command interface, science data interface, and power supplies. The MEP provided the electrical interface between IPEI and the spacecraft. Also, the MEP implements the operational modes of

IPEI: NORMAL, FAST, and AUTO. In the NORMAL mode the IT, HDM, and VDM provide measurements of the total ion concentration and the cross-track ion drift velocity at 32 Hz, while the RPA provides the in-track ion drift, the ion temperature, and the major ion composition at a nominal 1/2 Hz rate. In the FAST mode, these sample rates are 1024 Hz and 1/4 Hz respectively. The AUTO mode enables IPEI to switch from the default NORMAL mode to the FAST mode when sudden large changes in the ion concentration, commonly associated with plasma structures called bubbles, are detected. The unique feature of the AUTO mode allows scientists to investigate spatial structures with scale sizes as small as 16 meters [126, 127].

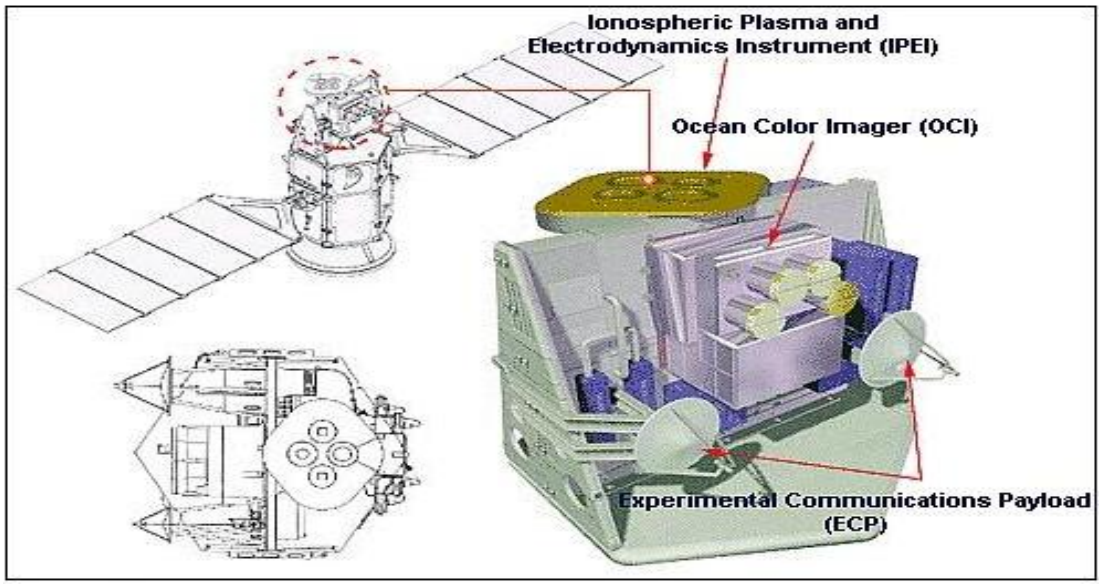


Figure 3.4: Accommodation of the payload on the spacecraft (image credit: NSPO)

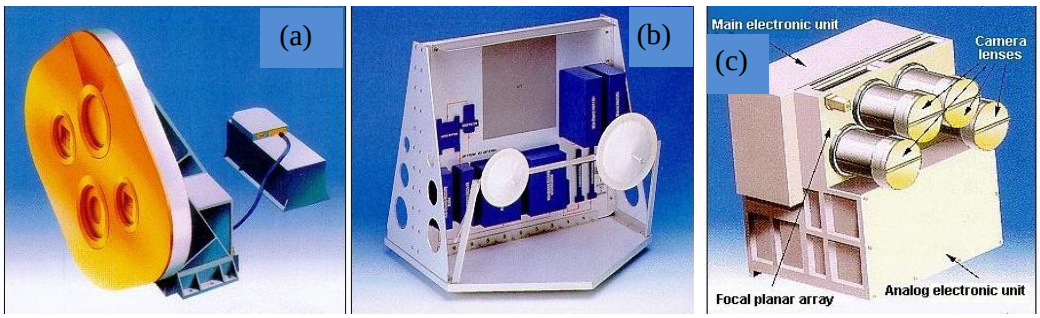


Figure 3.5: View of IPEI device (a), ECP instrument (b), and OCI instrument (c), image credit: NSPO

***Retarding Potential Analyze (RPA):*** The RPA provided a measure of the ram energy of the incoming ions with respect to the spacecraft (figure 3.6). The planar sensor views approximately along the satellite velocity vector and presented a circular

gridded 4-cm diameter entrance aperture (G1) to the incoming ions. The internal retarding grid (G2) presented a potential that controlled the minimum energy required by ions to have access to the ion collector. The suppressor grid (G3) prevented ambient thermal electrons from reaching the collector. The shield grid (G4) prevented potential variations applied to the previous retarding grids from coupling to the collector and reduced microphonics to the collector caused by the suppressor grid [127].

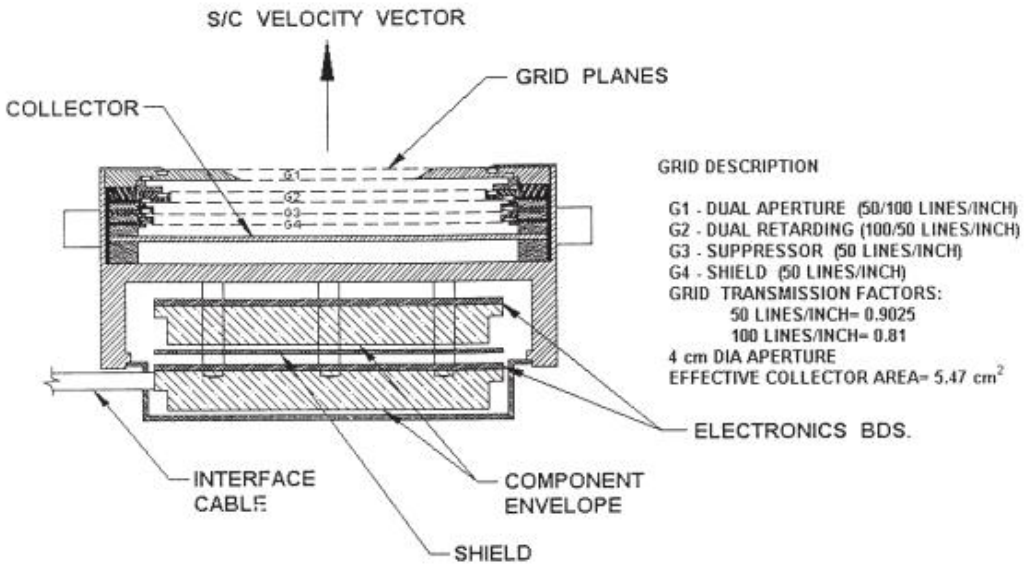


Figure 3.6: A schematic diagram for the cross-section of the Retarding Potential Analyzer, Chang et al. 1999

A retarding potential versus ion current characteristic curve is obtained by stepping the RV through a series of discrete steps. At each RV step, the ion current to the collector is measured by the RPA electrometer.

### 3.4.2 Derivation of Ionospheric Parameters

To investigate the ionospheric phenomena on the scale sizes of greater than 10 km (i.e., global scale), IPEI was supposed to take measurements with high precision and accuracy, as listed in table 3.2.

Table 3.2: Measurement for Global Scale only (> 10 km), Yeh et al. 1999

| Parameter | Dynamic Range | Accuracy |
|---|---|---|
| Ion Velocity Vector | ±2 km/s | ±10m/s |
| Total Ion Concentration | 50 to $5\times10^6$ $cm^{-3}$ | 10% |
| Ion Temperature | 500 to 10,000ºK | 10% |

Major features of the IPEI payload are summarized in table 3.3

Table 3.3: IPEI Specification Summary, yeh et al. 1999

| Instrument | RPA | IDM | IT |
|---|---|---|---|
| Measurement | Ion temperatures and Ram velocity | Transverse ion velocity components | Total ion concentration |
| Heritage | AE, DE, DMSP, Viking, and San Marco | | |
| Detector | Linear Electrometer, 8 ranges | Log Electrometers with Linear Diffe. Amplifier, 2 ranges | Log Electrometer |
| Range | $V_x$=±2 km/s<br>$T_i$= 500 -$10^4$K | V=±2 km/s | Ni=50 - $5x10^6$ $cm^{-3}$ |
| Accuracy | ΔV=±10 m/s<br>ΔTi=±10% | Δ V=±10 m/s | ΔNi/ Ni= ±10%<br>ΔNi/ Ni= ±1% |
| Sampling Rate | 32 Hz (Normal)<br>64 Hz (Fast) | 32 Hz (Normal)<br>1024 Hz (Fast) | 32 Hz (Normal)<br>1024 Hz (Fast) |
| Mass | < 14 kg (total weight) | | |
| Envelope Dimension(cm) | SEP: 17×37×36 | MEP: 7×21×27 | |
| Power(W) | 10W | | |
| DC Power Bus (V) | Minimum: 22 V | Nominal: 28 V | Maximum: 34 V |
| Pointing Direction | Ram | | |
| FOV (full angle) | 45º×45º | Conical | |
| Temperature | -20ºC | +50ºC | |
| Data Rates | Normal Mode: 2.224 kbps | Fast Mode: 53.376 kbps | |
| Duty Cycle | Normal Mode: 83% | Fast Mode: 17% | |

## 3.5 IRI MODEL DATA

The International Reference Ionosphere (IRI) is an international project funded and supported by the Committee on Space Research (COSPAR) and the International Union of Radio Science (URSI). The IRI model, based on all available data sources is believed to be the superior and most reliable among all the available empirical models today. For a given location, date, and time, IRI provides monthly averages of the ionospheric electron density, electron temperature, ion temperature, and ion composition, equatorial vertical ion drift, effects of ionospheric storms on F and E peak densities, etc. in the altitude ranging from 60 to 2000 km [128]. The main sources of data collection include the worldwide system of ionosondes, the great incoherent scatter radars (Jicamarca, Arecibo, Millstone Hill, Malvern, St. Santin), the ISIS and Alouette topside sounders, and in-situ instruments on several satellites and rockets.

IRI predictions are found most accurate in Northern mid-latitudes because of the generally high station density in this part of the globe. But at low and high latitudes the data coverage is rather sparse due to the harsh climate conditions, and as a result, the IRI predictions are less accurate at equatorial and auroral latitudes.

With the advent of new data collecting techniques, the IRI model has undergone numerous years of steady and critical testing and modifications by the international science and research communities, and hence several improved and advanced editions of the model have been released, For example, IRI-80, IRI-86, IRI-90, IRI-95, IRI-2000, IRI-2007, IRI-2012, and IRI-2016.

In the present research work, IRI-2012 and IRI-2016 model has been utilized for making comparisons with satellite measured values. The data for IRI-12 and IRI-16 model has been collected from the IRI homepage at

https://ccmc.gsfc.nasa.gov/modelweb/model/iri2012_vitmo.php and
https://ccmc.gsfc.nasa.gov/modelweb/models/iri2016_vitmo.php respectively.

## 3.6 SOLAR FLUX INDEX (F10.7) DATA

The solar radio flux at 10.7 cm (2800 MHz) is an excellent indicator of solar activity. Often called the F10.7 index, it is one of the longest-running records of solar activity. It has been discussed in detail in chapter 1 of the thesis. And the data for the solar flux index has been downloaded from https://omniweb.gsfc.nasa.gov/form/dx1.html.

## 3.7 SEISMIC ACTIVITY DATA

The seismic activity effects on the ionosphere are now very well known and have been studied by many scholars [128-130]. In the present work, the data of earthquakes were downloaded from the USGS website – NEIC (National Earthquake Information Center), https://earthquake.usgs.gov/earthquakes/search/. The USGS monitors and reports on earthquake's impacts and hazards and conducts targeted research on the causes and effects of earthquakes. It compiles and maintains an extensive, global seismic database on earthquake parameters and their effects that serve as a solid foundation for basic and applied earth science research.

## 3.8 GEOMAGNETIC INDICES DATA

Geomagnetic activity is caused due to the electric currents present in the magnetosphere and ionosphere of the earth. Magnetic measurements at different locations enable us to remotely sense these currents, monitor the global reaction of the magnetosphere/ionosphere and record the variations with time. Hence worldwide more than 200 ground-based geomagnetic observatories have been established. Indices of magnetic activity are prepared to have a common reference point from which all stations can study these variations commonly. Following are the geomagnetic indices used in the present study.

***Kp:*** The K-index is a quasi-logarithmic geomagnetic activity index, introduced by J. Bartels in 1949. This was designed to avail a homogeneous running record of the solar radiation effect on the earth; by measuring the intensity of geomagnetic activity caused due to the electric currents generated around the earth by that radiation [131]. It is based upon the 3-hourly fluctuations or deviations in the horizontal component of the earth's magnetic field, measured from several ground-based magnetometers all over the world. A three-hour interval indicates the intensity of geomagnetic activity

(ranging from 0 to 9) due to particle radiation from the sun at 00-03, 03- 06, 06-09 ....., 21-24 UTC intervals [132]. A zero Kp value infers small geomagnetic activity while value 9 refers to severe geomagnetic activity level. (https://www.spaceweather live.com/en/help/the-kp-index).

The finalized Kp-index is calculated by an algorithm that collects together all the K-values recorded at each station. Its final version is released from the GFZ in Potsdam, Germany, and is also updated twice a month. The finalized Kp-index is somewhat distinct from the K-index as it is measured on a scale of thirds having 28 values in total as 0, 0+,1-,1, 1+, 2-, 2, 2+,…….which are equivalent to 0,3,7,10,13,…. whereas the preliminary K-index has only 10 values ranging from 0-9. And in the Omni data set the Kp values are mapped as 0+ to 3, 1- to 7, 1 to 10, 1+ to 13, 2- to 17, etc.

Table 3.4: Table for converting Kp to ap

| **Kp** | $0_0$ | $0_+$ | $1_-$ | $1_0$ | $1_+$ | $2_-$ | $2_0$ | $2_+$ | $3_-$ | $3_0$ | $3_+$ | $4_-$ | $4_0$ | $4_+$ |
|---|---|---|---|---|---|---|---|---|---|---|---|---|---|---|
| **ap** | 0 | 2 | 3 | 4 | 5 | 6 | 7 | 9 | 12 | 15 | 18 | 22 | 27 | 32 |
| **Kp** | $5_-$ | $5_0$ | $5_+$ | $6_-$ | $6_0$ | $6_+$ | $7_-$ | $7_0$ | $7_+$ | $8_-$ | $8_0$ | $8_+$ | $9_-$ | $9_0$ |
| **ap** | 39 | 48 | 56 | 67 | 80 | 94 | 111 | 132 | 154 | 179 | 207 | 236 | 300 | 400 |

The geomagnetic indices ap, Ap, and the categorization of international quiet days (Q-days, in sense of low geomagnetic activity) and disturbed days (D-days, in sense of high geomagnetic activity) are set according to the Kp index values. In the present work data for Kp index or Kpmax has been obtained from the website ‘WDC for Geomagnetism, Kyoto http://wdc.kugi.kyoto-u.ac.jp/kp/index.html.

***Ap:*** The Ap index is the most primitively occurring index, associated with geomagnetic storms which provide the geomagnetic activity level for each day. It is obtained by calculating the average of eight 3-hour ap values in a row. It means, firstly every 3-hour K-value is changed into a linear scale called the a-index. Then the average computed for 8 daily a-values provides the Ap-index of a day. Hence the Ap-index is a reliable geomagnetic activity index which signifies that the higher the Ap-value a day, the higher is the level of geomagnetic activity.

For example, if the *K*-indices for a day are 3, 4, 6, 5, 3, 2, 2, and 1, then the daily *A*-index is the average of the corresponding equivalent amplitudes:

$$\text{i.e. } Ap = (15 + 27 + 80 + 48 + 15 + 7 + 7 + 4) / 8 = 25.375$$

***Dst:*** The strength of geomagnetic storms can be measured using the Disturbance storm time (Dst) index an hourly index, which is calculated by averaging deviations for the horizontal component of the earth's magnetic field [133-134] at four lower latitude stations. At these stations, the magnetosphere ring current dominates over the H component of the magnetic perturbations. The large intensity of the ring current is represented by large negative perturbations in the Dst value [135]. Hence, the Dst index is actually an indication of the strength of the geomagnetic storms.

The intensity of geomagnetic storms is divided into five categories (according to Loewe and Prolss 1997) based on the minimum Dst such as weak (-30 to -50 nT), moderate (-50 to -100 nT), strong (-100 to - 200 nT), severe (-200 to -350 nT), and great (<-350 nT). During quiet times, Dst is in between ±20 nT. In this thesis work, the Dst data is taken through the website https://omniweb.gsfc.nasa.gov/form/dx1.html.

***IMF, Bz data- The*** interplanetary magnetic field (IMF) is a constituent of the sun's magnetic field which flows out into the interplanetary space by the solar wind. The IMF lines are also said to be 'frozen in' to the solar wind plasma.

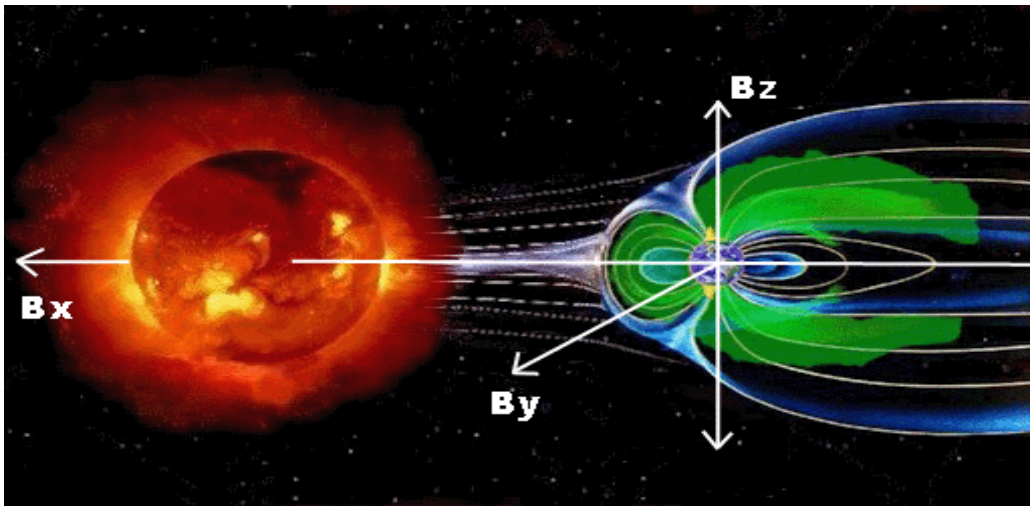


Figure 3.7: The Interplanetary Magnetic-field, Image Credit: Space Weather live.com

The solar wind drives the sun's magnetic field out in the solar system. Hence, the sun's extended magnetic field is known as the interplanetary magnetic field. The IMF is a three axial-vector quantity, where Bx and By are orientated along the ecliptic (figure 3.7) and the Bz component is perpendicular to the ecliptic plane and is formed due to various disturbances in the solar wind. When the IMF and the earth's magnetic field lines are leaning opposite or 'antiparallel' to each other then they reconnect/merge together such that transfer of energy, mass, and momentum from the solar wind to the magnetosphere takes place. Since the Bz, directed towards the south, peels off the sunlit side geomagnetic field lines, so larger the Bz value, the larger is the amount of energy transfer to the Earth's magnetosphere and subsequently causes a stronger geomagnetic storm or a more vivacious aurora. In the present thesis the data for IMF, Bz is taken from https://omniweb.gsfc.nasa.gov/form/dx1.html

# CHAPTER 4

# VARIATION OF IONOSPHERIC PARAMETERS DURING LSA AND HSA AS MEASURED BY SROSS-C2 SATELLITE

## 4.1 INTRODUCTION

Satellite navigation and communication system have become an integral part of today's world. This dependence necessitates the study and forecasting of changes in the F2 region ionosphere. The incoming solar flux is a predominant factor of ionization. However, other dynamical processes like electrodynamic drifts, transport mechanisms diffusion, etc. also determine the variability and structure of the ionosphere. The variations in ionospheric or plasma parameters (Ne, Te, Ti, Ni, and icon composition) are yet partially understood. Hence, analyzing the complexity of the ionosphere and predicting its behaviour has become extremely important for forecasting ionospheric weather and improvement of existing ionospheric models.

The structure and variability of the low latitude ionosphere are significantly different from the high and mid-latitude ionosphere. There, the exceptional orientation of geomagnetic field lines gives birth to various unique physical features such as electro dynamical drift, equatorial electrojet, and equatorial ionization anomaly (EIA), etc. Owing to these unique features like EIA, E × B drifts, the low latitude ionosphere has been studied and analyzed extensively [136-139]. These reports indicate that the ionospheric structure depends predominately on the E × B drift over F region of the low latitude ionosphere. This drift further gets modified due to seasons, solar cycle and level of geomagnetic activity, etc.

Ion density/composition studies are much more composed of ionospheric temperature studies [59]. Ion and electron temperatures are determined by energy flow as well as heating and cooling of ionospheric plasma [140]. However, few comprehensive and detailed studies on ionospheric temperatures can be found reported in the literature [41, 58]. In literature, one can find many studies related to electron density and its temperature with the help of satellite measurements [141,142]. But the studies on the relationship of ion densities with their corresponding temperatures are less.

The present study aims to statistically analyze the behaviour and relationship of total ion density Ni with ion temperature Ti during a high and low solar activity using SROSS-C2 satellite data and compare it with IRI-2012 model data. The relative study of Ni and Ti as obtained from SROSS-C2 and as estimated by IRI-2012 brings out symmetry/asymmetry variations in the two sources of data. The co-relation between the Ni and Ti and its comparison with IRI-2012 model data further helps in understanding their behaviour. These studies also help in the improvement of existing ionospheric models.

## 4.2 DATA COLLECTION AND ANALYSIS

The data of ionospheric parameters (ion temperature and density – Ti, Ni) used in the present study have been taken from retarding potential analyzer (RPA) of the SROSS-C2 satellite. The region selected for the present work spans from 5-35˚Geog. N and 65-95˚ Geog. E. The study has been carried over low latitude and at an average altitude of ~ 500 km.

The diurnal pattern of ion temperature and density measured by SROSS-C2 satellite has been compared with the international ionosphere reference model IRI-2012 data. The IRI-2012 model data has been obtained online from OMNIWEB NASA site. To study the effect of solar activity on ion temperature and density, the data of solar flux - F10.7 have been retrieved from the Omniweb NSSDC site for the years 1995 and 2000.

Figure 4.1 shows the data count of ion density (Ni) and ion temperature (Ti) for which SROSS-C2 satellite has been used and solar flux (F10.7) during year low (1995) and high (2000) solar activity years. The solar flux F10.7 is around ~77 in the year 1995 and ~177 in the year 2000. As IRI-2012 model gives the estimated values so its data counts have not been considered.

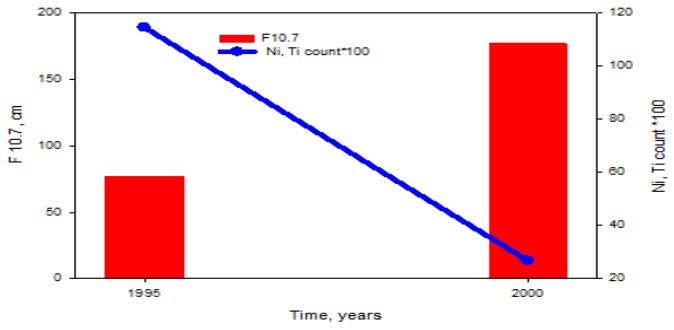


Figure 4.1: Ni and Ti data count (blue line) and F10.7 during LSA (1995) and HSA (2000)

## 4.3 DIURNAL VARIATION OF Ni AND Ti DURING LSA AND HSA

Figure 4.2 represents the diurnal variation of total ion density, Ni (a - SROSS and b - IRI), and ion temperatures (c – SROSS and d - IRI) during low (1995) and high (2000) solar activity years. As EUV flux coming from the Sun is the main source of ionization, it is important to understand the distribution of this energy which is expended in heating and ionizing the ions. Diurnal variation of Ni and Ti as measured by SROSS – C2 data have been compared with IRI - 2012 modelled data for low (1995) and high (2000) solar activity years.

During low solar activity year – 1995 (figure 4.2 - a); the diurnal features of total ion density are as follows, the minimum magnitude of density during nighttime, gradual increase during sunrise, day time peak, then gradual decrement of density until night time minimum is achieved. Ni varies from ~$2.5\times10^{11}$ to $4.5\times10^{10}$/ $m^3$ during daytime maximum to nighttime minimum. Total ion density is minimal just before sunrise at 04.00 LT during the year 1995. Thereafter during sunrise, photoelectron production begins in the ionosphere. These photoelectrons ionize the neutral particles and the density of ions gradually begins to increase which attains maxima/ peak at 12 LT. As the sun sets, ion density decreases gradually. Density keeps decreasing all through the evening sector till the nearly constant value is achieved during nighttime. The major cause of this temporal pattern of Ni during low solar activity is photo-ionization due to solar EUV flux.

During high solar activity year – 2000 (figure 4.2 -a); the diurnal features exhibited by total ion density are the minimum magnitude of density during nighttime, steeper increase during sunrise, day time peak, secondary or evening peak, and then gradual decrement of density till night time minimum is achieved. The ion density is minimal just before sunrise at 05 LT during the year 2000. Thereafter during sunrise, through ionization of neutral particles, Ni steeply begins to increase and attains maxima/ peak at 15 LT. As sunsets, a secondary/ evening enhancement during 21 LT is observed. Thereafter a gradual decrease in ion density can be observed. Density keeps on decreasing all through the evening sector till the nearly constant value is achieved during nighttime.

As the sun transverses from low to high activity phase, there is a huge increment in the magnitude of ion density (indicating higher EUV flux) via photoionization which is the main cause of the diurnal distribution of ion density. However, other factors - plasma movement due to E × B drift in low latitude F- region also comes into play. The secondary enhancement during late evening hours during high solar activity years is due to the movement of E × B drift in F- region. The typical 24 hours diurnal variation states that the magnitude of the velocity of vertical F-region E × B drift increases till day time peak velocity is attained thereafter decreases till sunset. During post-sunset drift velocity suddenly increases, then reverses and increases in the reverse direction during night time. Thus the attainment of the secondary peak during high solar activity period is completely attributed to the movement of E × B drift and is known as a pre-reversal enhancement (PRE).

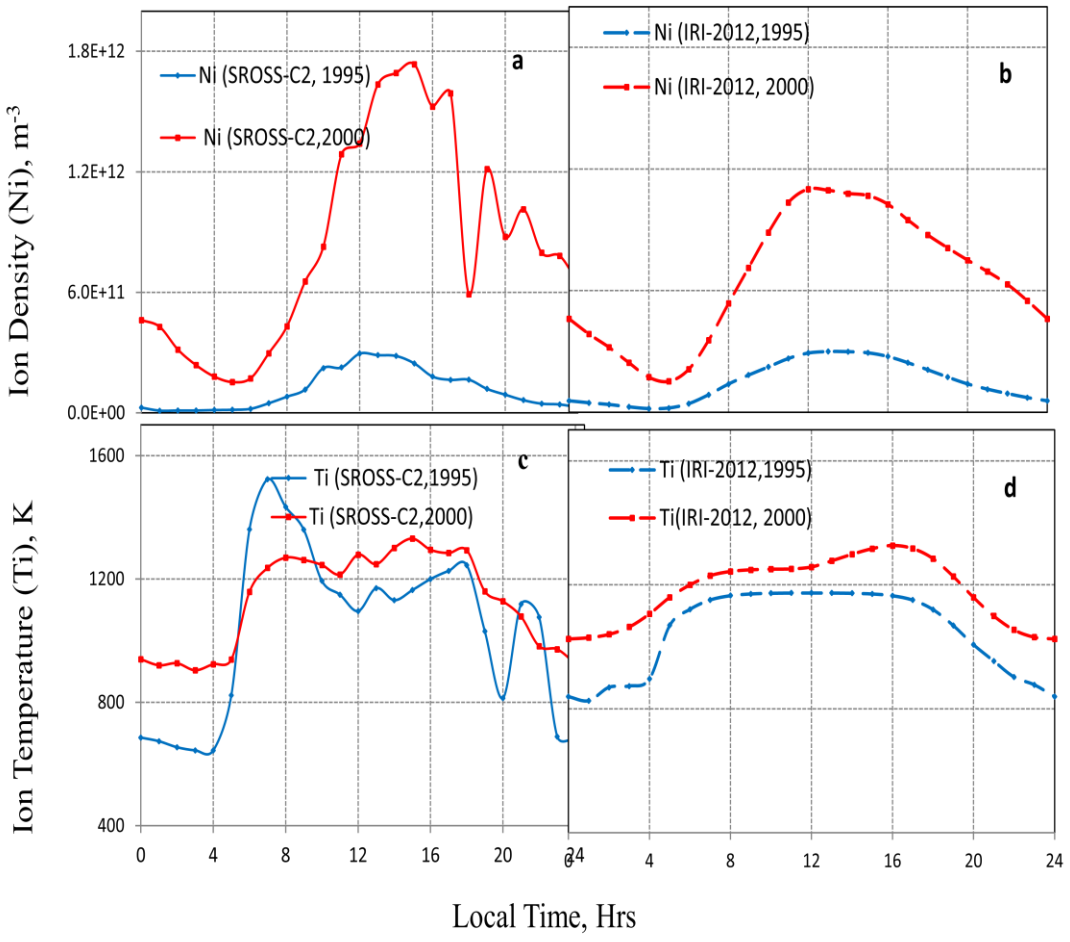


Figure 4.2: Diurnal variation of total ion density, Ni (a-SROSS and b-IRI), and ion temperatures (c-SROSS and d- IRI) during low (1995) and high (2000) solar activity years.

Figure 4.2-b represents the diurnal variation of total ion density, Ni as estimated by IRI model during low (1995) and high (2000) solar activity years. IRI model underestimates the daytime Ni value during high solar activity year – 2000. During night time RPA measured values are almost similar to IRI estimated values. During low solar activity year, the diurnal features and magnitude value of Ni as measured by SROSS-C2 satellite are in fair agreement with IRI estimated values. Diurnal features as estimated by model data are a minimum magnitude of density during nighttime; which is minimal just before the sunrise, gradual increase during sunrise, day time peak, and then gradual decrement of density till night time minimum is achieved. Magnitude values of Ni as estimated by IRI in the year 1995 remains lower than 2000, which is in agreement with SROSS-C2 values; however, the typical diurnal feature of evening enhancement in the year 2000 can't be observed in IRI plot.

Diurnal features of Ti exhibited by figure 4.2c are a minimum magnitude of temperatures during nighttime, morning peak during sunrise, day time trough, and evening enhancement during low solar activity year (1995). However, in high activity year – 2000 the secondary or evening enhancement is negligibly observable. Ti varies from ~ 650K – 1500K and 900K- 1300K during low and high solar activity years respectively. Ti is minimal just before sunrise at 4 and 5LT during the years 1995 and 2000 respectively.

It is found that – as ion density decreases, ion temperature increases and vice versa during the daytime. During sunrise, when ion density is less, ion temperature (Ti) shoots up. It is called morning overshoot [58, 59]. At sunrise, the photoelectron production begins in the ionosphere through the ionization of neutrals. As the photoelectrons share their high energy with ambient electrons, the electron temperature rises [141]. These electrons further increase the temperature of ions and similar kind of observations in Ti is expected as electron energy gets transferred via elastic electron-ion collision [63]. This increase is rapid in the early morning due to low ion density. As the day progresses more and more ions are produced due to ionization, thus the energy shared by each ion decreases, and a daytime trough in Ti is observed. During this daytime peak in Ni (total ion density) is observed. This process is much pronounced during the low solar activity year. The evening enhancement of Te is attributed to vertical E × B drift [10]. During nighttime (20.00 – 04.00 LT) in

absence of solar flux – UV and EUV emissions, Te and Ti decrease gradually and attain almost a constant value.

The daytime magnitude value and diurnal features of Ti as measured by SROSS-C2 are higher and differ from IRI model value and pattern during low solar activity year - 1995. During high solar activity year, the daytime diurnal/ temporal pattern and magnitude value of the model and the measured data are almost similar. However, during nighttime the IRI model data overestimates Ti magnitude value than SROSS-C2 measured value by a moderately higher value. Magnitude values of Ti as estimated by IRI in the year 1995 remains lower than 2000. However, SROSS-C2 Ti values are higher during morning and evening enhancements in the year 1995 compared to the year 2000.

## 4.4 RELATIVE VARIATION OF $Ti_{SROSS-C2}$ AND $Ti_{IRI-2012}$ FOR YEARS 1995 AND 2000

Figure 4.3a represents the variation of Ti as measured by SROSS-C2 satellite, relative to Ti as estimated by IRI – 2012 model on the diurnal scale during years 1995 and 2000. Here value 1 represents no asymmetry in SROSS-C2 and IRI model values. Below one indicates IRI overestimated values and higher than one indicates underestimation compared to SROSS-C2 values. During low solar activity year, 1995 (blue), in night (23 – 4 LT) overestimation of Ti values by IRI is observed by a factor of ~ 0.8. During sunrise, the measured Ti values by SROSS-C2 are much higher than IRI values by almost ~1.2 times. Day time values show an equilibrium value of nearly approaching one, indicating similar daytime values. Again during the evening sector asymmetry in both the values (SROSS-C2 and IRI) is observed. During high solar activity year - 2000 (red) IRI estimated values are in good agreement with SROSS-C2 measured values. During sunrise, day, and evening time value is almost ~1, thus both the values -modelled and measured are in agreement with each other. Only during night time, a little variation or asymmetry is observed.

## 4.5 RELATIVE VARIATION OF $Ni_{SROSS-C2}$ AND $Ni_{IRI-2012}$ FOR YEARS 1995 AND 2000

Figure 4.3b discusses the relative variation of ion density, Ni. During the year 1995 (blue), it can be seen that all through diurnal time scale (0-24 hrs), the values are

below 1, indicating an overestimation by IRI-2012. During the year 2000 (red), the values are generally above 1, pointing to underestimation by IRI. Only during 5 -10 LT, IRI overestimates the SROSS-C2 values. Ni values as measured by SROSS-C2 and IRI-2012 are highly asymmetrical. The asymmetry varies from 0.2(lower side) to 0.9 (upper side) in year 1995 and from 0.6 (lower side) to 1.7 (upper side) in year 2000 respectively.

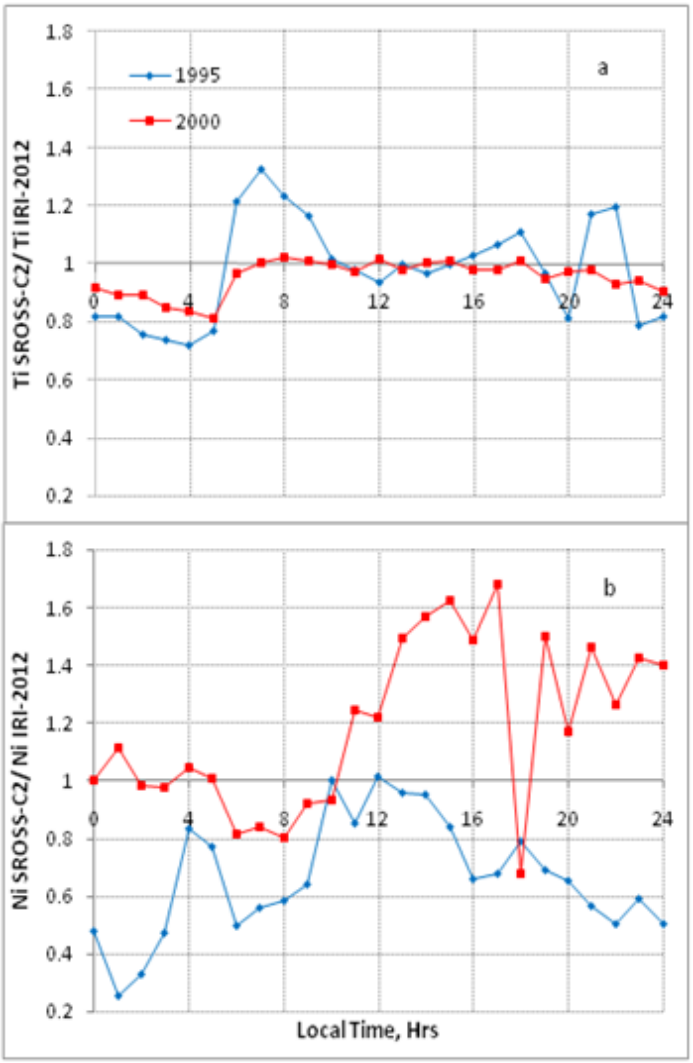


Figure 4.3: Relative variation of Ti (a), Ni (b) with measured and estimated values for years 1995 and 2000

## 4.6 LINEAR OR NON-LINEAR RELATIONSHIP OF Ni WITH Ti

Generally, as the temperature increases the density decreases and vice-versa, over low latitude F2 regions. This trend can be observed from many reports [139, 142]. This kind of observation indicates a poor or negative co-relation between these two ionospheric parameters. The negative/ poor correlation in Ne or Ni (ion density) and

Te during local daytime is widely accepted. Some positive correlations have been found during periods of high solar activity [143] and also in the equatorial area at sunset in December month [144]. It would be interesting to understand how they (Ni and Ti) are co-related and their comparison with IRI values would further help in improvising the model. IRI is revised periodically and any small parameter's statistical variation/ asymmetry with measured values would help in improving it. Figure 4.4 represents a relationship of Ni Vs Ti during 1995 and 2000 as measured by SROSS-C2 satellite and IRI-2012 model over 0-24 hrs diurnal scale.

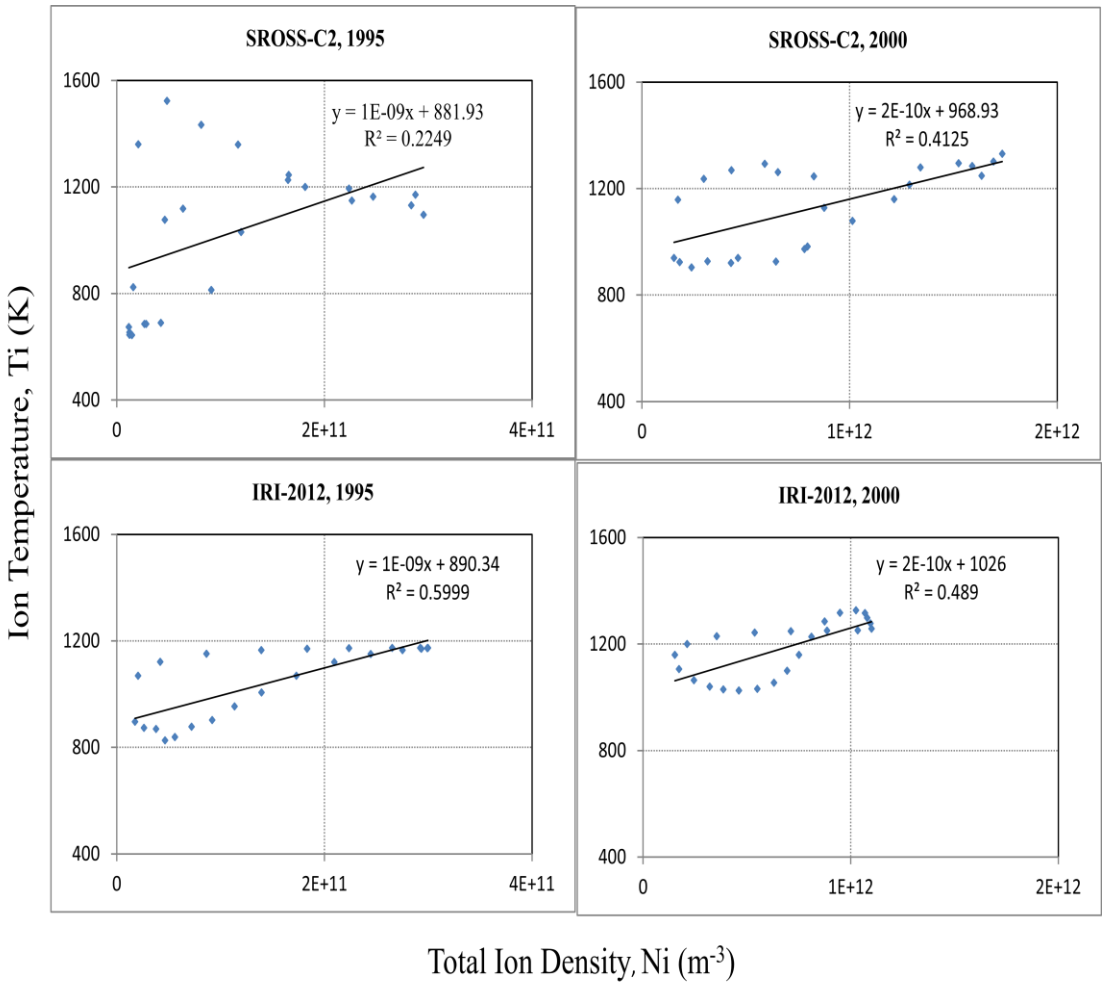


Figure 4.4: Ni Vs Ti during low (1995) and high (2000) solar activity years as measured by SROSS-C2 satellite and IRI-2012 model.

During year 1995, the Ni and Ti are weakly/ poorly co-related - $R^2 = 0.22$ as measured by SROSS-C2, and $R^2 = 0.599$ as estimated by IRI-2012 respectively. The co-relation factor $R^2$ shows a lot of dissimilarity during low solar activity year, 1995. During the year 2000, the Ni and Ti are weakly/ poorly co-related - $R^2 = 0.41$ as measured by SROSS-C2, and $R^2 = 0.48$ as estimated by IRI-2012 respectively, which shows the

variation of Ni with Ti as estimated values by IRI and measured by SROSS-C2 are symmetrical. Thus the nature of interaction and their behaviours also coincide. Few researchers have also reported weak/negative co-relation [69]. The whole diurnal temporal scale of 24 hrs includes highly dynamic times – sunrise and evening time. Thus it would be interesting to understand the Ni Vs Ti relationship in rather quiet times (day and night time). Figure 4.5, shows the relationship of Ni Vs Ti during 1995 and 2000 as measured by SROSS-C2 satellite and IRI-2012 model during day and night time. The daytime is considered from 10-14LT and night time from 22-04 LT in this section. During the daytime in the year 1995, the Ni and Ti are poorly co-related having a correlation factor of - $R^2 = 0.39$ as measured by SROSS-C2, and $R^2 = 0.16$ as estimated by IRI-2012 respectively. It shows a moderate variation in both the $R^2$ values. During daytime in the year 2000, the Ni and Ti are poorly co-related by a correlation factor of - $R^2 = 0.2$ as measured by SROSS-C2, and $R^2 = 0.27$ as estimated by IRI-2012 respectively. $R^2$ values are almost the same indicating similar kinds of interactions as assumed by IRI model and as actually measured values by SROSS-C2 satellite. During night time in the year 1995, the Ni and Ti are poorly co-related by a correlation factor of $R^2 = 0.49$ as measured by SROSS-C2, and $R^2 = 0.007$ as estimated by IRI-2012 respectively, showing a large deviation in both the values. In the year 2000, the Ni and Ti are poorly co-related by a correlation factor of $R^2 = 0.69$ as measured by SROSS-C2, and $R^2 = 0.38$ as estimated by IRI-2012 respectively during night time. Thus during night time both the years show appreciable variations in $R^2$ values.

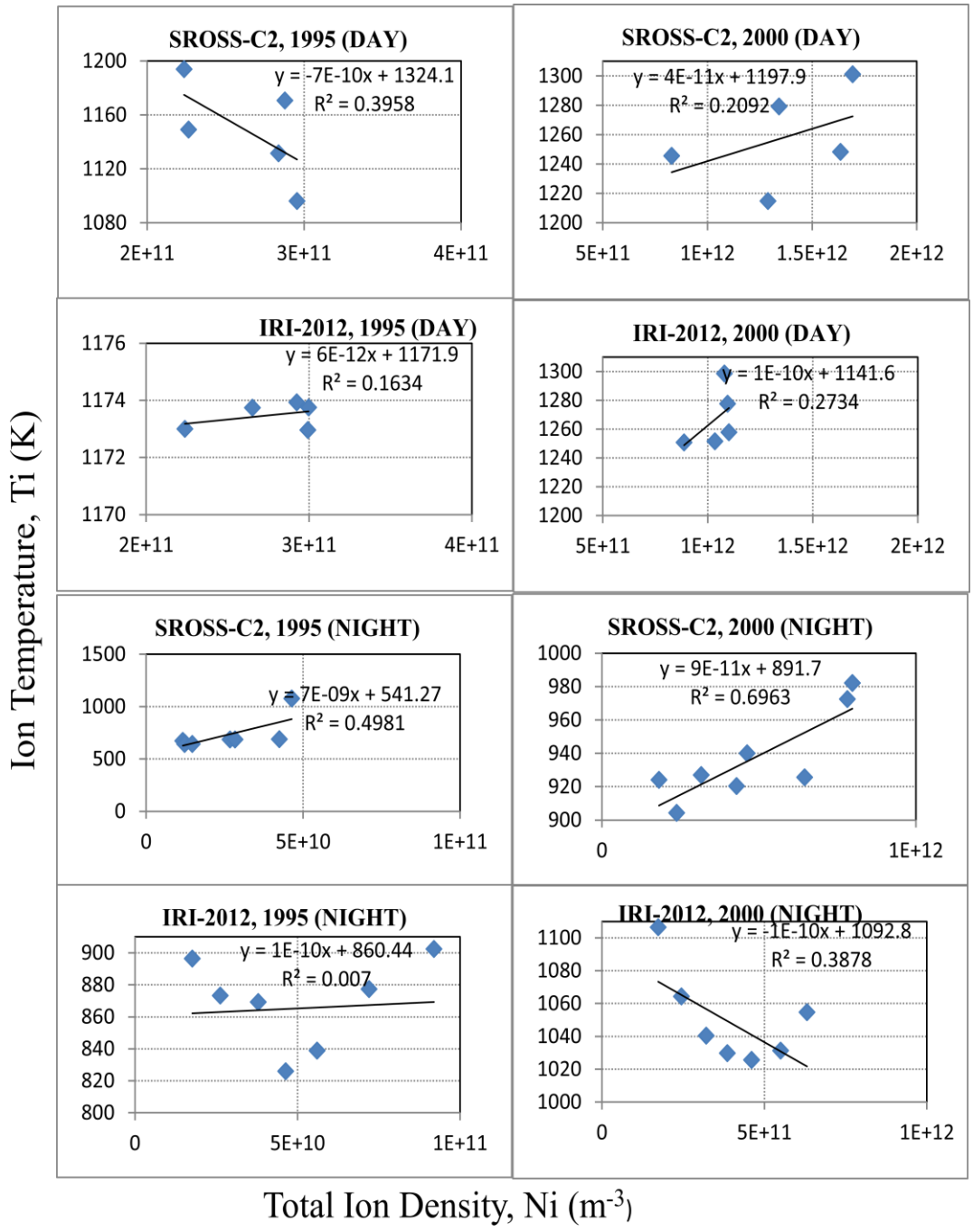


Figure 4.5: Ni Vs Ti during low (1995) and high (2000) solar activity years as measured by SROSS-C2 satellite and IRI-2012 model at day and nighttimes.

## 4.7 CONCLUSION

The behaviour of ionospheric ion parameters (total ion density - Ni and ion temperature - Ti) as measured by SROSS-C2 satellite have been analyzed and compared with estimated IRI – 2012 model values at an average altitude of ~ 500 km during low (year 1995, $F_{10.7}$ = 77) and high (year 2000, $F_{10.7}$ = 177) solar activity over

5°-35°N geog. latitude and 65°-95°E geog. longitude. From the present study, the following can be concluded.

1. As solar activity increases, total ion density Ni also increases by the factor of $10^2$ emphasizing the main source of ionization as solar flux. Ti varies from ~ 650K – 1500K and 900K- 1300K during low and high solar activity years respectively. Ni and Ti are minima just before sunrise. During sunrise, Ti increases rapidly owing to the low density of Ni, known as morning overshoot. During the evening sector, PRE (pre-reversal enhancement) is evident in Ni during high solar activity and in Ti during low solar activity. Thus, highlights the role of E × B drift in determining the Spatio-temporal structure of ionospheric ion parameters over the low latitude.
2. The relative variation shows that IRI-2012 and SROSS-C2 Ti values are in good agreement with each other during low and high solar activity years. However, during the nighttime of the year 1995 (low solar activity), it shows asymmetry. Ni values as obtained from SROSS-C2 and IRI-2012 show asymmetrical behaviour during both high and low solar activity years. IRI overestimates Ni values during low solar activity and underestimates during high solar activity.
3. The relationship between Ni and Ti shows weak /poor co-relation. The correlation factor is weaker in low solar activity compared to high solar activity. The $R^2$ values as obtained from SROSS-C2 are similar during high solar activity and differ during low solar activity with IRI-2012 modelled values.

# CHAPTER 5

# VARIABILITY OF IONOSPHERIC PARAMETERS USING ROCSAT-1 MEASUREMENTS

## 5.1 INTRODUCTION

Solar radiations are the primary cause of the ionization of the Earth's atmosphere. Specifically, the X-ray and extreme ultraviolet radiations are the basic drivers at the base of the plasma density distribution in the ionosphere. It is well known that ionospheric plasma and temperature vary with respect to latitude, altitude, seasons, geomagnetic and solar activities [145]. And in particular, the morphology and dynamics of equatorial and low latitude regions are different compared to the mid and high latitude ones. So to understand the really complex dynamics of low latitude ionosphere, the coupling between the topside ionosphere and protonosphere, and all related processes, many researchers have worked to study the variations of low latitude ionospheric parameters [50, 64, 53, 67, 142, and 144]. The atmospheric neutral winds along with the ionospheric dynamics are considered the dominant factors for perturbing the behaviour of plasma density and temperature [144, 146, 147, and 148].

Previous studies have shown that for low latitudes, sufficient theories and observations are available for total electron content TEC and electron density but there is a gap concerning the ion density and the ion temperature. The present study focuses on the variations of total ion density (Ni) and ion temperature (Ti), in the low latitude topside ionosphere, for different solar activities, as recorded by ROCSAT-1between 1999 and 2003; a comparative study with the output of the IRI-2016 model has been also performed. Although the IRI model has been continuously improved [149], it still shows some shortcomings at equatorial and low latitude regions. Hence, the present analysis is then an additional contribution for testing and understanding the advantages and disadvantages of the IRI model.

## 5.2 DATA COLLECTION AND ANALYSIS

The ion density and ion temperature data used in the present study have been taken from the ionospheric plasma electrodynamics instrument (IPEI) onboard ROCSAT-1

satellite. The selected region for the analysis lies between 5-35ºGeo.N to 65-95°Geo. E in the altitude range of around 600±50 km.

The ROCSAT-1 satellite was launched in 1999 and its mission ended in 2004. It had a circular orbit at an average altitude of around 600 km with an orbit inclination angle of 35°[150, 127]. The instrument IPEI onboard the satellite had four sensors and made measurements for ion density, ion temperature, ion composition, and drift velocity. Detailed information about IPEI is given in [151].

The IRI-2016 model data has been obtained online from https://ccmc.gsfc.nasa.gov/modelweb/models/iri2016_vitmo.php.

The solar flux index (F10.7) data has been retrieved from the website https://omniweb.gsfc.nasa.gov/form/dx1.html. Based upon the strength of yearly solar flux magnitude F10.7, the years (1999-2003) have been categorized as rising, higher, and declining phases of solar activity. The year 1999 (F10.7~153.9 sfu),-is considered as a rising phase of solar activity; the year 2000 (F10.7~180 sfu), 2001(F10.7~ 181.1 sfu) and 2002 (F10.7~179.4 sfu) as high solar activity years; the year 2003(F10.7~128.4 sfu) as the declining phase of solar activity. Figure 5.1 represents the variation of F10.7 flux during the years 1999-2003(upper panel) and yearly averaged data count from 1999-2003 as measured by ROCSAT-1 satellite (lower panel).

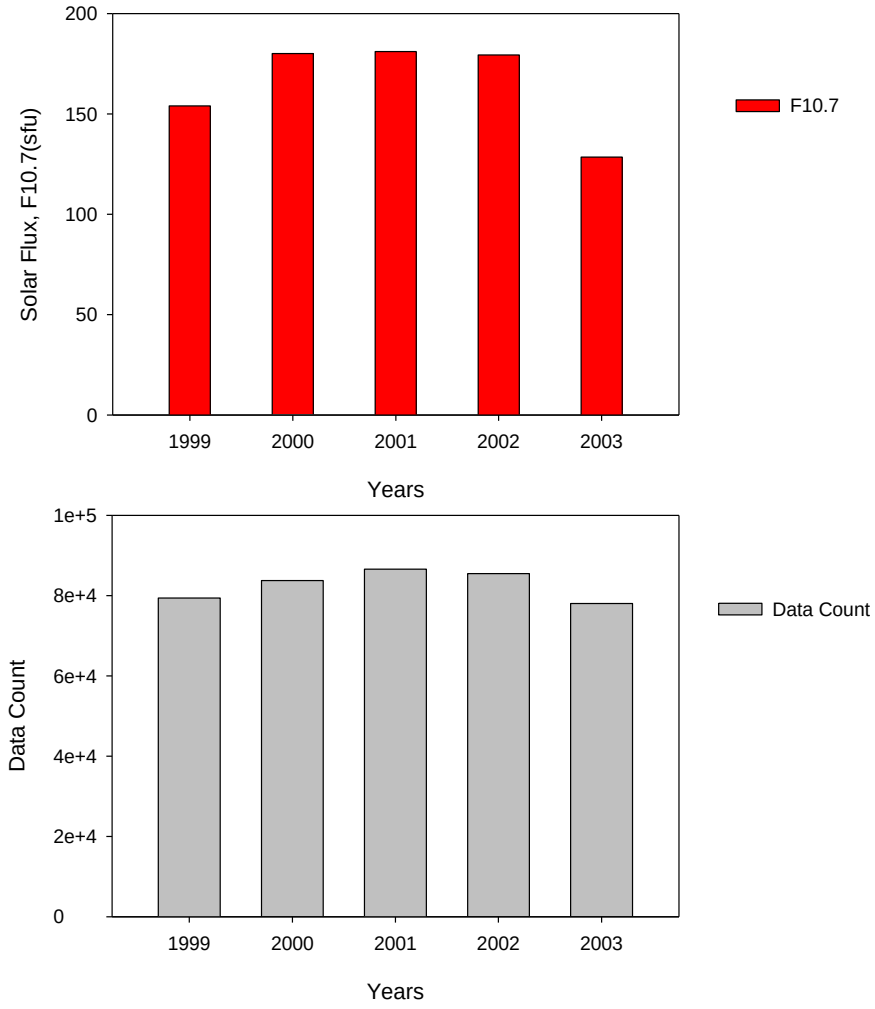


Figure 5.1: Variation of Solar Flux (F10.7, sfu) (upper panel) and yearly averaged data count as measured by ROCSAT-1 satellite (lower panel), between years 1999-2003.

## 5.3 ANNUAL DIURNAL VARIATION OF Ni AND Ti FOR YEARS 1999-2003

***Variation of total ion density, Ni:*** Figure 5.2, represents the annual variation of hourly averaged total ion density measured by ROCSAT-1 satellite (red coloured triangles) and estimated by IRI-2016 (black coloured circles), during different solar activity phases. The calculations for the IRI model have been made for each month and thereafter the monthly values were averaged for every year. The diurnal features shown by Ni as measured by ROCSAT-1 satellite during the year1999-2003 are a daytime peak; nighttime minima; an absolute minimum just before the local sunrise.

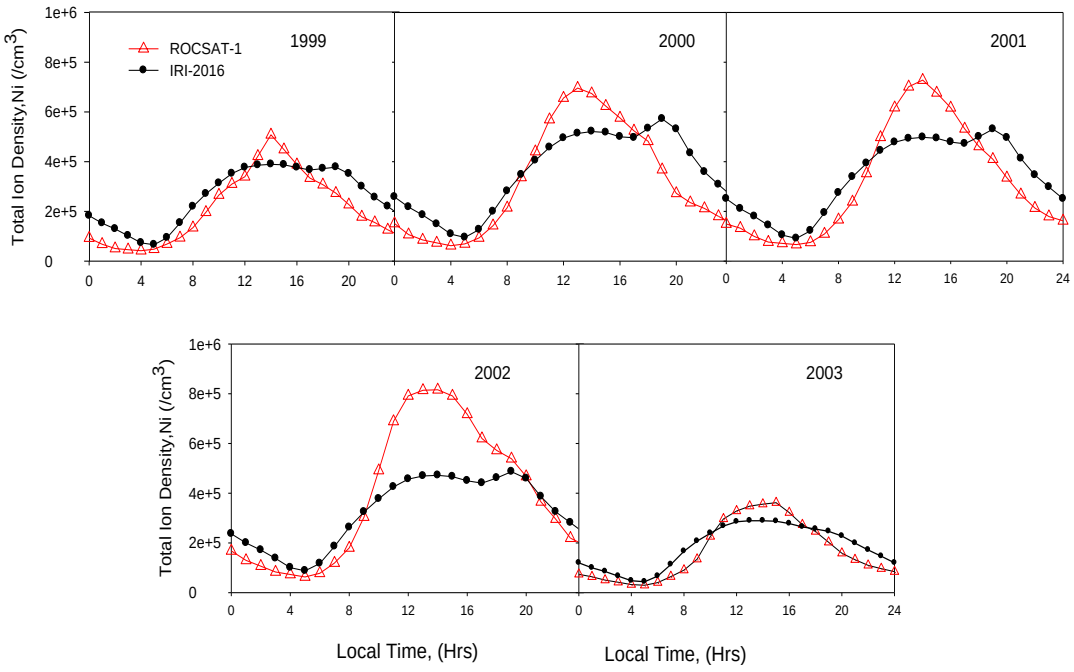


Figure 5.2: Annual variation of Ni ($cm^{-3}$) measured by ROCSAT-1 (red color) and estimated by IRI-2016 model (black color) for years 1999-2003.

During the rising (1999) and declining (2003) phases of solar activity, Ni shows a minimum of ~4.16E+04 and ~2.94E+04 $cm^{-3}$ respectively during pre-sunrise hours (~04:00/05:00 LT). Analysis by using SROSS-C2 data measurements has also shown a minimum density of Ni just before local sunrise [63]. Thereafter, Ni increases gradually due to photoionization of the neutral particles and attains a maximum value of 5.08E+05 to ~3.62E+05 $cm^{-3}$ during the daytime (~14:00 /15.00 LT). Ni then starts decreasing continuously through the evening and nighttime hours.

During high solar activity years 2000, 2001and 2002 the minimum values of Ni observed during pre-sunrise hours (~04:00/05:00 LT) are ~6.16E+04, 6.66E+04and 6.30E+04 $cm^{-3}$ respectively. The peak value of Ni observed in the afternoon hours (~ 13.00/14.00 LT) is 6.96E+05, 7.28E+05, and 8.16E+05 $cm^{-3}$during 2000, 2001, and 2002 respectively.

According to the IRI model, the diurnal features shown by Ni are a daytime relative maximum; a secondary absolute maximum during late evening hours; nighttime minima with an absolute minimum during pre-sunrise hours. During the years 1999 and 2003, Ni shows an absolute minimum of ~6.5E+04 $cm^{-3}$ and ~4.39E+04$cm^{-3}$

respectively at ~05:00 LT; the daytime peaks as 3.8E+05 $cm^{-3}$ and~2.8E+05 $cm^{-3}$ respectively at ~14:00 LT. The secondary absolute peak during 1999 is 3.78E+05 $cm^{-3}$ at ~19:00 LT whereas, in the year 2003 there is no secondary peak, so the daytime maximum becomes the absolute one.

During the high solar activity years 2000, 2001 and 2002 the absolute minimum values of Ni observed at ~5:00 LT is ~ 9.48E+04, 9.13E+04 and 8.77E+04 $cm^{-3}$ respectively; the day time peaks at ~14:00 LT is 5.21E+05, 4.97E+05 and 4.72E+05 $cm^{-3}$ respectively; the evening absolute maximum is modelled at ~19:00 LT as 5.71E+05, 5.30E+05 and 4.86E+05 $cm^{-3}$.The results of Figure 5.2 show that during high solar activity years higher day-time peaks of Ni are attained as compared to the rising and declining phases of solar activity. Hence, photoionization can be considered as the primary cause of daytime peaks. Moreover, this figure also shows that during all the investigated years (1999-2003), if compared to measurements made by ROCSAT -1, the IRI model predicts higher values of Ni in the pre-sunrise hours and lower values of Ni during the daytime. A further feature is that the IRI model shows evening enhancement that is not been observed by ROCSAT-1.

***Variation of ion temperature, Ti:*** The annual variation of hourly averaged ion temperature measured by ROCSAT-1(red coloured triangles) and estimated by IRI-2016 (black coloured circles) during different phases of solar activity is represented in Figure 5.3. The study region for Ti is around 600 km which is not the isothermal region of the ionosphere because the temperature is found to increase in the topside ionosphere.

The diurnal features observed by ROCSAT-1 measurements for Ti during years1999-2003 shows that Ti presents a minimum value during pre-sunrise hours and as the sun progresses, the Ti exhibits a sharp increment known as the morning overshoot [58]. Owing to photoionization, photoelectrons gain higher energy which they share with the surrounding electrons and ions through coulomb-collision; consequently, because of lesser electron/ion density in early morning hours, ion temperature starts increasing rapidly and attains a maximum/peak value at ~07:00 LT [50, 51, 59,]. After attainment of the morning peak, Ti experiences a daytime trough, and then, due to the pre-reversal enhancement phenomenon [139], it shows an evening enhancement followed by a nighttime decrease.

During the years 1999 and 2003, at ~ 07:00 LT, Ti shows morning peaks of ~1565 K and ~1491K respectively, while secondary peaks present values of ~1348 K and ~1292 K respectively at ~ 17/18:00 LT. During the high solar activity years, 2000, 2001, and 2002, the morning peaks are 1525K, 1504 K, and 1457 K (at 07:00 LT),

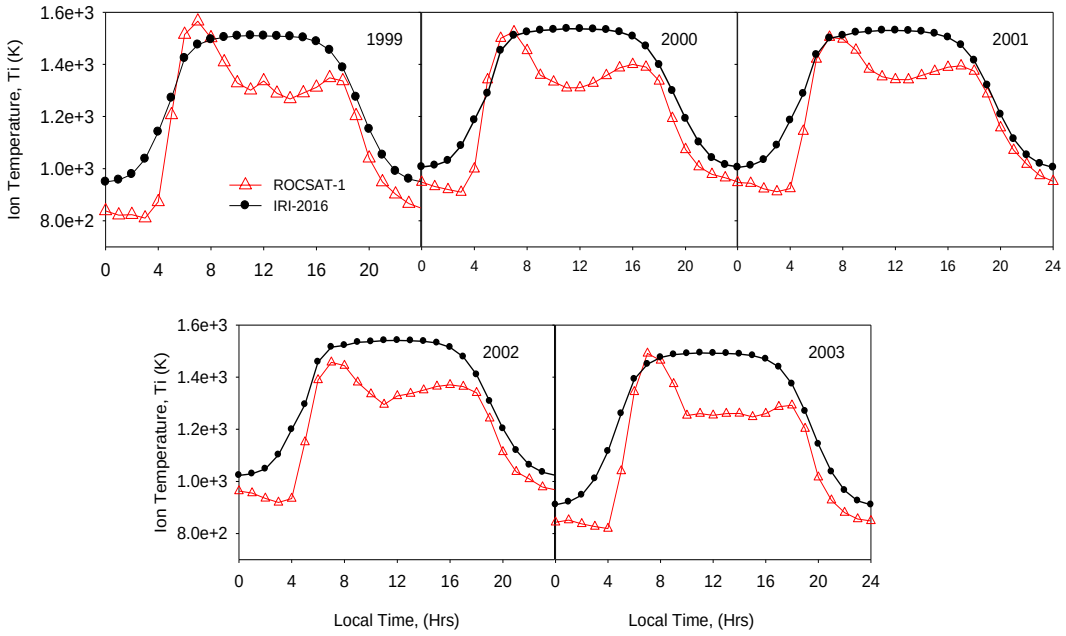


Figure 5.3: Annual variation of Ti (K) measured by ROCSAT-1 (red color) and estimated by IRI-2016 (black color) for years 1999-2003.

whereas the secondary peaks are ~1400K, 1394 K, and 1370K respectively at 16/17:00 LT. The nighttime Ti values are also observed to be higher during high solar activity years (~950 K) as compared to those of rising and declining solar activity years (~850 K). This may be due to the adiabatic expansion and compression of the plasma, flowing across the equator and along the field lines [152]. The same nighttime plasma features have been observed with the help of the Orbiting Geophysical Observatory satellite (OGO-6) at an altitude of 500 km [153].

According to the IRI model, the diurnal features shown by Ti are typical diurnal ones, with higher values during daytime and lower values during nighttime. For years 1999 and 2003, the morning peaks of Ti are observed as ~1475K and 1449 K respectively at ~ 07:00 LT. For years 2000-2002, the morning peaks of Ti are of higher magnitude i.e. ~1500K. The secondary peak of Ti visible in ROCSAT-1 measurements is not represented by IRI-2016 model.

The annual-diurnal behaviours of Ni and Ti show a different variation pattern. Specifically, during the daytime, when Ti presents a trough, Ni shows a peak value. For the topside ionosphere over India, also [69] investigated Ni and Ti and they observed a positive correlation between them during high solar activity and a negative correlation during low solar activity.

## 5.4 RELATIVE VARIATION OF $Ni_{ROCSAT-1}$ AND $Ni_{IRI-2016}$ DURING 1999-2003

To perform an analysis of the relative variation of Ni as measured by ROCSAT-1 and calculated by IRI-2016 model, the ratios ($Ni_{ROCSAT}/Ni_{IRI}$) have been plotted in Figure 5.4 (upper panels). This figure shows that during the whole investigated period (1999-2003) the IRI model overestimates the Ni measurements by ROCSAT-1 during nighttime and pre-sunrise hours, whereas underestimates them during the daytime. The largest differences of ratios are obtained during 12-14:00 LT and 22-04:00 LT where values vary from 0.4 (lower side; year 1999) to 1.7(upper side; year 2002). Only during the local time ~09-11:00 and ~17-18:00 LT, the ratio is equal to ~1, which means that the Ni value measured by ROCSAT-1is similar to that modelled by IRI.

Anyhow, Figure 5.2 shows that the diurnal pattern of Ni as measured by ROCSAT-1 and estimated by IRI are similar. Concerning this issue, Figure 5.4 (lower panels) shows the scatterplots between the two data sets (measured and estimated), along with the corresponding linear fit and the value of the correlation coefficient $R^2$. $R^2$ for 1999 and 2003 is found to be 0.84 and 0.89 respectively; while during high solar activity years (2000-2002) is found to vary from 0.73-0.85.

## 5.5 RELATIVE VARIATION OF $Ti_{ROCSAT-1}$ AND $Ti_{IRI-2016}$ DURING 1999-2003

To perform an analysis of the relative variation of Ti as measured by ROCSAT-1 and measured by IRI-2016 model, the ratios ($Ti_{ROCSAT}/Ti_{IRI}$) have been plotted in Figure 5.5 (upper panels).

From the graphs, it can be seen that during all the years (1999-2003) the ratio values are below 1, which means overestimated values of Ti modelled by the IRI model except during few morning peak hours in years 1999, 2000, and 2003.

Figure5.5 (lower panels) shows scatter plots between modelled and measured data, along with the corresponding linear fit and the value of correlation factor $R^2$. $R^2$ is found to be 0.86 during the years 1999 and 2003, while, during high solar activity years 2000-2002, is found to vary from 0.87-0.90.

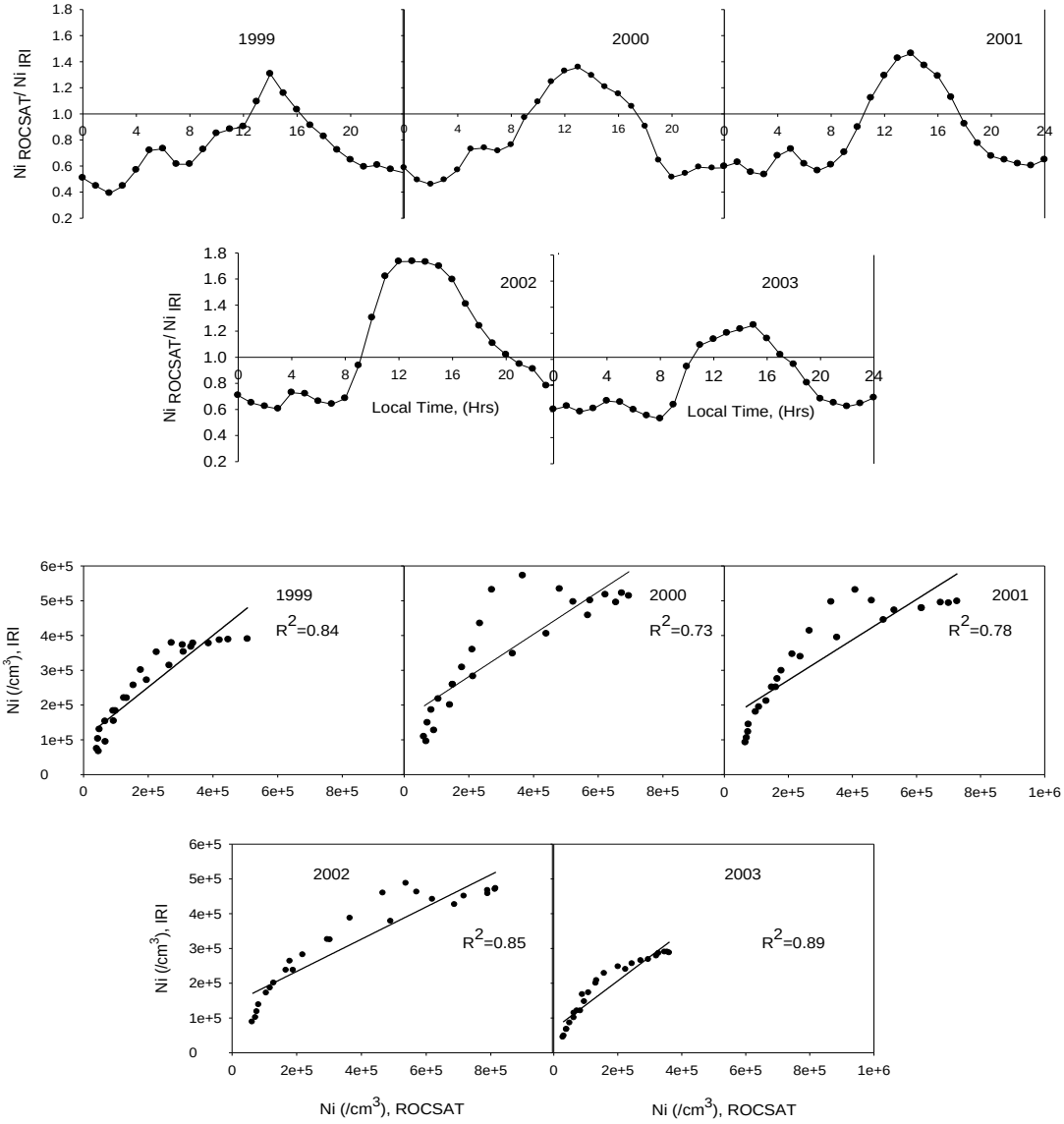


Figure 5.4: Variation of Ni measured by ROCSAT-1 relative to Ni estimated by IRI-2016 on a diurnal scale for years 1999-2003(upper panels). Scatter plots of two data sets, along with the corresponding linear fits and correlation coefficient values obtained for hourly averaged daytime values (10-16 LT) of Ni (lower panels).

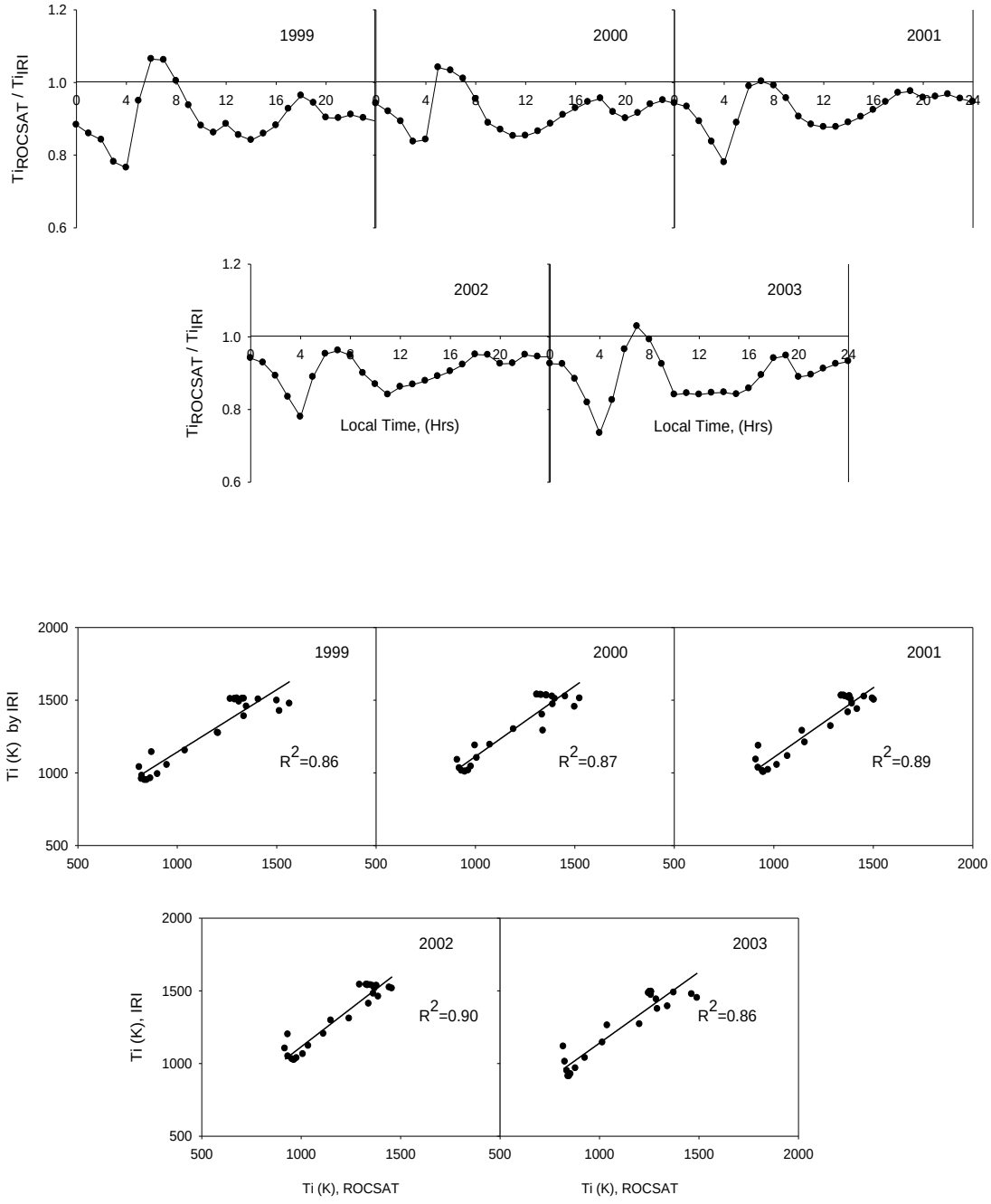


Figure 5.5: Variation of Ti measured by ROCSAT-1 relative to Ti estimated by IRI-2016 on a diurnal scale for years 1999-2003 (upper panels). Scatter plots of two data sets, along with the corresponding linear fits and correlation coefficient values obtained for hourly averaged daytime values (10-16 LT) of Ti (lower panels).

## 5.6 RELATIONSHIP OF Ni AND Ti WITH SOLAR FLUX INDEX, F10.7

The solar flux, F10.7 is very often used as an index to monitor solar activity. Since the solar radio emission takes place from the chromosphere and corona, it indicates variations occurring in the Sun during different phases of solar activity [25]. Figure 5.6 shows the scatter plots of Ni vs. F10.7 and Ti vs. F10.7.

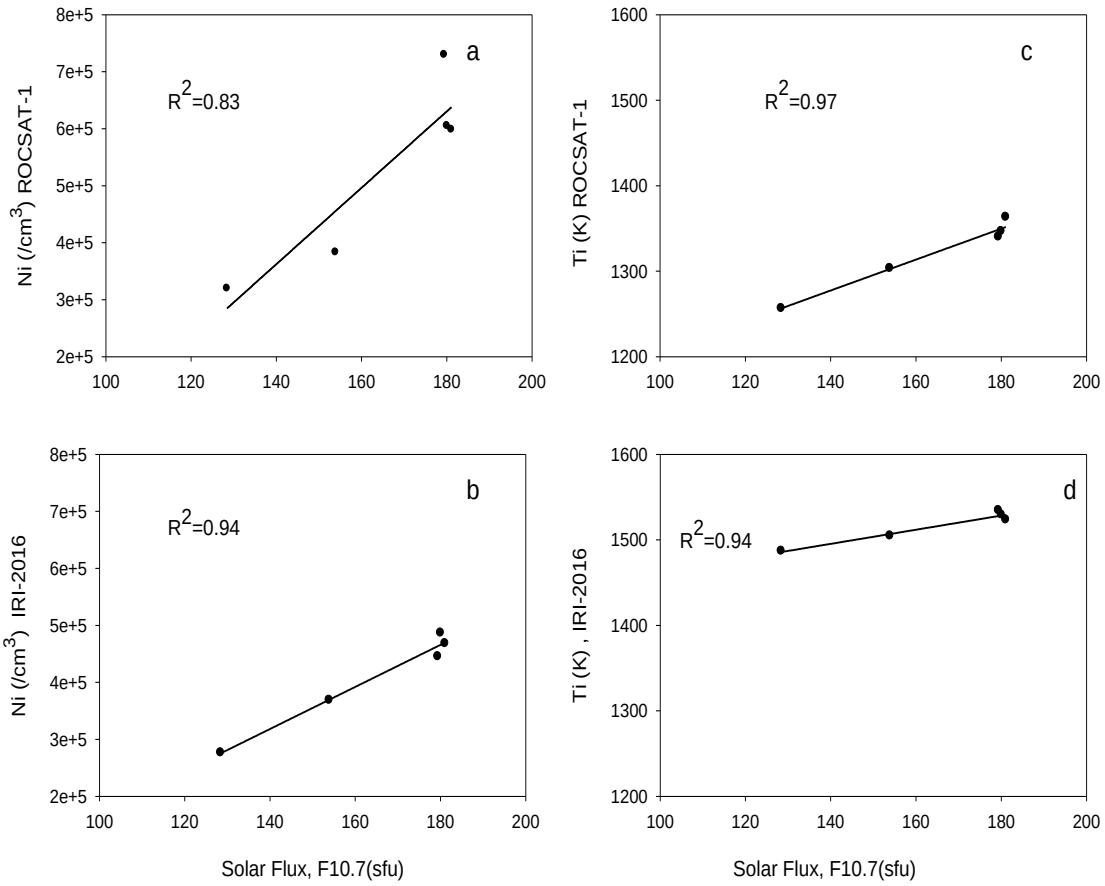


Figure 5.6: Scatter plots between yearly averaged values of (left panels) Ni, $cm^{-3}$ and solar flux F10.7, sfu, and between averaged values of (right panels) Ti (K) and solar flux F10.7, sfu, for (upper panels) ROCSAT-1 and (lower panels) IRI-2016, for years 1999-2003.

To plot this figure, yearly averaged values of F10.7, Ni, and Ti during the daytime (10:00-16:00 LT) have been utilized. The correlation coefficient $R^2$ between Ni and F10.7 is found to be 0.83 for ROCSAT measured values (Figure 5.6a) and 0.97 between IRI estimated values and F10.7 (Figure 5.6 b). This shows that photoionization via extreme ultraviolet radiation remains a major source of ionization in our selected region of study. This confirms what was found by [63] who observed

higher photoionization during high solar activity in the year 2000 compared to that of the low solar activity in the year 1995, using SROSS-C2 satellite data.

Instead, the correlation coefficient $R^2$ between Ti and F10.7 is found to be 0.97 for ROCSAT measured values (Figure 5.6 c) and 0.94 for IRI estimated values (Figure 5.6 d). Both $R^2$ values are pretty similar to each other during the years 1999-2003, which indicates that Ti data during daytime (10:00-16:00 LT) is in good agreement with the solar flux index.

## 5.7 CONCLUSION

In the present study, we have examined the variation of topside ionospheric parameters, specifically the total ion density, Ni, and the ion temperature, Ti, at low latitudes during different phases of solar activity (1999-2003). The Ni and Ti data has been obtained from ROCSAT-1 satellite and then a comparison is made with the estimations of the IRI-2016 model. The findings of the present analysis can be summarized in the following points.

1. The annual diurnal analysis of Ni (measured by ROCSAT-1) shows a minimum value just before local sunrise (~04:00/05:00 LT), a daytime peak (~13:00/14:00 LT), and then a gradual decrement through the evening and nighttime.
2. During high solar activity years, measured Ni data exhibited steeper enhancements with a higher magnitude of the peak density as compared to those during the rising and declining phases of solar activity. This shows a direct dependency of the ion density on solar flux.
3. During all the considered years (1999-2003), the IRI-2016 model overestimates Ni data, specifically in the nighttime and pre-sunrise hours. On the contrary, the model underestimates Ni during the daytime. Also, the IRI model predicts evening enhancements in Ni which are not observed in ROCSAT-1 measurements.
4. The annual diurnal analysis of Ti (measured by ROCSAT) shows that Ti exhibits a morning peak (morning overshoot, ~07:00 LT), a daytime trough, and a secondary peak (evening enhancement) followed by nighttime minima and a minimum before the sunrise.

5. According to ROCSAT-1 measurements, secondary peaks of Ti are of higher magnitude (~1500K) for years 2000-2002 as compared to the years 1999 and 2003 (~1400K ). On the contrary, the IRI-model cannot model the Ti secondary peaks measured by ROCSAT-1.
6. For each year scatter plots between Ni data measured by ROCSAT-1 and those estimated by the IRI model for years 1999-2003 have been generated; they indicate $R^2$ value ranging from 0.7-0.8. Analogous scatter plots for Ti show $R^2$ values ranging from 0.8-0.9.
7. We have found that Ni and Ti are strongly positively correlated with solar-flux (F10.7). In this case, the correlation coefficient factor $R^2$ obtained for Ni and Ti during daytime (10:00-16:00 LT) was ~ 0.8 and ~ 0.9 respectively.

At last, it can be concluded that an overall evaluation demonstrates a moderate agreement between the IRI-2016 model's estimations and ROCSAT-1 measurements. However, the model still requires some improvements to be done, left as a scope for future work.

# CHAPTER 6

# IONOSPHERIC RESPONSE TO GEOMAGNETIC STORMS OVER LOW LATITUDE INDIAN REGION

## 6.1 INTRODUCTION

The study of 'geomagnetic storm effects' falls under one of the most significant research areas while learning about the solar-terrestrial environment. The above study is important due to the following reasons. Firstly, the ionosphere acts in a very complex manner during the geomagnetic storm. Secondly, Geomagnetic storms affect the solar-terrestrial environment, the ground-based communication systems, ionospheric radio propagation, and military and commercial operations [154, 155]. Thirdly, it also helps in improving the prevailing ionospheric models. Thus, the study of 'geomagnetic storm's effects' on ionospheric parameters has become a necessity.

The geomagnetic storm (GS) is a phenomenon that occurs in the near-Earth environment in response to solar activity. When the Earth's magnetic field is severely disturbed, a "magnetic storm" is said to occur. The Earth's magnetic field is affected by solar events like solar flares, high-speed solar wind streams, and coronal mass ejections which results in geomagnetic field disturbances and causing geomagnetic storms.

The primary sources causing geomagnetic storms are coronal mass ejection (CMEs), solar flares, or a high-speed stream (co-rotating interaction region or CIRs) associated with the solar winds [30]. In all the cases if the interplanetary magnetic field (IMF) field is directed southward, opposite to the geomagnetic field lines orientation then the disturbed Earth's magnetic field can be noticed as an abrupt drop in the Earth's magnetic field strength, known as the main phase. This reduced magnetic field strength may last for a few hours to a period of several days and then recovers back to its original value, known as the recovery phase [96, 156].

The equatorial and low latitude ionosphere's response towards geomagnetic storm is different as compared to mid and high latitude regions because of exhibiting some unique characteristics such as plasma fountain, equatorial ionization anomaly (EIA), the equatorial temperature and wind anomaly (ETWA), equatorial electrojet, EEJ,

plasma bubble and spread F, etc. The horizontal orientation of the geomagnetic field lines at the equator and the shift between geographic and geomagnetic equator is considered to be the principal reason for these irregularities at the low latitude ionosphere [157].

In the present chapter, the variations in the ionospheric parameters ($O^+$, $H^+$ density, and ion temperature ) due to a weak and moderate geomagnetic storms have been studied over the low latitude, F2 (~600 km altitude) region using ROCSAT-1 satellite data. The novelty of the present study covers two aspects. Firstly, one can find abundant literature that analyses the effects of high magnitude geomagnetic storms (severe or great storms) on ionospheric parameters over high/mid-latitudes using GPS data but the effects of weak/moderate magnitude geomagnetic storms, over the low latitudinal region are still sparse. Thus more work needs to be done in this direction. Secondly, most of the earlier work focuses on the study of variation of electron and ion density due to geomagnetic storms. A very few reporting on electron and ion temperature over the low latitudes can be found. The ROCSAT-1 satellite measures ion density and ion temperature. Thus, provides us with an opportunity to study the anomalous behaviour of ion temperature as well, during geomagnetic storms. Moreover, the study has also been compared with the IRI-2016 model.

## 6.2 DATA COLLECTION AND ANALYSIS

### *Data collection*

To analyze the variations in the ionospheric ion densities and the temperature during geomagnetic storms, data from Ionospheric Plasma and Electrodynamics Instrument (IPEI) onboard the Republic of China Satellite (ROCSAT-1) has been used. ROCSAT- 1was launched on January 27, 1999, at an average altitude of 600 km, with an inclination angle of $35^o$ in a circular orbit [127, 150, 151 ]. The IPEI onboard satellite had four sensors for measurement of the ion density, ion temperature, and the ion drift velocity vector. The ROCSAT-1 satellite successfully completed its journey for 5 years, from January 1999 to June 2004. The ROCSAT-1 data is well calibrated. The error limits for ion temperature are ± 10% in the temperature range from 500 to 10,000 K and similar (± 10%) for total ion density Ni in the range from 50 to $5\times10^6$ $cm^{-3}$ [151].

The geomagnetic storm data for the years 1999 and 2000 have been taken from the website https://www.spaceweatherlive.com/en/auroral-activity/top-50-geomagnetic-storms.

The earthquake activity data during the study period has been taken from USGS website i.e. https://earthquake.usgs.gov/earthquakes/search.

$Kp_{max}$ index and Dst index data have been taken from the website http://wdc.kugi.kyoto-u.ac.jp/kp/index.html and https://omniweb.gsfc.nasa.gov/form/dx1.html respectively.

***Data Analysis***

To study the behaviour of the ionospheric parameters: $H^+$, $O^+$ and Ti, the ROCSAT-1 satellite and IRI 2016 model data was sorted out for the region encompassed between 5-35° geog. N and 65-95° geog. E at an average altitude of about 600 km. In the IRI-2016 model the average values for $H^+$, $O^+$ and Ti were calculated over a latitudinal range of 5° to 35° N geog latitude and 77° E geog longitude as an input.

In the present work, two geomagnetic storm events are selected (from list of top 50 geomagnetic storms, https://www.spaceweatherlive.com/en/auroral/top-50-geomagnetic- storms) which are: one on 30 July 1999 ($Kp_{max}$ = 8-, Dst= ~ -53 nT), a weak GS and second on 13 November 1999 ($Kp_{max}$ = 6+, Dst= ~ -106 nT), a moderate GS [29]. Although according to the storm selection scheme introduced by Loewe and prolss, these storms falls under the category of moderate and strong but as the Dst values -53 and -106 nT are very close to -50 and -100 nT and also these storms did not end up with significant results or variations hence we considered them as weak and moderate storms.

Data selection is the most crucial part of this analysis as satellite rarely passed over the selected region during storm time.

The present study has been explained in two sections. In section one, the variations in ion density and temperature have been observed specifically during the main phase and recovery phase of the GS.

Whereas, in section two the variations in ion density and temperature have been observed during a time window of 15-24 UTC. This time window has been restricted to ±3 hours of the $Kp_{max}$ range (1800-2100 UT) to get a more precise analysis and is kept the same for both quiet and disturbed days. The quietest days are selected from WDC Kyoto (http://wdc.kugi.kyoto-u.ac.jp/qddays/index.html). Also, this analysis has been compared with IRI-2016 modelled values which demonstrate marked differences.

The ionospheric parameters also vary due to seismic activities over the low latitude F2 region. Thus, only those geomagnetic storms have been selected which are free from earthquakes in the coverage area of ROCSAT-1. This is done by first selecting all the geomagnetic storms with $K_{p_{max}} \geq 5$. After that, all the days associated with earthquakes with a magnitude of 4-10 and within 0-30 km depth have been excluded from the present analysis. Recently, it has been observed that seismo-ionospheric coupling is an emerging field of research. One can find enough literature that suggests the anomalous behaviour of ionospheric parameters due to seismic activities. [96, 101-105]. Aggarwal et al. [2016] have also observed changes in total electron content over Qinghai station using GPS data. Large-scale plasma irregularities present in the EPZ (Earthquake Preparation Zone) have been reported using topside sounders [103]. [159 and 160] statistically analyzed a larger database of plasma densities using Intercosmos-24. [160] have analyzed the anomalous behaviour of ionospheric densities using 3000 orbits of Intercosmos-24 satellite co-relating global distribution of seismic activity and ion density variations.[159] observed precursory type significant changes in the ion density distribution pattern over earthquake epicentres during the night time over 500 km altitude. Hence, there is the necessity of excluding the events that are affected by seismic activities.

## 6.3 RESULTS AND DISCUSSIONS

### 6.3.1 Variation in $O^+$, $H^+$, and Ti during Main and Recovery Phase of Weak GS

***Section 1:*** In this section, in particular, the main phase and the recovery phase of both the GS have been studied.

In the figure 6.1, the passes of ROCSAT-1 satellite during quiet and disturbed days during the two GSs events (30 July 1999 and 13 Nov 1999), considered in the present

study have been shown. It cleared that the spatial coverage of the ROCSAT-1 satellite during the disturbed and quiet days was same.

A geomagnetic storm that commenced on 30 July 1999 at around 1800 UT was associated with M class flare and interplanetary coronal mass ejection (ICME). The maximum X-ray intensity of solar flare as recorded by GOES satellite was 8.6E-03 $W/m^2$ during the peak flare time. The maximum velocity of ICME was 660 km/sec as reported on the website http://www.srl.caltech.edu/ACE/ASC/DATA/level3/icmetable2.htm. On 30 July, the maximum solar wind proton density and solar wind velocity were around 41.5 $N/cm^3$ and 670 km/sec at about 20 UTC and 23 UTC respectively as observed by http://www.spaceweatherlive.com/en/archive/1990/07/30/aurora.

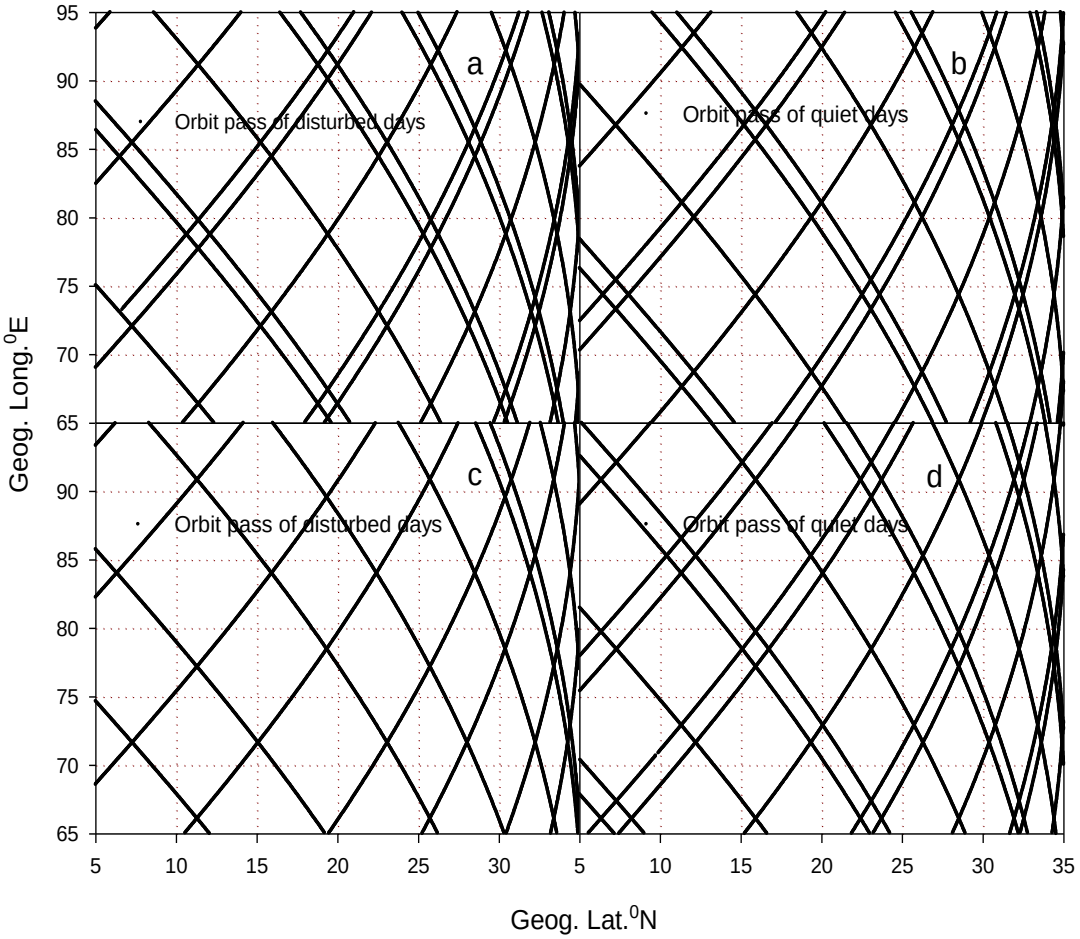


Figure 6.1: Orbit Pass of ROCSAT-1 satellite on disturbed days (a-13 Nov 1999 event, c-30 July 1999 event) and quiet days (b-13 Nov 1999 event, d-30 July 1999 event).

Figure 6.2 represents the variation of southward component of interplanetary magnetic field IMF Bz (a) Dst index (b) solar wind (c) and solar wind proton density (d) during 30, 31 July and 1 Aug. 1999. From Figure, it is observed that there were southward as well as some northward excursions of the IMF Bz bearing a maximum value of -10.7 nT at 20 UTC, which might have resulted in ring current. However, the magnitude of the ring current was not large enough to produce a significant decrease in the Dst. The Dst value started decreasing significantly from around 21UTC on 30 July, consequently on setting its main phase from thereon, which stays till 25 UTC (i.e. 1 am on 31 July) where Dst fell to its maximum value of about -53 nT and thereafter recovery phase took place up till 50 UTC (i.e. 2 am on 1 August, where the Dst value returns to about $1/4^{th}$ (~ -15 nT) of its maximum value).

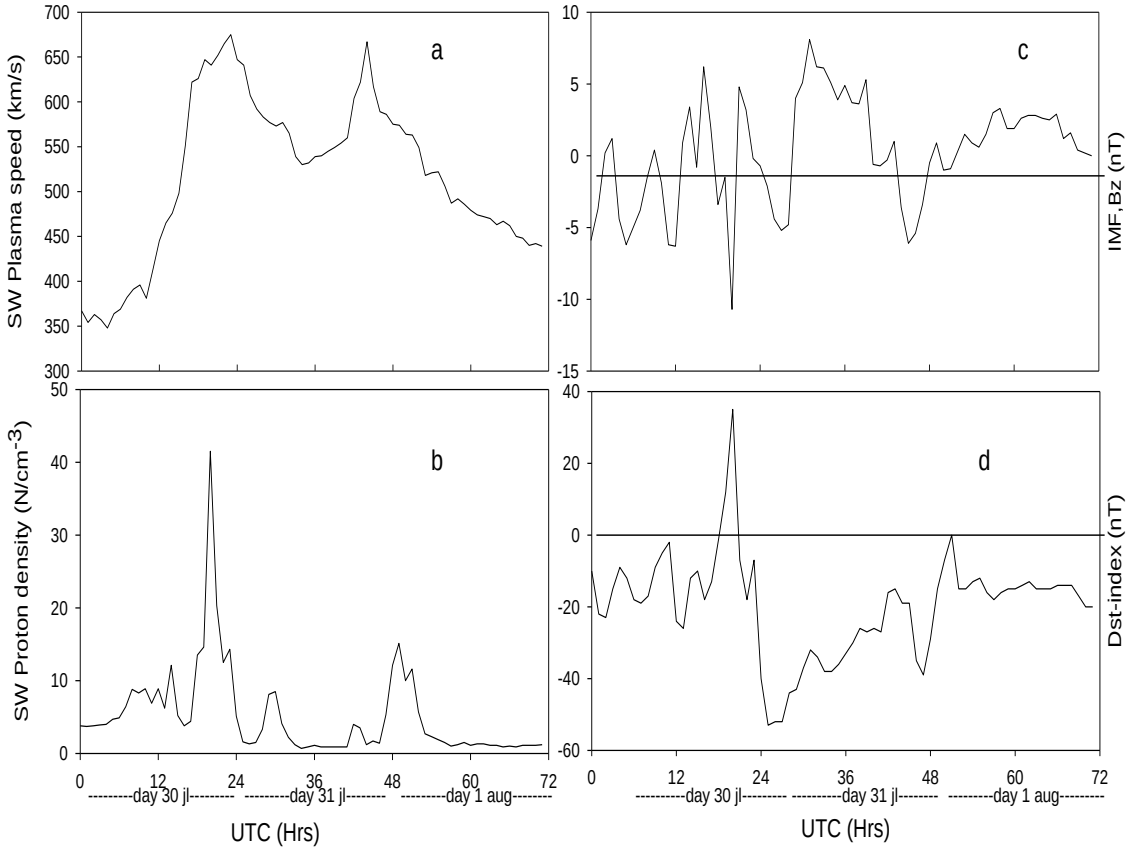


Figure 6.2: Representation of solar wind speed, ($SW_V$, (km/s)) (a), solar wind proton density, ($SW_D$, ($cm^{-3}$)) (b), IMF Bz, nT (c) and Dst index, nT (d) during 30, 31 July and 1 August 1999.

Figure 6.3 represents the variation of $O^+$ density (a), $H^+$ density (b), and ion temperature (c) during the main and recovery phase of the GS. Since this was a weak magnitude GS, and even took place in the nighttime so the ion density and temperature were not expected to show many variations. The ROCSAT data analysis also reflects the same behaviour that $O^+$ density and Ti did not exhibit any significant variation during the main and recovery phase but Ti decreases notably near the end of the recovery phase (on 1 August). On the other hand, $H^+$ density shows marked variations, it increased significantly during the recovery phase than in the main phase.

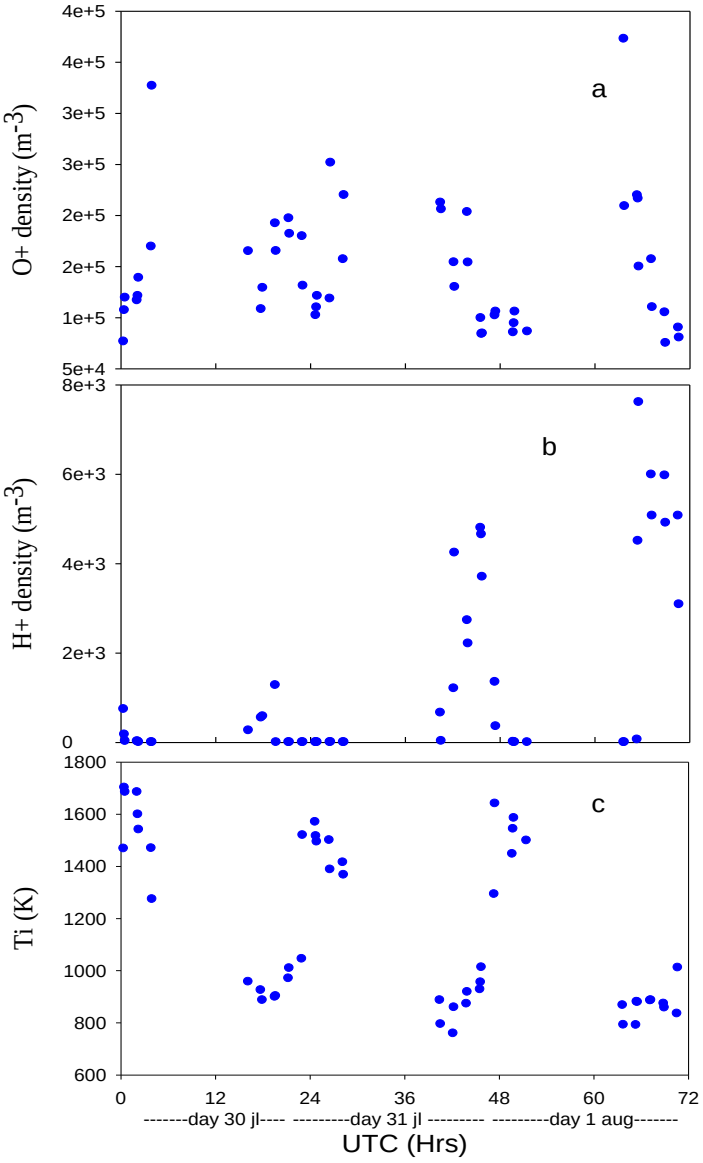

Figure 6.3: Variation of $O^+$ density, $cm^{-3}$ (a), $H^+$ density, $cm^{-3}$ (b) and Ti, K (c) during main phase (21-25 UTC) and recovery phase (25-50 UTC) for GS on 30 July 1999.

### 6.3.2 Variation in $O^+$, $H^+$, and Ti during Main and Recovery Phase of Moderate GS

Another geomagnetic storm that commenced on 13 November 1999 was associated with M class flare and ICME. The maximum X-ray intensity of solar flare as recorded by GOES satellite was 8.4E-02 W/m2 during the peak flare time. The maximum velocity of ICME was 480 km/sec as reported on the website http://www.srl.caltech. edu/ACE/ASC/DATA/level3/icmetable2.htm. The maximum solar wind velocity and solar wind proton density were around 480 km/s and 5 $N/cm^3$ at around16UTC and 21UTC respectively as observed by https://www.spaceweath erlive.com/en/archive/ 1999/07/30/aurora.

Figure 6.4 represents the variation of southward component of interplanetary magnetic field IMF Bz (a) Dst index (b) solar wind (c) and solar wind proton density (d) during 13, 14, and 15 November 1999. This strong GS evolved gradually with small southward Bz bearing a maximum value of -11.5 nT for 18-19 UTC. On 13 November, the Dst at around 16 UTC started dropping continuously and reached up to a maximum value of ~ -106 nT. Hence, after staying in the main phase (16-22 UTC) on 30 July, it then entered in its recovery phase. It recovered back completely at 65 UTC (i.e. 17 UTC on 15 Nov) where the Dst value returned to about $1/4^{th}$ (~ -26 nT) of its maximum value.

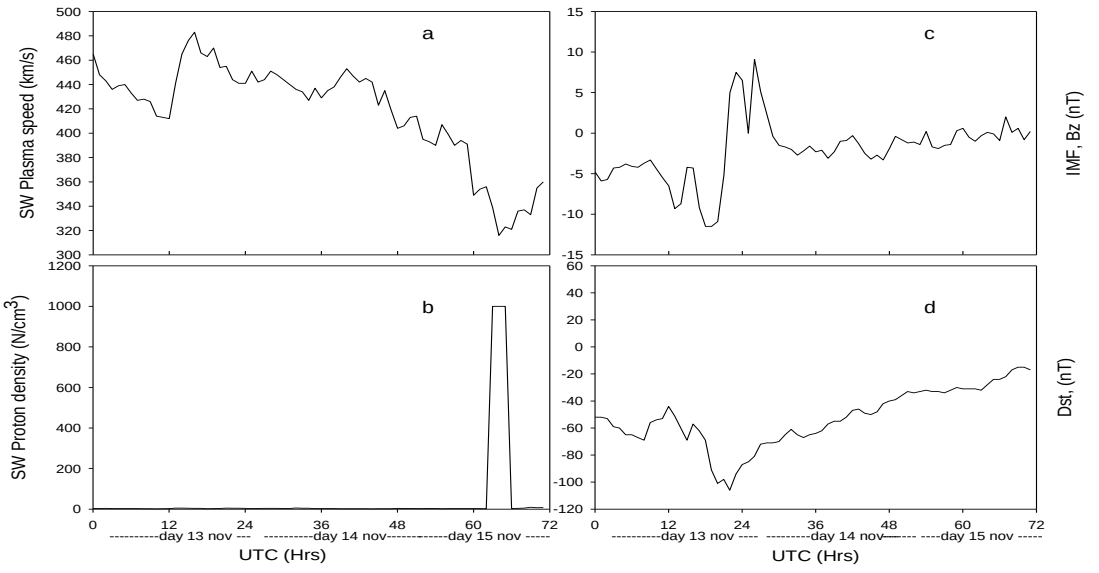

Figure 6.4: Representation of solar wind speed, ($SW_V$, (km/s)) (a), solar wind proton density, ($SW_D$, ($cm^{-3}$)) (b), IMF Bz, nT (c) and Dst index, nT (d) during 13, 14 and 15 November 1999.

Figure 6.5 represents the variation of $O^+$ density (a), $H^+$ density (b), and ion temperature (c) during the main and recovery phase of strong GS. Since it was a strong magnitude GS, the figure also represents an expected variation in $O^+$ and $H^+$ densities. $O^+$ density was found to increase during the main phase (13 Nov) than in the recovery phase. However, the $H^+$ density increased in the recovery phase than the main phase. And Ti did not show any significant variation during main and recovery phase except a notable decrement near the end of the recovery phase (on 15 Nov).

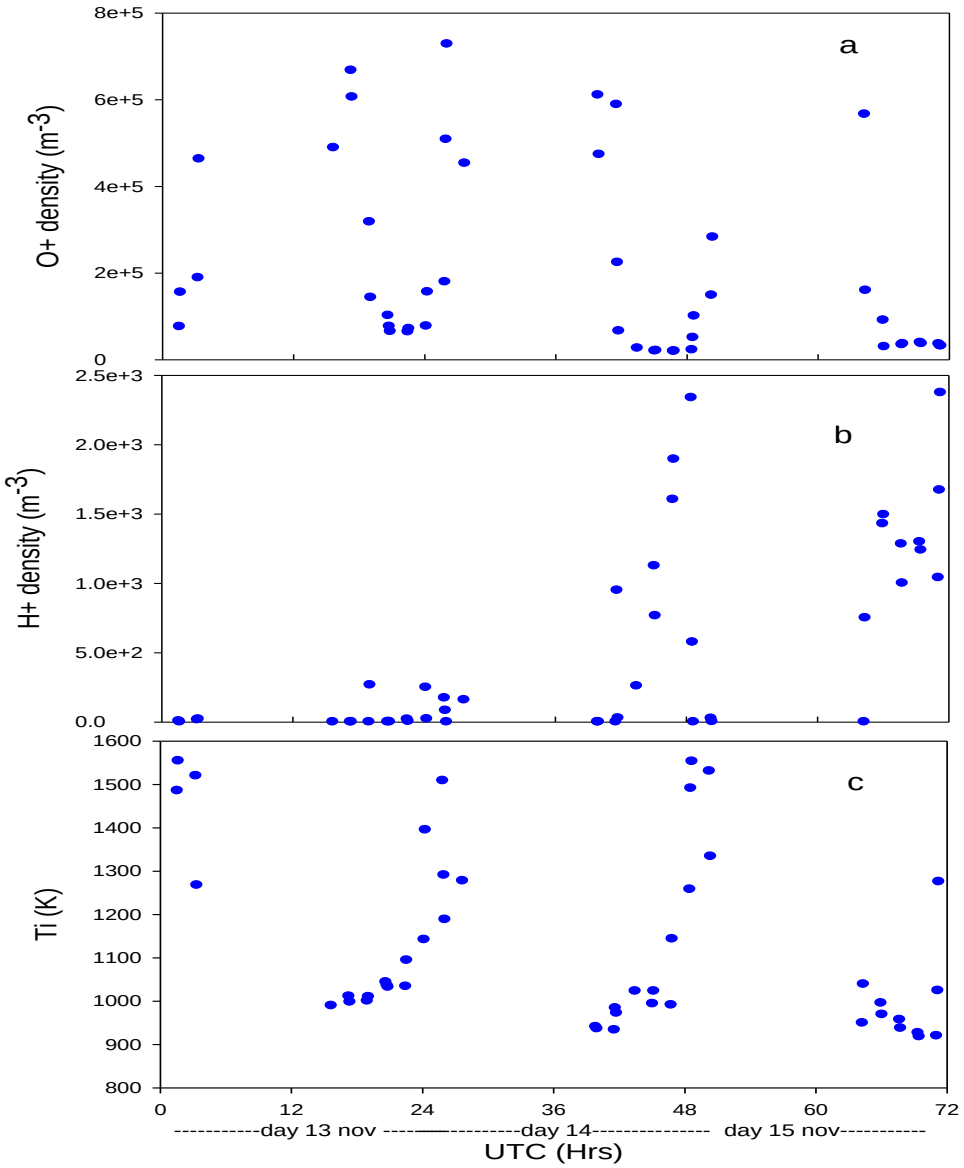


Figure 6.5: Variation of $O^+$ density, $cm^{-3}$ (a), $H^+$ density, $cm^{-3}$ (b) and Ti, K (c) during main phase (16-22 UTC) and recovery phase (22-65 UTC) for GS on 13 November.

***Section 2***

## 6.4 ION DENSITY AND TEMPERATURE VARIATION DURING 15-24 UTC HOURS

In this section, the variations in ion density and temperature have been observed in a certain time window of 15-24 UTC. This time window was kept same for both quiet and disturbed days and was restricted to ±3 hour of the $Kp_{max}$ range. For both of the

storms, the Kp index was maximum in the 3-hour interval of 18-21 UTC. Hence, this time window was set to study the variations in ion density and temperature during disturbed days and quiet days which were then further compared with the IRI-2016 modelled values.

In Figure 6.6, the variation of ion density and temperature (event - 30 July 1999), measured and modelled in an interval of 15-24 UTC have been shown with their average values during disturbed days (shown in red colour) and quiet days (shown in black colour). The disturbed days were 30, 31 July and 1 August whereas the quiet days selected were 16, 17 and 18 July.

The average ionospheric $O^+$ density during disturbed days was 1.49E+05 $cm^{-3}$ and 7.98E+04 $cm^{-3}$ during the quiet days. Thus the $O^+$ density during disturbed days was found to be ~1.8 times higher than the normal day's ion density. Whereas by the IRI model, this incremental ratio ($O_D^+/O_Q^+$) was ~1.06.

The average $H^+$ density observed during disturbed days was 1.27E+03 $cm^{-3}$ and during the quiet days 2.36E+03 $cm^{-3}$, which illustrated that $H^+$ density during quiet days was ~1.8 times higher than the disturbed days. Whereas by the IRI model, this incremental ratio ($H_Q^+/H_D^+$) was ~2.51.

Similarly, the average ion temperature during disturbed days was 975 K and 895 K during quiet days which showed an average increment by a factor of ~1.08 during disturbed days as compared to the quiet days whereas, with the modelled values, the ratio ($T_{iD}/T_{iQ}$) was found ~1.05.

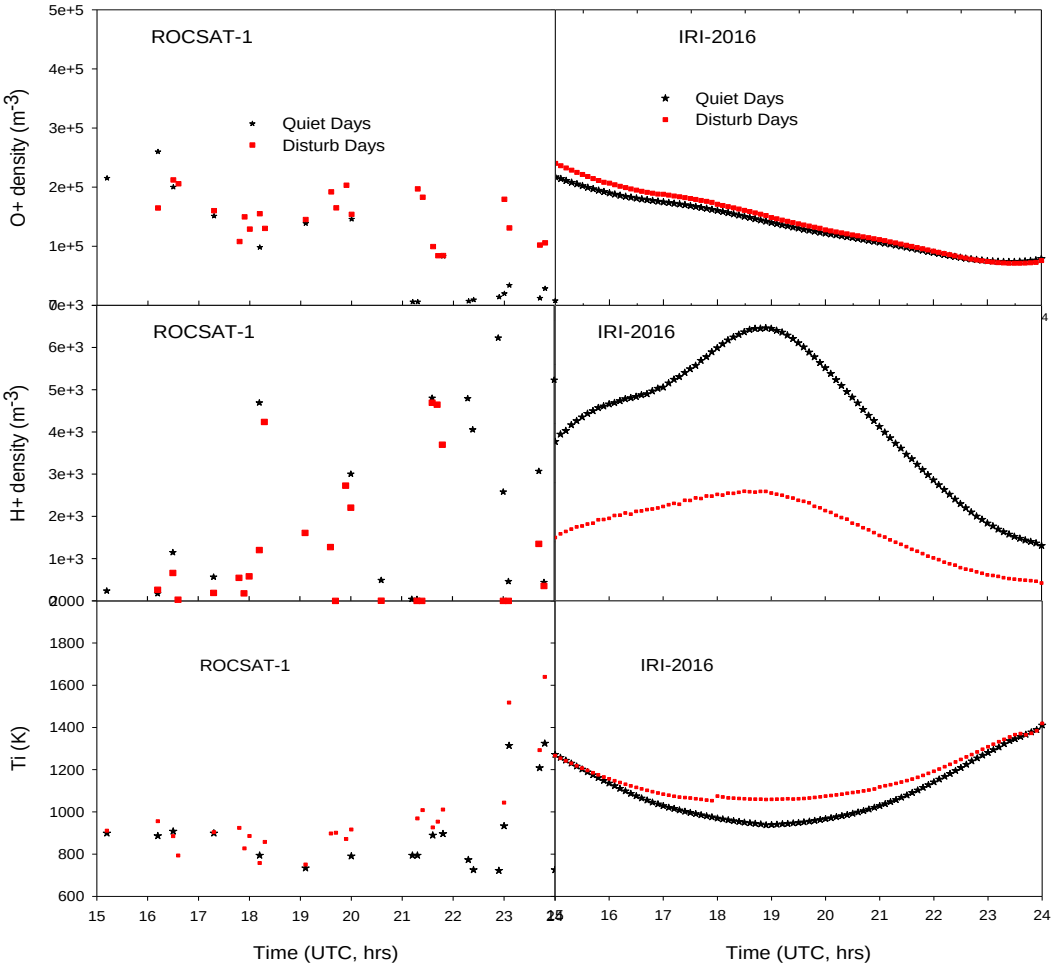


Figure 6.6: Representation of ROCSAT-1 measurements (Left panels) ) and IRI-2016 estimations (Right Panels) for average $O^+$ density($cm^{-3}$), $H^+$ density($cm^{-3}$) and Ti(K), during quiet days (black) and disturbed days (red) for GS on 30 July 1999.

In Figure 6.7, (event – 13 Nov. 1999), illustrates the ion density and temperature variations, measured and modelled with their average values in an interval of 15-24 UTC during disturbed days (shown in red colour) and quiet days (shown in black colour). The disturbed days were 13, 14, 15 November, whereas the quiet days selected were 26, 27 and 28 November 1999.

The average ionospheric $O^+$ density calculated during disturbed days was 2.07 E+05 $cm^{-3}$ and 7.51E+04 $cm^{-3}$ during the quiet days. Thus the $O^+$ density during disturbed days was found to be ~2.7 times higher than the normal day's ion density. Whereas by the IRI model, this incremental ratio ($O_D^+/O_Q^+$) was ~1.1.

The average $H^+$ density observed during disturbed days was 3.67 E+02 $cm^{-3}$ and during the quiet days 2.34 E+03 $cm^{-3}$, which illustrated that $H^+$ density during quiet days was ~6.3 times higher than the disturbed days. Whereas by the IRI model, this incremental ratio ($H_Q^+/H_D^+$) was ~2.8. Similarly, the average ion temperature during disturbed days was 1007 K and 986 K during quiet days which showed an average increment by a factor of ~1.02 during disturbed days as compared to the quiet days whereas, with the modelled values, the ratio ($T_{iD}/T_{iQ}$) was found ~1.13.

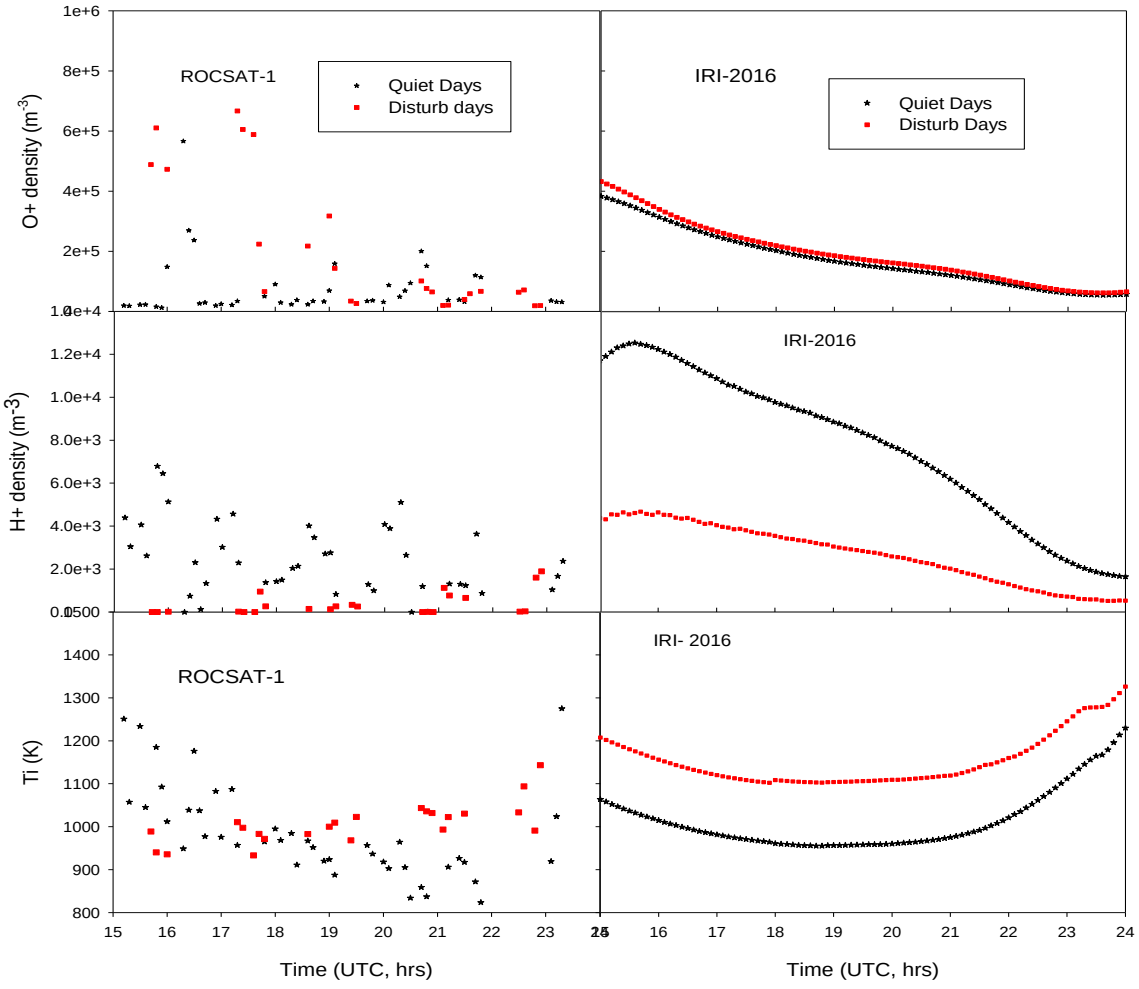


Figure 6.7: Representation of ROCSAT-1 measurements (Left panels) ) and IRI-2016 estimations (Right Panels) for average $O^+$ density($cm^{-3}$), $H^+$ density($cm^{-3}$) and Ti(K), during quiet days (black) and disturbed days (red) for GS on 13 November 1999.

Table 6.1 summarizes the details about the $O^+$, $H^+$ density and Ti variations during selected geomagnetic storms.

Table 6.1: Variations observed in O+, H+ and Ti by ROCSAT-1 and IRI-2016, during a weak (30 July, 1999) and moderate (13 November, 1999) geomagnetic storm

| ***30 July 1999*** | | | | | | |
|---|---|---|---|---|---|---|
| **Parameter** | **ROCSAT-1** | | | **IRI-2016** | | |
| Avg. $O^+$ density | Disturb Days (D) | Quiet Days (Q) | Ratio factor | Disturb Days (D) | Quiet Days (Q) | Ratio factor |
| | 1.49e+5 | 7.98e+4 | D/Q= 1.8 | 1.41e+5 | 1.34e+5 | 1.0 |
| Avg. $H^+$ density | 1.27e+3 | 2.36e+3 | Q/D= 1.8 | 2.47e+3 | 6.20e+3 | 2.5 |
| Avg. Ti | 975.28 | 895.48 | D/Q= 1.08 | 1154.44 | 1092.90 | 1.05 |
| ***13 November 1999*** | | | | | | |
| **Parameter** | **ROCSAT-1** | | | **IRI-2016** | | |
| Avg. $O^+$ density | Disturb Days (D) | Quiet Days (Q) | Ratio factor | Disturb Days (D) | Quiet Days (Q) | Ratio factor |
| | 2.07e+05 | 7.51e+04 | D/Q= 2.7 | 1.91e+05 | 1.74e+05 | 1.1 |
| Avg. $H^+$ density | 3.67e+02 | 2.34e+03 | Q/D= 6.3 | 2.71e+03 | 7.69e+03 | 2.8 |
| Avg. Ti | 1007.065 | 986.3135 | D/Q= 1.02 | 1153.19 | 1013.63 | 1.13 |

This anomalous variation observed in ion density could be due to the movement of both meridional and storm-induced winds towards the equator. These winds uplift the ionosphere from the equator towards the poles. However, over the low latitudes, these ions diffuse down hence, showing an increment in ion density [63]. The enhanced ion density might also be attributed to the prompt penetration of electric field which triggers the expansion of equatorial ionization anomaly in such a manner that the two formed crest regions expand towards the higher latitudes. Hence, varies the pattern of ion distribution. [161] have also shown with his data analysis that actually during the main phase of geomagnetic storms the ionospheric westward (eastward) electric field increases which results in the variations in ionospheric parameters.

## 6.5 CONCLUSION

In the present study, the variations in ionospheric parameters - ion densities and ion temperature ($H^+$, $O^+$ and Ti) over the low latitude Indian region, using ROCSAT-1 satellite observations and IRI-2016 estimations, in response to a weak and moderate

magnitude GS occurred on 30 July 1999 ($K_{p_{max}} = 8-$, $D_{st} = \sim -53$ nT) and 13 November 1999 ( $K_{p_{max}} = 6+$ , $D_{st} = \sim -106$ nT ) has been analyzed. The conclusion of the study has been explained in the following points.

1. For weak GS, both the average $O^+$ and $H^+$ density has been found to increase by a factor of around 1.8 during disturbed and quiet days respectively as calculated by ROCSAT-1. According to the IRI-2016 model, only $H^+$ density has increased by a factor of around 2.5 during quiet days as modelled by IRI-2016 model–whereas any significant–variations has not been shown by Ti as measured by both ROCSAT-1 and IRI-2016 model values.
2. For moderate GS, the average $O^+$ and $H^+$ density has been found to increase by a factor of around 2.7 and 6.3 respectively during disturbed and quiet days respectively as calculated by ROCSAT-1 whereas according to IRI-2016 model the $O^+$ and $H^+$ density has increased by a factor of around 1.1 and 2.8 respectively during disturbed and quiet days respectively. Again, no significant variation has been observed, except by factor of around 1.1 with the modelled values only.
3. The study of both the GSs by ROCSAT -1 reveals that $O^+$ density showed variation according to the strength of GS. For weak storm, it showed little variation and a significant variation for moderate GS. For the $H^+$ density it has been noticed that for both weak and moderate GS, it varied notably with measured and modelled values. And the Ti has been observed showing the least or negligible variation both by measured and modelled values during both weak and moderate GSs.

# CHAPTER 7

# CONCLUSION AND FUTURE SCOPE

## 7.1 CONTRIBUTION OF THE THESIS

In the present study, efforts have been put to study the variability of ionospheric parameters at low latitude regions during different phases of solar activity years. As in today's world, the dependence on technological systems is spontaneously increasing, so it becomes extremely important to study the variabilities occurring in the ionosphere.

In the present research work, the ionospheric parameters are used as a tool to study or analyze the behavioural pattern of the ionosphere under different circumstances. The analysis of ion density and ion temperature behaviour provides an insight into the low latitudinal ionosphere's characteristics. The study shows that the sun is the predominant factor which governs the Earth and Earth's atmosphere due to which the ionospheric properties are found completely coupled with solar activities.

A comparative study on ionospheric ion density and temperature has been done in chapter 4 and 5. The behaviour of ionospheric ion parameters (total ion density - $N_i$ and ion temperature - $T_i$ ) as measured by SROSS-C2 satellite have been analyzed and compared with estimated IRI – 2012 model values at an average altitude of ~ 500 km during LSA (year 1995, $F_{10.7}$ = 77) and HSA (year 2000, $F_{10.7}$ = 177) over 5°-35°N geog. latitude and 65°-95°E geog. longitude.

As solar activity increases, total ion density Ni also increases by the factor of $10^2$ emphasizing the main source of ionization as solar flux. Ti varies from ~ 650K – 1500K and 900K- 1300K during low and high solar activity years respectively. The relationship between Ni and Ti shows weak /poor co-relation. The correlation factor is observed weaker in low solar activity compared to high solar activity.

Topside ionospheric parameters- $N_i$ and $T_i$ have been analyzed at low latitude region with changing solar phases (years 1999 to 2003). The Ni and Ti data collected from ROCSAT-1 satellite has been compared with the estimated values of the IRI-2016 model. The distinct annual diurnal feature observed by IRI model is presence/absence

of a secondary peak in Ni/Ti which is vice-versa in ROCSAT-1 measurements. Some other discrepancies observed in the model are overestimation of Ni during all the years, specifically in the morning and evening time; overestimation of Ti, during the entire day except in the morning peak hours of the year 1999, 2000, and 2003. For each year, the hourly averaged ROCSAT-1 measured value of Ni and Ti has also been correlated with the estimated value of IRI-2016 model. The correlation coefficient factor $R^2$ is ~ 0.8 for Ni and ~ 0.9 for Ti respectively. The variations of Ni and Ti with changing solar flux have also been studied.

This comparison-based study will be beneficial to amend the models so that these empirical models can be utilized further with advanced precision.

Efforts have also been put to understand the coronal mass ejections which trigger the geomagnetic storms with an increase in solar wind velocity, density, temperature, and southward interplanetary magnetic field. The geomagnetic storms affect the ionosphere and thus make ionospheric studies a necessity from the point of view of space-weather-related processes. In this study, three moderate magnitude storms effect is analyzed over low latitude ionosphere which shows increment and decrement in ionospheric parameters density. The ionospheric plasma parameters (ion temperature - Ti and ion densities - $O^+$, $H^+$) show anomalous behaviour during storm-affected days compared to normal days. $O^+$ ion density and ion temperature (Ti) increases whereas $H^+$ ion density decreases during storm-affected days. This can lead to disturbance in satellite-based navigation and communication systems.

At this stage, the thesis provides information on the ionosphere, its structure and evolution, and the effects of solar activity on the ionospheric plasma. The main focus area of the study is low latitudinal F-2 region and topside ionosphere. The thesis has a significant contribution to the application of ionosphere-based studies. A better understanding of ionospheric plasma variations, related to the solar activity effects will not only increase our knowledge of ionospheric chemical and dynamical processes but also will provide an insight into space weather-related problems. The present work also suggests some significant improvements in the ionospheric IRI models. Thus, the research work in the present thesis has significant importance in the field of ionospheric physics.

## 7.2 FUTURE WORK

It is well accepted that the main drive for the navigation and communication systems is the behaviour of the ionosphere. Larger irregularities in the ionospheric plasma density can result in the failure of communication systems. So for a better understanding of the behaviour of the ionosphere, ionospheric parameters due to the solar activity effects on it, the study needs to be extended more. This will assist us to have a global understanding of ionospheric electrodynamics.

The interaction of ionospheric plasma with geomagnetic field lines is different at low and high latitudes. The low latitudes occupy a larger part of the earth's surface area (because of being bulged at equators) and with the countries which are still developing or are underdeveloped. Hence it requires advanced technology or satellite-based research studies in these regions. Further, the research work can be extended to mid and high latitudes to find more correlations of one on another.

Complete knowledge of coupling processes between the Earth's upper atmosphere and the Sun can unfold many unresolved questions. Regarding that, an intensive study on finding correlations between parameters of the ionosphere and the Sun is still a big deal.

The study of the relationship between solar flares and coronal mass ejections is an essential issue of today's active research. The prediction of CME and then its forecasting is still uncertain. Therefore it requires related extensive studies which will help the astronomers to understand the evolution of CMEs and their impact on the Earth.

# REFERENCES


[1] P. K. Subhadra Devi, "Behaviour of Ionosphere and its interaction with solar magnetosphere system," *Thesis, Mirror Shodhganga*, 2014, http://hdl.handle.net/10603/28485.

[2] M. C. Kelley, "The Earth's Ionosphere: Plasma Physics and Electrodynamics, *Academic,* San Diego, Calif., 1989.

[3] S. Raizada, "Ionospheric irregularities in the f region at low latitudes," *Thesis, Mirror Shodhganga*, 2015, http://hdl. handle.net/10603/48581.

[4] Balan, N., K. Shiokawa, Y. Otsuka, S. Watanabe, and G. J. Bailey (2009a), Super plasma fountain and equatorial ionization anomaly during penetration electric field, *J. Geophys. Res*., 114, A03310,

[5] H. Rishbeth and O. K. Garriott, "Introduction to ionospheric physics," 1st ed., *Academic Press,* New York, Vol. 47, pp. 234, 1969.

[6] S. Sau, "Study of dynamical coupling of the atmosphere ionosphere system at low latitudes," *Thesis, Mirror Shodhganga,* 2018, http://hdl.handle.net/ 10603/248906.

[7] L. Alexander, V. N. Radhika, T. John, P. Subrahmanyam, P. Chopra, M. Bahl, H. K. Maini, V. Singh, D. Singh, S. C. Garg, "Study of the evolution of Te and Ti at the low-latitude upper ionosphere using SROSS-C2 RPA observations," *Journal of Atmospheric and Solar-Terrestrial Physics*., Vol. 66, 2004, pp. 1075-1083, 10.1016/j.jastp.2004.04.002.

[8] L. Zou, H. Rishbeth, I. C. F. Muller-Wodarg, A. D. Aylward, G. H. Millward, T. J. Fuller-Rowell, D. W. Idenden, and R. J. Moffett, "Annual and semiannual variations in the ionospheric F2-layer," I. Modelling, *Ann. Geophys.*, Vol. 18, 2000, pp. 927.

[9] L. Liu, B. Zhao, W. Wan, B. Ning, M. L. Zhang, and M. He, "Seasonal variations of the ionospheric electron densities retrieved from Constellation

Observing System for Meteorology, Ionosphere, and Climate mission radio occultation measurements," *J. Geophys. Res.*, Vol. 114, A02302, 2009.

[10] M. Klimenko, V. Klimenko, I. Cherniak, I. Zakharenkova, K. Ratovsky and A. Karpachev, *40th COSPAR Scientific Assembly*, 2014.

[11] M. A. Abdu, "Major phenomena of the equatorial ionosphere thermosphere system under disturbed conditions," *J. Atmos. Terr. Phys.*, Vol. 59, 1997, pp. 1505-1519.

[12] Abdu, M. A., "Outstanding problems in the equatorial ionosphere - thermosphere electrodynamics relevant to spread F, *J. Atmos. & Sol. Terr. Phys.*, 63, 2001, 869-884.

[13] M. A. Abdu, I. S. Batista, H. Takahashi, J. MacDougall, J. H. Sobral, A. F. Medeiros, and N. B. Trivedi, "Magnetospheric disturbance induced equatorial plasma bubble development and dynamics: A case study in Brazilian sector," *J. Geophys. Res.*, Vol. 108(A12), 2003, pp.1449, doi:10.1029/2002JA009721.

[14] D. T. Farley, E. Bonelli, B. G. Fejer, and M. F. Larsen, "The prereversal enhancement of the zonal electric field in the equatorial ionosphere," *J. Geophys. Res.*, Vol. 91(A12), 1986, pp. 13723– 13728, doi:10.1029/JA091iA12p13723.

[15] P. R. Fagundes, J. A. Bittencourt, J. R. Abalde, Y. Sahai, M. J. A. Bolzan, and W. L. C. Lima, "F layer postsunset height rise due to electric field prereversal enhancement: 1. Traveling planetary wave ionospheric disturbance effects," *J. Geophys. Res*., Vol. 114, 2009, doi: 10.1029/2009JA014390.

[16] M. C. Kelley, R. R. Ilma and G. Crowley, "On the origin of pre-reversal enhancement of the zonal equatorial electric field," *Ann. Geophys*., Vol. 27, 2009, pp. 2053–2056, https://doi.org/10.5194/angeo-27-2053-2009, 2009.

[17] R. W. Schunk and A. F. Nagy, "Ionospheres: Physics, Plasma Physics, and Chemistry," *Cambridge: Cambridge University, In Press*, N. York, 2000, doi: 10.1017/CBO9780551772.

[18] K. A. Zawdie, J. D. Huba, M. S. Dhadly and K. Papadopoulos, “The Effect of Plasma Releases on Equatorial Spread *F*- a Simulation Study.” *Front. Astron. Space Sci*., 2019, doi: 10.3389/fspas.2019.00004.

[19] S. Ravindran, “Electrodynamics of the equatorial ionosphere,” Thesis, *Mirror Shodhganga*, 1994, http://hdl. handle.net/10603/122994.

[20] R. R. Raghava, L. E. Wharton, N. W. Spencer, H. G. Mayr and L. H. Brace, “An equatorial temperature and wind anomaly (ETWA),” *Geophys. Res. Lett*., Vol. 18, 1991, pp. 1193-1196.

[21] J. Lei, “A brief review of the equatorial thermosphere anomaly,” *Journal of University of Science and Technology of China*, Vol. 43, 2013, pp. 922-928.

[22] P. T. Jayachandran, P. Sri Ram, V. V. Somayajulu and P. V. S. Rama Rao, "Effect of equatorial ionization anomaly on the occurrence of spread-F,” *Ann. Geophysicae*, Vol. 15, 1997, pp. 255–262.

[23] B. Mangla, “Study of ionic behavior of ionosphere F2 region using satellite data,” Thesis, *Mirror Shodhganga*, 2018, http://hdl. handle.net/10603/214144.

[24] B. Rathore, D. Gupta, and K. Parashar, “Relation between Solar Wind Parameter and Geomagnetic Storm Condition during Cycle-23,” *International Journal of Geosciences,* 2014, Vol. 05. pp. 1602-1608, 10.4236/ijg.2014.513131.

[25] K. F. Tapping, “The 10.7 cm solar radio flux (F10.7),” Space Weather, Vol. 11, 2013, pp. 394-406, 10.1002/swe.20064.

[26] Güyer, Sinan & Can, Zehra, “Solar flare effects on the ionosphere”. RAST 2013 - *Proceedings of 6th International Conference on Recent Advances in Space Technologies*, 2013, pp. 729-733, 10.1109/RAST.2013.6581305.

[27] W. D. Gonzalez, J. A Joselyn, Y. Kamide, H. W. Kroehl, G. Rostoker, B. T Tsurutani, V. M. Vasyliunas, “What is a geomagnetic storm,” *Journal of Geophysical Research*, Vol. 99, 1994, pp. 5771–5792,

[28] W. D Gonzalez, B. T. Tsurutani, and A. L. Clua de Gonzalez, "Interplanetary origin of magnetic storms," *Space Sci. Rev*., Vol. 88, 1999, pp. 529– 562.

[29] C. A. Loewe and G. W. Prolss, "Classification of mean behavior of magnetic storms," *Journal of Geophysical Research*, Vol. 102(A7), 1997, pp. 14, 209–14,213,

[30] B. T. Tsurutani, W. D. Gonzalez, G. S. Lakhina and S. Alex, " The extreme magnetic storm of 1- September 1859," *J. Geophys. Res,* Vol. 108, 2003, pp. 1268.

[31] Y. Kamide, N. Yokoyama, W. Gonzalez, B. T. Tsurutani, I. A. Daglis, A. Brekke, and S. Masuda, "Two-step development of geomagnetic storms," *J. Geophys. Res*., Vol. 103, 1998, pp. 6917-6921, doi: 10.1029/97JA03337.

[32] T. F. Tascione, "Introduction to the Space Environment", *Orbit Book Company Inc*., Malabar, Florida, 1988.

[33] K. Davies, "Ionospheric Radio", *Institution of Engineering and Technology,* London, U. K., Vol. 31, 1990.

[34] L. F. McNamara, "The Ionosphere: Communications, Surveillance, and Direction Finding," *Krieger, Malabar, Fla*., 1991.

[35] V. Depuev and T. Zelenova, "Electron density profile changes in a pre-earthquake period," *Advances in Space Research*, Vol. 18, 1996, pp.115-118.

[36] J. Rai, M. Rao, and B.A. P. Tantry, "Bremsstrählung as a Possible Source of UHF Emissions from Lightning," *Nature Physical Science*., Vol. 238, 1972.

[37] D. K. Sharma., J. Rai, M. Israil and P. Subrahmanyam, "Diurnal, seasonal and latitudinal variation of ionospheric temperatures of the topside F region over Indian region during solar minimum year 1995-96," *J. Atmos. Solar-Terr. Phys*, Vol. 67, 2005, pp. 269-274.

[38] J. Y. Liu., Y. J. Chuo, S. J. Shan, Y. B. Tsai, Y. I. Chen, S. A. Pulinets and S. B. Yu, "Preearthquake ionospheric anomalies registered by continuous GPS TEC measurements," *Annales Geophysicae*, Vol. 22, 2004, pp. 1585-1593.

[39] R. R. Babcock Jr. and J. V. Evans, "Effects of geomagnetic disturbances and neutral winds and temperatures in the thermosphere observed over Millstone Hill," *J. Geophys. Res.*, Vol. 84, 1979, pp. 5349-5354.

[40] W. L. Oliver, T. Takami, S. Fukao, T. Sato, M. Yamamoto, T. Tsuda, T. Nakamura, and S. Karo, "Measurements of ionospheric and thermospheric temperatures and densities with the middle and upper atmosphere radar," *J. Geophys. Res.*, Vol. 96, 1991, pp. 17827.

[41] S. Watanabe, K. I. Oyama and M. A. Abdu, "A computer simulation of electron and ion densities and temperature in the equatorial F region and comparison with Hinotori results," *J. Geophys. Res.*, Vol. 100, 1995, pp. 14,581.

[42] P. M. Banks and A. F. Nagy, "Concerning the influence of elastic scattering upon photoelectron transport and escape," *J. Geophys. Res.*, Vol. 75, 1970, pp. 1902.

[43] G. V. Khazanov and M. W. Liemohn, "Nonsteady-state ionosphere-plasmasphere coupling of superthermal electrons," *J. Geophys. Res.*, Vol. 100, 1995, pp. 9669.

[44] G. J. Bailey, R. J. Moffett, and W. E. Swartz, "Effects of photoelectron heating and interhemisphere transport on daytime plasma temperature at low latitudes," *Planet. Space Sci.*, Vol. 23, 1975, pp. 599.

[45] P. G. Richards and D.G. Tort, "Thermal coupling of conjugate ionospheres and the tilt of the Earth's magnetic field," *J. Geophys. Res.*, Vol. 91, 9017, 1986.

[46] W. Kohnlein, "A model of the electron and ion temperatures in the ionosphere," *Planet. Space Sci.*, Vol. 34, 1986, pp. 609.

[47] L. H. Brace and R. F. Theis, “An empirical model of daytime electron temperature in the thermosphere at solar minimum,” *Geophys. Res. Lett.*, Vol. 5, 1978, pp. 275.

[48] L. H. Brace and R. F. Theis, “Global empirical models of ionospheric electron temperature in the upper F region and plasmasphere based on in situ measurements from the Atmosphere Explorer-C, ISIS-1 and ISIS-2 satellites,” *J. Atmos. Terr. Phys.*, Vol. 43, 1981, pp. 1317.

[49] K. I. Oyama, N. Balan, S. Watanabe, T. Takahashi, F. Isoda, G. J. Bailey, and H. Oya, “Morning overshoot of Te enhanced by downward plasma drift in the equatorial topside ionosphere,” *J. Geomagn. Geoelectr.*, Vol. 48, 1996, pp. 959.

[50] N. Balan, Y. Otsuka and S. Fukao, “New aspects in the annual variations of the ionosphere observed by the MU radar,” *Geophy. Res. Lett.*, Vol. 24, 1997 , 2287-2290, 1997b.

[51] K. I. Oyama, M. A. Abdu, N. Balan, G. J. Bailey, S. Watanabe, T. Takahashi, E. R. de Paula, I. S. Batista, F. Isoda and H. Oya, “High electron temperature associated with the prereversal enhancement in the equatorial ionosphere,” *J. Geophys. Res.*, Vol. 102, 1997, pp.417.

[52] J.P. McClure, “Thermospheric temperature variations inferred from incoherent scatter observations,” *J. Geophys. Res.*, Vol. 76, 3106, 1971.

[53] S. Watanabe and K. I. Oyama, “Effects of neutral wind on the electron temperature at a height of 600 km in the low-latitude region,” *Ann. Geophysicae*, Vol. 14, 1996, pp. 290–296.

[54] S. Fukao, W. L. Oliver, Y. Onishi, T. Takami, T. Sato, T. Tsuda, M. Yamamoto, and S. Karo, “F-region seasonal behavior as measured by the MU radar,” *J. Atmos. Terr. Phys.*, Vol. 53, 1991, pp. 599.

[55] Y. Z. Su, K. I. Oyama, G. J. Bailey, T. Takahashi, and S. Watanabe, “Comparison of satellite electron density and temperature measurements at

low latitudes with a plasmasphere-ionosphere model," *J. Geophys. Res.*, Vol. 100, 14591, 1995.

[56] D. L. Hysell, E. Nossa, M. F. Larsen, J. Munro, M. P. Sulzer, S. A. González, "Sporadic E layer observations over Arecibo using coherent and incoherent scatter radar: assessing dynamic stability in the lower thermosphere," *J Geophys Res.*, Vol. 114, 2009, doi: 10.1029/2009JA014403.

[57] N. Balan, K. I. Oyama, G. J. Bailey, S. Fukao, S. Watanabe and M. A. Abdu, "A plasma temperature anomaly in the equatorial topside ionosphere," *J. Geophys. Res*., Vol. 102, 1997a, pp. 7485-7492.

[58] M. Aggarwal, H.P. Joshi, and K.N. Iyer, "Solar activity dependence of electron and ion temperatures using SROSS C2 RPA data and comparison with IRI model," *Journal of Atmospheric and Solar-Terrestrial Physics*, Vol. 69, 2007, pp. 860-874.

[59] A. Bardhan, D.K. Sharma, M.S. Khurana, M. Aggarwal, S. Kumar, "Electron-ion-neutral temperatures and their ratio comparisons over low latitude ionosphere," *Advances in Space Research*, Vol. 56, 2015, pp. 2117-2129.

[60] J. Lei, L. Liu, W. Wan, and S. R. Zhang, "Variations of electron density based on long-term incoherent scatter radar and ionosonde measurements over Millstone Hill," *Radio Sci.*, Vol. 40, 2005, pp. 1-10, doi:10.1029/2004 RS003106.

[61] K. H. West and R. A. Heelis, "Longitude variations in ion composition in the morning and evening topside equatorial ionosphere near solar minimum," *Journal of Geophysical Research*, Vol. 101, 1996, pp. 7951-7960.

[62] V. Truhlik, L. Trikosva, and J. Smilauer, "Manifestation of solar activity in the global topside ion composition-a study based on satellite data," *Annales Geophysicae*, Vol. 23, 2005, pp. 2511-2517.

[63] A. Bardhan, D. K. Sharma, S. Kumar, and J. Rai, "Variation of O+ ion density during low and high solar activity as measured by SROSS-C2 satellite," *Atmosfera*, Vol. 27(3), 2014, pp. 227-237.

[64] P.K. Bhuyan, P.K. Kakoty, S.C. Garg and P. Subrahmanyam, “Electron and ion temperature and electron density at ±10° magnetic latitudes from SROSS C2 measurements over India and comparison with the IRI,” *Advances in Space Research*, Vol. 29, 2002a, pp. 865-870.

[65] P. K. Bhuyan, M. Chamua, P. Subrahmanyam, S. C. and Garg, “Diurnal, seasonal and latitudinal variations of electron temperature measured by the SROSS C2 satellite at 500 km altitude and comparison with the IRI,” *Ann. Geophys.*, Vol. 20, 2002 b, pp. 807–815, doi:10.5194/angeo-20-807-2002b.

[66] F. Su, W. Wang, A. G. Burns, X. Yue, and F. Zhu, “The correlation between electron temperature and density in the topside ionosphere during 2006–2009,” *J. Geophys. Res. Space Physics,* Vol. 120, 2015, pp. 10724–10739, doi:10.1002/2015JA021303.

[67] S. R. Zhang and J. M. Holt, “Ionospheric temperature variations during 1976 – 2001 over Millstone Hill,” *Adv. Space Res.,* Vol. 33, 2004, pp. 963 – 969, doi:10.1016/j.asr.2003.07.012.

[68] [68] D. Bilitza, V. Truhlik, P. Richards, T. Abe, and L. Triskova, “solar cycle variation of mid-latitude electron density and temperature: Satellite measurements and model calculations,” *Adv. Space Res.,* Vol. 39 (5), 2007, pp. 779–789, doi:10.1016/j.asr.2006.11.022.

[69] A. Borgohain and P. Bhuyan, “Effect of solar cycle on topside ion temperature measured by SROSS C2 and ROCSAT 1 over the Indian equatorial and low latitudes,” *Annales Geophysicae,* Vol. 30, 2012, pp. 1645-1654.

[70] Y. Kakinami, S. Watanabe, M. Y. Yamamoto, and C. K. Chao, “Correlations between ion density and temperature in the topside ionosphere measured by ROCSAT-1,” *J. Geophys. Res. Space Physics*, Vol. 119, 2014, pp. 9207–9215.

[71] R.B. Bent, and S.K. Liewellyn, “Documentation and Description of the Bent Ionospheric Model,” *Space and Missiles Organization,* Los Angeles, CA. AFCRL-TR- 73-0657, 1973.

[72] R. Ezquer, M Mosert, S. Radicella, and C. Jadur, “The study of the electron density variability at fixed heights over San Juan and Tucuman,” *Advances in Space Research,* Vol. 29, 2002, pp. 993-997.

[73] M. Figurski and P. Wielgos, “Intercomparison of TEC obtained from the IRI model to the one derived from GPS measurements,” *Advances in Space Research,* Vol. 30, 2002, pp. 2563-2568.

[74] D. Bilitza, “The importance of EUV indices for the international reference ionosphere,” *Physics and Chemistry of the Earth, Part C: Solar, Terrestrial & Planetary Science,* Vol. 25, 2000, pp. 515-521.

[75] R. Leitinger, B. Nava and S. Radicella, “Electron density models for assessment studies - New developments,” *Acta Geodaetica Et Geophysica Hungarica,* Vol. 37, 2002, pp. 183-193.

[76] C. T. Hsu and R. A. Heelis, “Modeling the daytime energy balance of the topside ionosphere at middle latitudes,”*J. Geophys. Res. Space Physics,*Vol. 122, 2017, pp. 5733– 5742.

[77] B. MacPherson, S. A. Gonzfilez, G. J. Bailey, R. J. Moffett, and M.P. Sulzer, “The effects of meridional neutral winds on the O+-H + transition altitude over Arecibo,” *Geophys. Res.,* Vol. 103, 1998, pp. 183-29.

[78] J. D. Huba, G. Joyce, and J. A. Fedder, “Sami2 is another model of the ionosphere (SAMI2): A new low-latitude ionosphere model,” *J. Geophys. Res.,* Vol. 105, 2000, pp. 23 035–23053.

[79] D. K. Sharma, Malini Aggarwal, Ananna Bardhan, “Variability of ionospheric parameters during solar minimum and maximum activity and assessment of IRI model,” *Advances in Space Research,* Vol. 60, 2017, pp. 435-443.

[80] E. Mengistu, M. B. Moldwin, B. Damtie, and M. Nigussie, “The performance of IRI-2016 in the African sector of equatorial ionosphere for different geomagnetic conditions and time scales,” *Journal of Atmospheric and Solar-Terrestrial Physics*, Vol. 186, 2019, pp. 116-138.

[81] G. W. Prolss, “Ionospheric F-region storms,” In: *Handbook of atmospheric Electrodynamics* (H. Volland, Ed.), CRC Press, Boca, Raton, FL, Vol. 2, 1995, pp. 195-248.

[82] M. J. Buonsanto, “Ionospheric storms- A review,” *Space Sci. Rev.*, Vol. 88, 1999, pp. 563-601.

[83] G. Zhang and L.F. Burlaga, “Magnetic clouds, geomagnetic disturbances and cosmic ray decrease,” *J. Geophys. Res.*, Vol. 93, 1998, pp. 2511-2518.

[84] J. T. Gosling, D. J. McComas, J. L. Philips, and S. J. Bame, “Geomagnetic activity associated with earth passage of interplanetary shock disturbances and coronal mass ejections,” *J. Geophys. Res*., Vol. 96, 1991, pp. 7831-7839.

[85] C. C. Wu, and R. P. Lepping, “The effects of magnetic clouds on the occurrences of geomagnetic storms: The first four years of Wind,” *J. Geophys. Res.*, Vol. 107, 2002, pp.1314-1321.

[86] J. E. Borovsky and J. T. Steinberg, “The “calm before the storm” in CIR/magnetosphere interactions: Occurrence statistics, solar wind statistics, and magnetospheric preconditioning,” *J. Geophys. Res.*, Vol. 111, 2006, doi: 10.1029/2005JA011397.

[87] A. Nishida, N. Iwasaki, and T. Nagata, “The origin of fluctuations in the equatorial electrojet: a new type of geomagnetic variation,” *Ann. Geophys.*, Vol. 22, 1966, pp. 478-484.

[88] J. H. Sastri, M. A. Abdu, and J. H. A. Sobral, “Response of equatorial ionosphere to episodes of asymmetric ring current activity,” *Ann. Geophys.*, Vol. 15, 1997, pp. 1316-1323.

[89] R. W. Spiro, R. A. Wolf and B. G. Fejer, “Penetration of high latitude-electric-field effects to low latitudes during SUNDIAL 1984,” *Ann. Geophys*., Vol. 6, 1988, pp. 39-50.

[90] M. Blanc and A. D. Richmond, “The ionospheric disturbance dynamo,” *J. Geophys. Res.*, Vol. 85, 1980, pp. 1669-1686.

[91] L. Scherliess and B. G. Fejer, “Storm time dependence of equatorial disturbance dynamo zonal electric fields,” *J. Geophys. Res.*, Vol. 102, 1997, pp. 24037-24046.

[92] [92 ] E. Astafyeva, I. Zakharenkova, K. Hozumi, P. Alken, P. Coisson, M. R. Hairston and W.R. Coley, “Study of the equatorial and low-latitude electrodynamic and ionospheric disturbances during the 22-23 June 2015 geomagnetic storm using ground-based and spaceborne techniques,” *J. Geophys. Res.*, Vol. 123, 2018, pp. 2424-2440.

[93] T. J. Fuller-Rowell, G. H. Millward, A. D. Richmond and M. V. Codrescu, “Storm-time changes in the upper atmosphere at low latitudes,” *J. Atmos. Sol. Terr. Phys.*, Vol. 64, 2002, pp. 1351-1360.

[94] N. Maruyama, A. D. Richmond, T. J. Fuller-Rowell, M. V. Codrescu, S. Sazykin, F. R. Toffoletto, R. W. Spiro and G. H. Millward, “Interaction between direct penetration and disturbance dynamo electric fields in the storm-time equatorial ionosphere,” *Geophys. Res. Lett.*, Vol. 32, 2005, doi: 10.1029/2005GL023763.

[95] V. Sreeja, S. Ravindran, T. K. Pant, C. V. Devasia and L. J. Paxton, “Equatorial and low-latitude ionosphere-thermosphere system response to the space weather event of August 2005,” *J. Geophys. Res.*, Vol. 114, 2009, doi: 10.1029/2009JA014491.

[96] M. S. Bagiya, H. P. Joshi, K. N. Iyer, M. Aggarwal, S. Ravindran and B. M. Pathan, “TEC variations during low solar activity period (2005-2007) near the Equatorial ionospheric anomaly crest region in India,” *Ann. Geophys*., Vol. 27, 2009, pp. 1047-1057.

[97] M. Chakraborty, S. Kumar, B. K. De and A. Guha, “Effects of geomagnetic storm on low latitude ionospheric total electron count: A case study from Indian sector,” *J. Earth Syst. Sci.*, Vol. 124, 2015, pp.1115-1126.

[98] M. Aggarwal, H.P. Joshi, K.N. Iyer, and Y.S. Kwak, “Response of the EIA ionosphere to the 7-8 May 2005 geomagnetic storm,” *Advances in Space Research*, Vol. 52, 2013, pp. 591-603.

[99] S. Sharma, P. Galav, N. Dashora, and R. Pandey, “Longitudinal study of the ionospheric response to the geomagnetic storm of 15 May 2005 and manifestations of TADs,” *Ann. Geophys.*, Vol. 29, 2011, pp. 1063-1070.

[100] C. S. Huang, J. C. Foster, L. P. Goncharenko, P. J. Erickson, W. Rideout, and A. J. Coster, “A strong positive phase of ionospheric storms observed by the Millstone Hill incoherent scatter radar and global GPS network,” *J. Geophys. Res*., Vol. 110, 2005.

[101] A. Komjathy, Y. M. Yang, X. Meng, O. Verkhoglyadova, A. J. Mannucci, and R. B. Langley, “Review and perspectives: Understanding natural-hazards-generated ionospheric perturbations using GPS measurements and coupled modeling,” *Radio Sci*., Vol. 51, 2016, doi:10.1002/2015RS005910

[102] T. I Zelenova and A. D. Legen'ka, “Ionospheric effects related to the Moneron earthquake of September 5(6), 1971,” *Izvestiya USSR Academy of Sciences: Physics of the Solid Earth*, Vol. 6, 1989, pp. 89–95,

[103] S. A. Pulinets, A. D. Legen’ka, A. T. Karpachev, N. A. Kochenova, M. D. Fligel, V. V. Migulin, and V. N. Oraevsky, “The earthquakes prediction possibility on the base of topside sounding data,” *IZMIRAN preprint N, (paper presented at VII IAGA Scientific Assembly, Buenos-Aires, Argentina, 1993),* Vol. 34, 1991, pp. 25.

[104] E. Astafyeva, L. Rolland, P. Lognonne, K. Khelfi, and T. Yahagi, “ Parameters of seismic source as deduced from 1 Hz ionospheric GPS data: Case study of the 2011 Tohokuoki event,” *J. Geophys. Res. Space Physics*, Vol. 118, 2013, doi:10.1002/jgra.50556.

[105] A. Komjathy, D.A. Galvan, P. Stephens, M.D. Butala, V. Akopian, B.D. Wilson, O. Verkhoglyadova, A.J. Mannucci, and M. Hickey. “Detecting Ionospheric TEC Perturbations Caused by Natural Hazards Using a Global

Network of GPS Receivers: the Tohoku Case Study," *Earth, Planets and Space*, Special Issue on "The 2011 Tohoku Earthquake" Vol. 64, 2012, pp. 1287–1294.

[106] H. Yang, "ADDTID: An Alternative Tool for Studying Earthquake/Tsunami Signatures in the Ionosphere. Case of the 2011 Tohoku Earthquake," *Remote Sens*., Vol. 11, pp. 1894, 2019, doi:10.3390/rs11161894

[107] H. Ahmamedov, "Interferometer temperature measurements in the ionosphere F-2 region during the Iranian earthquake of June 20 1990," Geomagnetism and Aeronomy, 33:163.

[108] G. A. Mikhailova, O. V. Kapustina, V. M. Kostin and M. Yu Mikhajlov, "Anomalous spectra of VLF emission in the outer ionosphere related to the Iranian earthquake of June 1990," *Geomagnetism and Aeronomy*,30:837.

[109] D. D. Sentman, E. M. Wescott, D. L. Osborne, D. L. Hampton and M. J. Heavner, "Preliminary results from the sprites 94 aircraft campaign: 1. Red sprites," *Geophys. Res. Lett.* Vol. 22, 1995, pp. 1205-1208.

[110] C. Rodger, "Red sprites, upward lightning, and VLF perturbations," *Reviews of Geophysics*, Vol. 37, 1999, 10.1029/1999RG900006.

[111] T. Otsuyama, Y. Hobara, and M. Hayakawa, "EM radiation associated with sprites," Proc. *Book on 11th International Conference on Atmospheric Electricity held at Alabama (USA)*, 1999, pp. 96-98.

[112] E. M. Wescott, D. D. Sentman, M. J. Heavner, D. L. Hampton, D. L. Osborne, and O. H. Vaughan Jr, "Blue starters: Brief upward discharges from an intense Arkansas thunderstorm,2 *Geophys Res Let.*, Vol. 23, 1996, pp. 2153-2156.

[113] R. P. Singh and R. P. Patel, "Lightning generated ELF, VLF, optical waves and their diagnostic features," Proc. National Workshop on Recent Developments in *Atmospheric and Space Sciences*, IIT Roorkee, 2001, pp. 9-32.

[114] V. Yukhimuk, R. A. Roussel-Dupre, and E. M. D. Symbalisty, "Optical characteristics of blue jets produced by runaway air breakdown simulation results," *Geophys Res Lett*, Vol. 25, 1998, pp. 3289- 329

[115] K. B. Eack, D. M. Suszcynsky, H. B. William, R. A. Roussel-Dupre and E. M. D. Symbalisity, "Gamma-ray emissions observed in a thunderstorm anvil," *Geophys. Res. Lett.*, Vol 2, 2000, pp. 185-188

[116] E. M. Wescott, D. D. Sentman, H. C. Stenbaek-Nielsen, P. Huet, M. J. Heavner, and D. R. Moudry, "New evidence for the brightness and ionization of blue starters and blue jets," *J. Geophys. Res.*, Vol. 106, 2001, pp. 21,549 – 21,554.

[117] V. P. Pasko, M. A. Stanley, J. D. Mathews, U. S. Inan, and T. G. Wood, "Electrical discharge from a thundercloud top to the lower ionosphere," *Nature*, Vol. 416, 2002, pp. 152 – 154.

[118] S. C. Garg and U. N. Das, "Aeronomy experiment on SROSS-C2," *J. Spacecr. Tech.*, Vol. 5, 1995, pp. 11–15.

[119] S. C. Garg, J. R. Anand, M. Bahl, P. Subrahmanyam, S. S. Rajput, H. K. Maini, P. Chopra, T. John, S. K. Singhal, V. Singh, D. Singh, U. N. Das, S.M. Bedekar, Soma, Venkteshwarlu and D. P. Goel, "RPA aeronomy experiment onboard the Indian satellite SROSS-C2 - Some important aspects of the payload and satellite," *Indian Journal of Radio and Space Physics*, Vol. 32, 2003, pp. 5-15.

[120] H. M. Mott-Smith and I. Langmuir, "The Theory of Collectors in Gaseous Discharges," *Phys. Rev.*, Vol. 28, 1926, pp.727-763.

[121] S. S. Rajput and S. C. Garg, "Instrumentation for charged particle traps," *Rev. Sci. Instrum.*, Vol. 68, 1997, pp. 4022–4026, doi:10.1063/1.1148376.

[122] S. S. Rajput and S. C. Garg, "Design and implementation of slope measuring instrument for measurement of charged particle temperatures," *Rev. Sci. Instrum.*, Vol. 69, 1998, pp. 294–298, doi:10.1063/1.1148512.

[123] S. S. Rajput and S. C. Garg, “Instrumentation for Retarding Potential Analyzer Experiment: Part I. Ion parameters,” *Rev. Sci. Instrum.*, Vol. 70, 1999, pp. 1435-1441,doi:10.1063/1.1149636.

[124] F. B. Hsiao, A. M. Wu, J. S. Chern, and C. J. Shieh, “Cost-effective Earth observation missions: Taiwan's perspective,” *Acta Astronautica*., Vol. 56, 2005, pp. 307-313.

[125] J. Liu, L. Chang, C. Chao, M. Chen, Y. Chu, L. Hau, C. Huang, C. Kuo, L. Lee, L. Lyu, C. Lin, C. Pan, J. Shue, C. Su, L. Tsai, Y. Yang, C. Lin, R. Hsu and H. Su, “The fast development of solar terrestrial sciences in Taiwan,” *Geoscience Letters*., Vol. 3, 2016.

[126] P. Chen, L. S. Lee and S. Lin, “OCI and ROCSAT-1 Development, Operations, and Applications,” *Korean Journal of Remote Sensing*, Vol. 15, 1999.

[127] Y. S.Chang, W. L. Chiang, S. J. Ying, B. J. Holt, C. R. Lippincott, and K. C. Hsieh, “System Architecture of the IPEI Payload on ROCSAT-1,” *TAO, Supplementary Issue*, 1999, pp. 7-18, doi: 10.3319/TAO.1999.10.S.7(ROCSAT).

[128] D. Bilitza, “International reference ionosphere,” *Radio Science*, Vol. 36, 2000, pp. 261-275.

[129] E. Astafyeva, S. Shalimov,E. Olshanskaya and P. Lognonné, “Ionospheric response to earthquakes of different magnitudes: Larger quakes perturb the ionosphere stronger and longer,” *Geophys. Res. Lett.*, Vol. 40, 2013, pp. 1675– 1681.

[130] D. K. Sharma, M. Israel, R. Chand, J. Rai, P. Subrahmanyam, and S. C. Garg, “Signature of seismic activities in the F2 region ionospheric electron temperature,” *J. Atmos. Sol. Terr. Phys.*, Vol. 68, 2006, pp. 691–696, doi:10.1016/j.jastp.2006.01.005.

[131] J. Bartels, N. H. Heck, and H. F. Johnson, "The three hour-range index measuring geomagnetic activity, *Terr. Magn. Atmos. Elec.*, Vol. 44, 1939, pp. 411-454, doi:10.1029/TE044i004p00411.

[132] J. Bartels, "Solar radiation and geomagnetism," *Terr. Magn. Atmos. Electr.*, Vol. 45, 1940, pp. 339– 343.

[133] M. Sugiura and T. Kamei, "Equatorial Dst index 1957-1986*," in IAGA Bull.*, Vol. 40, edited by A. Berthelier and M. Menvielle, ISGI Publ. Off., Saint-Maur-des-Fosses, France, 1991.

[134] M. Sugiura, "Hourly values of equatorial Dst for the IGY, *Annals of the International Geophysical Year*, Vol. 35, Part 1, 1965, pp. 9-45.

[135] A. Meloni, P. De Michelis and R. Tozzi, "Geomagnetic storms, dependence on solar and interplanetary phenomena: a review," *Memorie della Società Astronomica Italiana*, Vol. 76, 2005, pp.882.

[136] B. G. Fejer, "Low latitude electrodynamic drifts: a review," *Journal of Atmospheric and Terrestrial Physics*, Vol. 53, 1991, pp. 677-693.

[137] N. Balan, and G. J. Bailey, "Equatorial plasma fountain and its effects: Possibility of an additional layer," *Journal of Geophysical Research*, Vol. 100, 1995, pp. 21421-21 432.

[138] G. J. Bailey, N. Balan, and Y. Z. Su, "The Sheffield University plasmasphere ionosphere model – a review," *Journal of Atmospheric and Solar-Terrestrial Physics*, Vol. 59, 1997, pp. 1541-1552.

[139] N. Balan, K. I. Oyama, G. J. Bailey, S. Fukao, S. Watanabe and M. A. Abdu, "A plasma temperature anomaly in the equatorial topside ionosphere," *J. Geophys. Res.*, Vol. 102, 1997a, pp. 7485-7492.

[140] R. W. Schunkand A. F. Nagy, "Electron temperatures in the F region of the ionosphere:theory and observations," *Review Geophysical Space Physics*, Vol. 16, 1996, pp. 355-399.

[141] K. I. Oyama, S. Watanabe, Y. Su, T. Takanashi, and K. Hirao, “Season, local time, and longitude variations of electron temperature at the height of -600 km in the low latitude region,” *Advances in Space Research*, Vol. 18, 1996, pp. 269–278.

[142] Y. Z. Su, K. I. Oyama, G. J.; Bailey, T. Takahashi, and H. Oya, “Longitudinal variations of the topside ionosphere at low latitudes: Satellite measurements and mathematical modellings,” *Journal of Geophysical Research*, Vol. 101, 1996, pp. 17191–17205.

[143] Y. Kakinami, C. H. Lin, J. Y. Liu, M. Kamogawa, S. Watanabe and M. Parrot, “Daytime longitudinal structures of electron density and temperature in the topside ionosphere observed by the Hinotori and DEMETER satellites,” *Journal of Geophysical Research*, Vol. 116, 2011, pp. A05316.

[144] Liu, L.; Zhao, B.; Wan, W.; Venkatraman, S.; Zhang, M. L.; Yue, X. (2007): Yearly variations of global plasma densities in the topside ionosphere at middle and low latitudes, *Journal of Geophysical Research*, 112, pp. A07303.

[145] Y. Otsuka, S. Kawamura, N. Balan, S. Fukao and G. J. Bailey, “Plasma temperature variations in the ionosphere over the MU radar,” *J. Geophys. Res.*, Vol. 103, 1998, pp. 20705-20713.

[146] H. Risbeth and I. C. F. Muller-Wodarg, “Why is there more ionosphere in January than in July? The annual asymmetry in the F2-Layer,” *Ann. Geophys.*, Vol. 24, 2006, pp. 3293-3311.

[147] L. Zou, H. Rishbeth, I. C. F. Muller-Wodarg, A. D. Aylward, G. H. Millward, T. J. Fuller-Rowell, D. W. Idenden, and R. J. Moffett, “Annual and semiannual variations in the ionospheric F2-layer. I. Modelling,” *Ann. Geophys.*, Vol. 18, 2000, pp. 927.

[148] M. Mendillo, C. Huang, X. Pi, H. Rishbeth and R. Meier, “The global ionospheric asymmetry in total electron content,” *J. Atmos. Solar Terr. Phys.*, Vol. 67, 2005, pp. 1377-1387.

[149] D. Bilitza, D. Altadill, V. Truhlik, V. Shubin, I. Galkin, B. Reinisch, and X. Huang, "International reference ionosphere 2016: From ionospheric climate to real-time weather predictions," *Space Weather*, Vol. 15, 2017, pp. 418-429.

[150] S. Y. Su, H. C. Yeh, R. A. Heelis, J. M. Wu, S. C. Yang, L. F. Lee, and H. L. Chen, "The ROCSAT-1 IPEI preliminary results: Low-latitude plasma and flow variations," *Terr. Atmos. Oceanic Sci.*, Vol. 10, 1999, pp. 787-804.

[151] H. C. Yeh, S. Y. Su, R. A. Heelis and J. M. Wu, "The ROCSAT-1 IPEI preliminary results: Vertical ion drift statistics," *J. Terr. Atmos. Oceanic Sci.*, Vol. 10, 1999b, pp. 805-820.

[152] W. B. Hanson, A. F. Nagy, and R.J. Moffett, "Measurements of super cooled plasma in the equatorial exosphere," *J. Geophys. Res.*, Vol. 78, 1973, pp. 751-756.

[153] G. J. Bailey, R. J. Moffett, W. B. Hanson and S. Sanatani, "Effects of interhemisphere transport on plasma temperatures at low latitudes," *J. Geophys. Res.*, Vol. 78, 1973, pp. 5597-5610.

[154] H. Chandra and R. G. Rastogi, "Space weather event of 25 September 1998: Ionospheric response," *J. Ind. Geophys Union*, Vol. 15, 2011, pp. 45-59.

[155] S. Yadav, R. M. Das, R. S. Dabas, P. Subrahmanyam and A. K. Gwal, "Response of low latitude ionosphere of the Indian region during the super geomagnetic storm of 31 March 2001," *J. Geophys. Res.*, Vol. 116, 2011, doi: 10.1029/2010JA016373.

[156] E. Saiz, E. Cerrato, C. Cid, and J. Aguado, "Why are intense geomagnetic storms so important for human life?," Proceedings of 3rd Symposium of Astrophysics Group of the *Spanish Royal Physical Society*, Granada, Spain, 2007.

[157] W. B. Hanson and R. J. Moffett, "Ionization transport effects in the equatorial F-region," *J. Geophys. Res.*, Vol. 71, 1966, pp. 5559-5572.

[158] D. K. Sharma, A. Bardhan, and J. Rai, “Ionospheric electron and ion temperatures response to seismic activity,” *Indian J. Radio & Space Phys.*, Vol. 42, 2013, pp. 18-26.

[159] V. V. Afonin, O. A. Molchanov, T. Kodama, M. Hayakawa, and O. A. Akentieva, “Statistical study of ionospheric plasma response to seismic activity: search for reliable result from satellite observations,” In: M. Hayakawa, Atmospheric and Ionospheric Electromagnetic Phenomena Associated with Earth quakes, *Terra Scientific Publishing Company*, Tokyo, 1999, pp. 597-618.

[160] M. Hayakawa, O. A. Molchanov, T. Kodama, V. V. Afonin and O. A. Akentieva, “Plasma density variations observed on a satellite possibly related to seismic,” *Adv. Space Res.*, Vol. 26, 2000, pp. 1277-1280.

[161] C. S. Huang, J. C. Foster and M. C. Kelly, “Long-duration penetration of the interplanetary electric field to the low-latitude ionosphere during the main phase of geomagnetic storms,” *J. Geophys. Res.*, Vol. 110, 2005, doi: 10.1029/2005JA011202.

# BRIEF PROFILE OF THE RESEARCH SCHOLAR


## GEETA RANA

**Email**: geetikarana72@gmail.com


Geeta received her M.Sc (Physics) degree from Maharshi Dayanand University, Rohtak in 2007. She has vast experience of teaching at various schools and colleges. She had taught at Saraswati College for Women at Palwal and K. L. Mehta Dayanand College for Women at Faridabad. She is doing her Ph.D. under the guidance of Assistant professor, Dr. Mani Kant Yadav. Her area of interest for research is in Space and Atmospheric physics

# LIST OF PUBLICATIONS OUT OF THESIS

| S.No | Title of the paper | Name of the Journal/Conference with ISSN No. | Volume & Issue | Year | Pages |
|---|---|---|---|---|---|
| 1 | The Sun and its Activities | IJERGS<br>ISSN: 2091-2730 | Vol. 2, Issue 6 | 2014 | 784-791 |
| 2 | The Ionosphere and Radio propagation | IJECET<br>ISSN:0976 –6472 | Vol. 5,<br>Issue 11 | 2014 | 9-16 |
| 3. | Variability in Ionospheric Ion Temperature and Density with Varying Solar Activity over Low Latitude F2 Region | IJRAT<br>ISSN: 2321-9637 | Vol. 6,<br>Issue 10 | 2018 | 2691-2700 |
| 4 | Variations of ion density and temperature as measured by ROCSAT-1satellite and comparison with IRI-2016 model over low latitude region | Annals of Geophysics<br>ISSN: 2037-416X | Vol. 62,<br>Issue 6 | 2019 | 677 |
| 5 | Variability of ionospheric parameters during geomagnetic storms over low latitude using ROCSAT -1 satellite measurements | IJRSP | | 2020 | |
| 6 | Equinoctial Asymmetry Observed In Low Latitude Ionosphere during Mid and High Solar Activity Years | ICSTM-2018:<br>International Conference on Science, Technology & Management | | 2018 | |
| 7 | Study of the ionospheric parameters during different phase of solar activities | ICOEST-2018:<br>International Conference on Energy Storage Technologies and Systems | | 2018 | |